SPRINGER BRIEFS IN
ELECTRICAL AND COMPUTER ENGINEERING

Long Zhao · Hui Zhao
Kan Zheng · Wei Xiang

Massive MIMO in 5G Networks: Selected Applications

Springer

SpringerBriefs in Electrical and Computer Engineering

More information about this series at http://www.springer.com/series/10059

Long Zhao • Hui Zhao • Kan Zheng • Wei Xiang

Massive MIMO in 5G Networks: Selected Applications

Springer

Long Zhao
School of Information and Communication Engineering
Beijing University of Posts and Telecommunications
Haidian District, Beijing, China

Hui Zhao
School of Information and Communication Engineering
Beijing University of Posts and Telecommunications
Haidian District, Beijing, China

Kan Zheng
School of Information and Communication Engineering
Beijing University of Posts and Telecommunications
Haidian District, Beijing, China

Wei Xiang
College of Science and Engineering
James Cook University
Cairns, Queensland, Australia

ISSN 2191-8112 ISSN 2191-8120 (electronic)
SpringerBriefs in Electrical and Computer Engineering
ISBN 978-3-319-68408-6 ISBN 978-3-319-68409-3 (eBook)
https://doi.org/10.1007/978-3-319-68409-3

Library of Congress Control Number: 2017955546

Printed on acid-free paper

This Springer imprint is published by Springer Nature
The registered company is Springer International Publishing AG
The registered company address is: Gewerbestrasse 11, 6330 Cham, Switzerland

Preface

With the rapid development of wireless communications, space-domain technology has been widely studied in the past decades. Multiple-input multiple-output (MIMO), as a typical space-domain technology, has vast potential to provide high information rates and to improve system reliability, and thus was adopted in the fourth generation (4G) cellular networks. However, to satisfy the high spectral efficiency, energy efficiency as well as reliability requirements of the fifth generation (5G) cellular networks, some technical breakthroughs are essential. Therefore, massive MIMO technology was proposed and has become the key technique of 5G cellular networks among other advanced techniques such as dense networks and millimeter communications.

The objective of this monograph is to present the basic theory of massive MIMO and to examine several typical applications of massive MIMO. In Chap. 1, we elaborate on the significance of massive MIMO for 5G or future communications following a brief introduction to the requirements and key techniques of 5G as well as traditional MIMO techniques. Chapter 2 describes a variety of 5G scenarios and their improvements when massive MIMO is taken into account, followed by state-of-the-art physical-layer techniques and various networking techniques for interference mitigation and resource scheduling. Chapter 3 focuses on the physical-layer design, multiple access control (MAC) mechanism, and networking techniques alongside the performance of millimeter-wave communications aided by massive MIMO technology. In order to realize the full potential of wireless communications, massive MIMO is well exploited for hybrid information and energy transfer networks. A downlink precoder and an uplink pilot scheme are first proposed for single cell networks, and then both non-cooperative and cooperative energy transfer in multi-cell are presented in Chap. 4, following a short introduction to the state-of-the-art of wireless energy transfer. Finally, Chap. 5 suggests some open issues that help point out some new research directions in massive MIMO networks.

We are very grateful to Prof. Xuemin (Sherman) Shen, the *Springer Briefs* series editor on Wireless Communications. This book would not be possible without

his kind support. Special thanks are also attributed to Caroline Flanagan and Susan Lagerstrom-Fife at Springer Science+Business Media for their assistance throughout the preparation process of this monograph.

We would like to thank Jie Mei, Haojun Yang, and Zhe Yang from the Wireless Signal Processing and Network (WSPN) group at the Beijing University of Posts and Telecommunications (BUPT) for their contributions to this monograph. We also would like to thank all the members of the WSPN group for their thought-provoking discussions and insightful suggestions, creative ideas, and valuable comments.

This work is funded in part by the National Science Foundation of China (No. 61601044) and Fundamental Research Funds for the Central Universities (No. 2016RCGD10, 2014ZD03-02).

Beijing, China — Long Zhao
Beijing, China — Hui Zhao
Beijing, China — Kan Zheng
Cairns, QLD, Australia — Wei Xiang

Contents

Acronyms

2D	Two-Dimensional
3D	Three-Dimensional
3GPP	3rd Generation Partnership Project
4G	Fourth Generation
5G	Fifth Generation
AA	Antenna Array
ABS	Almost Blank Subframe
AEs	Antenna Elements
AoA	Azimuth of Arrival
AR	Augmented Reality
AWGN	Additive White Gaussian Noise
BE	Bandwidth Efficiency
BER	Bit Error Ratio
BF	Beamformer
BI-GDFE	Block-Iterative Generalized Decision Feedback Equalizer
BS	Base Station
CBSM	Correlation-Based Stochastic Model
CEP	Constant Envelope Precoding
CIRs	Channel Impulse Responses
CPS	Cyber-Physical System
CR	Correlation Rotation
CRE	Cell Range Extension
CRS	Cell Specific Reference Signals
CSI	Channel State Information
CSIT	CSI at the Transmitter
DASs	Distributed Antenna Systems
DL	Downlink
DoF	Degrees of Freedom
DPC	Dirty Paper Coding
EE	Energy Efficiency
eMBB	Enhanced Mobile Broadband

eNB	evolved Node B
EoAs	Elevation angle of Arrivals
FD	Frequency Domain
FDD	Frequency Division Duplex
FFR	Fractional Frequency Reuse
FFT	Fast Fourier Transform
FIR	Finite Impulse Response
HetNet	Heterogeneous Network
HetSNets	Heterogeneous and Small Cell Networks
HIET	Hybrid information and Energy Transfer
HomoNet	Homogeneous Network
ICI	Inter-cell Interference
ICIC	Inter-cell Interference Coordination
i.i.d.	Independent and Identically Distributed
IoT	Internet of Things
ISD	Inter-Site Distance
ISI	Inter-Symbol Interference
IUI	Inter-User Interference
LoS	Line of Sight
LS-MIMO	Large-Scale MIMO
LTE	Long Term Evolution
MAC	Media Access Control
MAP	Maximum Posterior Probability
MAX-MIN	Maximizing the Minimum
MeNB	Macro-cell eNB
MF	Matched Filter
MIMO	Multiple-Input and Multiple-Output
MIN-MAX	Minimizing the Maximum
ML	Maximum-Likelihood
mm-wave	millimeter-wave
MMSE	Minimum Mean Square Error
MMSE-SIC	MMSE based Soft Interference Cancellation
mMTC	Massive Machine Type Communications
MRC	Maximum Ratio Combining
MRT	Maximum Ratio Transmission
MSE	Mean Square Error
MU-MIMO	Multi-User MIMO
MUEs	Macro-cell UEs
NLoS	Non Line of Sight
NOMA	Non-Orthogonal Multiple Access
OFDM	Orthogonal Frequency Division Multiplexing
OFDMA	Orthogonal Frequency Division Multiple Access
PAPR	Peak to Average Power Ratio
PAs	Power Amplifiers
PBCH	Physical Broadcasting Channel

PDF	Probability Density Function
PDSCH	Physical Downlink Shared Channel
PSS/SSS	Primary/Secondary Synchronization Signals
QoE	Quality of Experience
QoS	Quality of Service
RF	Radio-Frequency
RMS	Root Mean Squared
RRC	Radio Resource Control
RRUs	Remote Radio Units
RSRP	Reference Signal Received Power
RTDD	Reversed TDD
RZF	Regularized ZF
SDMA	Spatial Division Multiple Access
SE	Spectrum Efficiency
SeNBs	Small-cell eNBs
SER	Symbol Error Ratio
SFR	Soft Frequency Reuse
SINR	Signal-to-Interference-plus-Noise Ratio
SNR	Signal-to-Noise Ratio
SUEs	Small-cell UEs
TD	Time-Domain
TDD	Time-Division Duplex
TPC	Transmit Precoding
TS	Tabu Search
Tx-Rx	Transmitter-Receiver
UEs	User Equipments
UL	Uplink
URLLC	Ultra-Reliable and Low Latency Communications
VP	Vector Perturbation
VR	Virtual Reality
WiGig	Wireless Gigabit Alliance
WPAN	Wireless Personal Area Networks
ZF	Zero-Forcing

Chapter 1
Introduction

Massive Multiple-Input and Multiple-Output (MIMO) technology is an important and timely topic, which is largely motivated by the requirements of the Fifth Generation (5G) or future wireless communications. By offering a large number of Degrees of Freedom (DoF), 5G is capable of simultaneously serving multiple users with high gains and thus improving the system Spectrum Efficiency (SE), Energy Efficiency (EE) and reliability. Different from existing studies in the literature, this book focuses specifically on the state-of-the-art of massive MIMO and its typical applications, such as millimeter-wave (mm-wave) communications and wireless energy transfer. In this chapter, we first present the motivations of massive MIMO following a short overview on the requirements and techniques of 5G communications. Then, basic concepts alongside the pros and cons of both MIMO and massive MIMO systems are given. The aim of the monograph is provided at the end of this chapter.

1.1 5G Brief

1.1.1 5G Requirements

Mobile Internet and the Internet of Things (IoT) are two key market drivers for 5G communications. The applications of 5G communications include cloud computing, eHealth services, automotive driving, tactile Internet, Augmented Reality (AR)/Virtual Reality (VR), Cyber-Physical System (CPS) and so on. These applications could be classified into three use scenarios, i.e., Enhanced Mobile Broadband (eMBB), Massive Machine Type Communications (mMTC), and Ultra-Reliable and Low Latency Communications (URLLC) [1, 2].

L. Zhao et al., *Massive MIMO in 5G Networks: Selected Applications*,
SpringerBriefs in Electrical and Computer Engineering,
https://doi.org/10.1007/978-3-319-68409-3_1

In order to support the requirements of the three use scenarios, some performance targets of 5G communications are defined, i.e., increasing throughput by 1000-fold, improving EE by 10-fold, shortening the end-to-end delay to 1/5–1/10, increasing the number of connected equipment by 10–100 folds, and prolonging the battery lifespan of low-power equipment by 10-fold. Some research projects for 5G communications have been launched at home and abroad in order to achieve the performance targets of 5G before 2020 year [1].

1.1.2 5G Technology

There are three key techniques for 5G communications from the perspective of system capacity. That is, the massive MIMO technique is first adopted to improve system SE; mm-wave spectral resources are employed to expand system bandwidth; and multi-layer and ultra-dense networks are deployed to increase geographic spectral reuse. The systems employing massive antenna arrays to serve multiple users are dubbed massive MIMO communication systems. Massive MIMO systems are capable of combatting the severe fading of mm-wave signals, providing the wireless backhaul, and suppressing interference in multi-layer and denser networks. Therefore, this monograph focuses on massive MIMO technology and their typical application scenarios in an attempt to provide the basic theory and paradigms for practical system designs.

1.2 MIMO Technology

Bandwidth Efficiency (BE) or SE is usually one of the most important metrics to select candidate technologies for next-generation wireless communications systems. Meanwhile, with excessive power consumption in wireless communications networks, both carbon emissions and operator expenditure increase year by year [3, 4]. As a result, EE has become another significant metric for evaluating the performances of wireless communications systems with some given BE constraints [5–7].

1.2.1 Traditional MIMO

MIMO technology has attracted much attention in wireless communications, because it offers significant increases in data throughput and link range without an additional increase in bandwidth or transmit power. In 1993 and 1994, a MIMO approach was proposed and the corresponding patent was issued [8], where multiple transmit antennas are co-located at one transmitter with the objective

of improving the attainable link throughput. Then, the first laboratory prototype of spatial multiplexing was implemented to demonstrate the practical feasibility of MIMO technology [9]. Nowadays, MIMO has been accepted as one of key technologies in Fourth Generation (4G) wireless communication systems. When an evolved Node B (eNB) equipped with multiple antennas communicates with several User Equipments (UEs) at the same time-frequency resources, it is referred to as Multi-User MIMO (MU-MIMO). MU-MIMO is capable of improving either the BE or the reliability by improving either the multiplexing gains or diversity gains [10].

1.2.2 Massive MIMO

In order to scale up these gains of traditional MIMO, the massive MIMO concept, which is also known as Large-Scale MIMO (LS-MIMO) scheme often also associated with the terminologies of large-scale antenna systems, very large MIMO, very large MU-MIMO, full-dimensional MIMO, hyper MIMO, etc., was proposed by Marzetta in [11]. More explicitly, massive MIMO refers to the system that uses hundreds of antennas to simultaneously serve dozens of UEs. Both theoretical and measurement results indicate that massive MIMO is capable of significantly improving the BE, which simultaneously reducing the transmit power [12, 13]. As a result, massive MIMO is regarded as a candidate technique for next-generation wireless communications systems conceived for the sake of improving both their BE and EE.

As the down tilt of an Antenna Array (AA) is fixed, traditional MIMO technology can only adjust signal transmission in the horizontal dimension. In order to exploit the vertical dimension of signal propagation, AAs, such as rectangular, spherical and cylindrical AAs, were studied by the 3rd Generation Partnership Project (3GPP) [14–16]. MIMO with these arrays can adjust both azimuth and elevation angles, and propagate signals in Three-Dimensional (3D) space, thus termed 3D MIMO. To further increase capacity, 3D MIMO deploys more antennas to achieve larger multiplexing gains. Meanwhile, massive MIMO adopts rectangular, spherical or cylindrical AAs in practical systems considering the space of AAs. Therefore, 3D MIMO with massive antennas can be seen as a practical deployment means of massive MIMO.

Massive MIMO can improve BE since it can achieve large multiplexing gains when serving tens of UEs simultaneously [11, 17]. The significant increase in EE is due to the fact that the use of more antennas helps focus energy with an extremely narrow beam on small regions where the UEs are located [18]. Apart from these advantages, massive MIMO can enhance transmission reliability owing to the excessive DoF [19]. Inter-User Interference (IUI) can also be alleviated because of the extreme narrow beam [12]. In a massive MIMO system, individual element failure of the AA is not detrimental to the performance of the entire system [12]. Simple low-complexity signal processing algorithms are capable of approximating

Table 1.1 Current research directions of massive MIMO

Topics	Description [12, 13, 22]
AA configuration	Rational antennas deployment
Channel model	Channel measurement and modeling
Channel estimation	Efficient estimation algorithms for pilot reuse
Precoding and detection	Low-complexity and efficient precoder and detector
Performance and limitation	BE, EE and reliability performance and limitation factors
Practical applications	Network deployment and optimization
Resource management	Management of frequency, time and spatial resources
Interference controlling	Pilot contamination alleviation and interference suppression
Massive distributed antennas	Design and analysis of distributed antennas in indoor or outdoor

the performance achieved by optimal methods, such as Maximum-Likelihood (ML) multiuser detection and Dirty Paper Coding (DPC) [13]. The latency of the air interface can be reduced and the protocols at the Media Access Control (MAC) layer can be simplified because of the channel harden phenomenon and sufficient capacity [20].

Certainly, the complexity of signal processing, including Transmit Precoding (TPC), channel estimation and detection, increases with the increasing number of antennas. On the other hand, the maximum number of orthogonal pilot sequences is limited by the coherence interval and coherence bandwidth. Therefore, the performance of massive MIMO systems is constrained by pilot contamination due to pilot reuse in multi-cell scenarios [11]. Moreover, compared to the Physical Downlink Shared Channel (PDSCH) employing either precoding or beamforming, the Signal-to-Interference-plus-Noise Ratio (SINR) of the Physical Broadcasting Channel (PBCH) is lower due to the omni-directional signal transmission [21].

According to the current literature related to massive MIMO, the major research directions about massive MIMO are listed in Table 1.1, some of which have been investigated in [12, 13] and [22] while others are not.

1.3 Aim of Monograph

Currently, fundamental theoretical problems and several physical-layer techniques of massive MIMO have already been widely investigated. For example, the capacity and realistic performance of precoding and detection for massive MIMO have been analyzed from the viewpoint of information theory [13, 22]. Additionally, the advantages and disadvantages, and the limitations of massive MIMO are spelt out in [12]. However, the performance of massive MIMO and its potential applications are much more influenced by practical factors, which have not been well investigated so far.

Therefore, in addition to a comprehensive investigation on the theoretical performance of massive MIMO, this monograph first pays more attention to discussing issues from the system or network point of view, such as practical application scenarios of massive MIMO, networking techniques and so on. Then, based on basic theory, two typical applications of massive MIMO, i.e., mm-wave communication networks and wireless energy transfer networks, are discussed in detail. In massive MIMO-aided mm-wave communication networks for 5G communications, both the physical-layer and networking-layer techniques are discussed and designed. However, in massive MIMO-aided wireless energy transfer networks for future true wireless communications, cooperative resource allocation is emphasized in an effort to improve energy transfer efficiency.

References

1. W. Xiang, K. Zheng, X. Shen, *5G Mobile Communications* (Springer, New York, 2017)
2. K. Zheng, L. Zhang, W. Xiang, W. Wang, *Heterogeneous Vehicular Networks* (Springer, New York, 2016)
3. Z. Hasan, H. Boostanimehr, V.K. Bhargava, Green cellular networks: a survey, some research issues and challenges. IEEE Commun. Surveys Tutor. **13**(4), 524–540 (2011)
4. D. Feng, C. Jiang, G. Lim, L. Cimini Jr., G. Feng, G. Li, A survey of energy-efficient wireless communications. IEEE Commun. Surveys Tutor. **15**(1), 167–168 (2012)
5. Y. Chen, S. Zhang, S. Xu, G.Y. Li, Fundamental trade-offs on green wireless networks. IEEE Commun. Mag. **49**(6), 30–37 (2011)
6. G.Y. Li, Z. Xu, C. Xiong, C. Yang, S. Zhang, Y. Chen, S. Xu, Energy-efficient wireless communications: tutorial, survey, and open issues. IEEE Wirel. Commun. **18**(6), 28–35 (2011)
7. G. Auer, V. Giannini, C. Desset, I. Godor, P. Skillermark, M. Olsson, M.A. Imran, D. Sabella, M.J. Gonzalez, O. Blume, How much energy is needed to run a wireless network? IEEE Wirel. Commun. **18**(5), 40–49 (2011)
8. T. Kailath, A.J. Paulraj, Increasing capacity in wireless broadcast systems using distributed transmission/directional reception (DTDR), US Patent 5,345,599, Sept 1994
9. G. Golden, C. Foschini, R. Valenzuela, P. Wolniansky, Detection algorithm and initial laboratory results using V-BLAST space-time communication architecture. Electron. Lett. **35**(1), 14–16 (1999)
10. A. Ghrayeb, T.M. Duman, *Coding for MIMO Communication System* (Wiley, New York, 2007)
11. T. Marzetta, Noncooperative cellular wireless with unlimited numbers of base station antennas. IEEE Trans. Wirel. Commun. **9**(11), 3590–3600 (2010)
12. E.G. Larsson, F. Tufvesson, O. Edfors, T.L. Marzetta, Massive MIMO for next generation wireless systems. IEEE Commun. Mag. **52**(2), 186–195 (2014)
13. F. Rusek, D. Persson, B.K. Lau, E. Larsson, T. Marzetta, O. Edfors, F. Tufvesson, Scaling up MIMO: opportunities and challenges with very large arrays. IEEE Signal Process. Mag. **30**(1), 40–60 (2013)
14. DoCoMo, Requirements, candidate solutions & technology roadmap for LTE R12 onward, 3GPP RWS-120010 (June 2012)
15. Samsung, Technologies for Rel-12 and onward, 3GPP RWS-120021 (Nov 2013)
16. HUAWEI and HiSilicon, Views on Rel-12 and onwards for LTE and UMTS, 3GPP RWS-120006 (2013)
17. J. Hoydis, S. ten Brink, M. Debbah, Massive MIMO in the UL/DL of cellular networks: how many antennas do we need? IEEE J. Sel. Areas Commun. **31**(2), 160–171 (2013)

18. H.Q. Ngo, E. Larsson, T. Marzetta, Energy and spectral efficiency of very large multiuser MIMO systems. IEEE Trans. Commun. **61**(4), 1436–1449 (2013)
19. L. Zhao, K. Zheng, H. Long, H. Zhao, Performance analysis for downlink massive MIMO system with ZF precoding. Trans. Emerg. Telecommun. Technol. **25**, 1219–1230 (2014)
20. B. Hochwald, T. Marzetta, V. Tarokh, Multiple-antenna channel hardening and its implications for rate feedback and scheduling. IEEE Trans. Inf. Theory **50**(9), 1893–1909 (2004)
21. I.C. Lin, C. Rowell, S. Han, Z. Xu, G. Li, Z. Pan, Toward green and soft: a 5G perspective. IEEE Commun. Mag. **52**(2), 66–73 (2014)
22. L. Lu, G. Li, A. Swindlehurst, A. Ashikhmin, R. Zhang, An overview of massive MIMO: benefits and challenges. IEEE J. Sel. Topics Signal Process. **8**(5), 742–758 (2014)

Chapter 2
Massive MIMO Technology

The escalating tele-traffic growth imposed by the proliferation of smart-phones and tablet computers outstrips the capacity increase of wireless communications networks. Furthermore, it results in substantially increased carbon dioxide emissions. As a powerful countermeasure, in the case of full-rank channel matrices, MIMO techniques are potentially capable of linearly increasing the capacity or decreasing the transmit power upon commensurately increasing the number of antennas. Hence, the concept of massive MIMO systems has attracted substantial research attention and been regarded as a promising technique for next-generation wireless communications networks. Therefore, this chapter surveys the state-of-the-art of massive MIMO systems. Firstly, some typical application scenarios are classified and analyzed. Then, key techniques of both the physical layer and network layer are also detailed. Finally, we conclude this chapter.

2.1 Main Application Scenarios

This section presents a set of application scenarios, which capture the major dynamics that are of interest in massive MIMO systems. As an essential step of the study, the definition of application scenarios may present a guide for developing key techniques. As shown in Table 2.1, all of these scenarios under different network deployments can be roughly classified into two types, i.e., *Case 1* Homogeneous Network (HomoNet) with only macro-cell deployment and *Case 2* Heterogeneous Network (HetNet) with both macro-cell and small cells. Next, more details of these scenarios are discussed.

L. Zhao et al., *Massive MIMO in 5G Networks: Selected Applications*,
SpringerBriefs in Electrical and Computer Engineering,
https://doi.org/10.1007/978-3-319-68409-3_2

Table 2.1 Typical application scenarios

	Type	Description	Feature
HomoNet	Case 1A	Multi-layer sectorization	Easy to implement High multiplexing gains
	Case 1B	Adaptive beamforming	Narrow beam and little interference Flexible with elevation and azimuth
	Case 1C	Large-scale cooperation	Coverage enhancement Efficient cooperation
HetNet	Case 2A	Wireless backhaul	Low infrastructure costs Flexible and extendible
	Case 2B	Hotspot coverage	High throughput Superior elevation resolution
	Case 2C	Dynamic cell	Adjusting cell adaptively Balancing network load

2.1.1 Homogeneous Network Scenarios

2.1.1.1 Multi-Layer Sectorization

Upon increasing the number of UEs and their carried tele-traffic in urban environments, increased system capacity is required for supporting customer requirements. Traditionally, sectorization techniques are used for providing services to a growing population, which simply divide a cell into multiple sectors, thus increasing network capacity. The equipment costs can also be reduced by allowing a single eNB to serve either three 120^{o} sectors or six 60^{o} sectors. However, although sectorization is capable of improving the area BE, this benefit comes at the expense of a potentially increased interference among sectors due to non-ideal sector-antenna patterns. Therefore, more efficient techniques are required to further increase the achievable network capacity.

As illustrated in Fig. 2.1, accurate sectorization in massive MIMO systems can be achieved by high-selectivity angular beamforming performed horizontally, which is capable of reducing the interference among sectors. Moreover, the coverage of each beam can be changed by adjusting the elevation angle of 3D beamforming. By this way, a conventional fixed sector can be further spitted into inner and outer sectors, each of which can be served by a 3D Beamformer (BF) with the same horizontal but different elevation angles. The same frequency radio resources are reused by all the sectors, which is capable of significantly increasing the number of UEs served and/ or of improving the network's throughput.

2.1.1.2 Adaptive Beamforming

Fixed BFs are so called because the weights that multiply the signals at each element of the AA remain unchanged during operation. By contrast, the weights

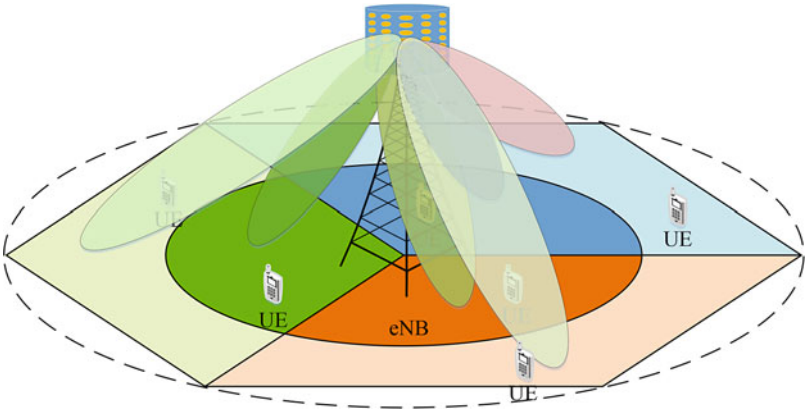

Fig. 2.1 Illustration of multi-layer sectorization

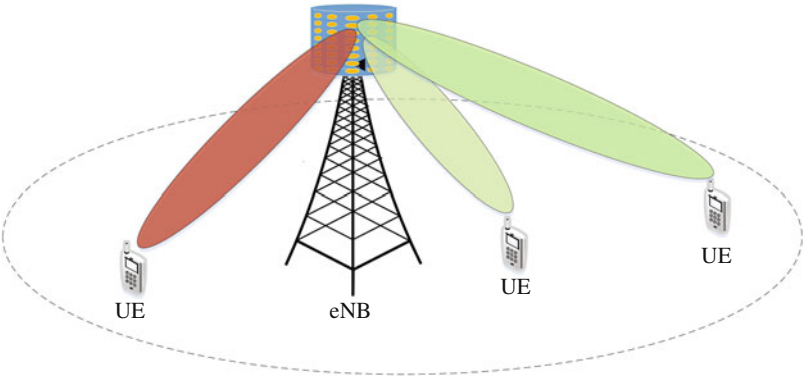

Fig. 2.2 Illustration of adaptive beamforming

of an adaptive BF are continuously updated based on the received signals in order to suppress spatial interference, e.g., as depicted in Fig. 2.2. This process may be carried out in either the Time-Domain (TD) or Frequency Domain (FD). Compared to the Two-Dimensional (2D) adaptive BF, a 3D BF may have more flexibility in reusing the radio resources in the spatial domain.

2.1.1.3 Large-Scale Cooperation

Most of the existing contributions on massive MIMO show different benefits in a co-located deployment scenario, where there is a large number of antennas installed at a single cell cite. However, such co-located deployments impose challenges both on their hardware design and on their field deployment. On the other hand, Distributed Antenna Systems (DASs) associated with spatially separated antennas have been conceived for improving the indoor coverage using a moderate number of antennas [1]. Recent studies have shown that apart from its improved

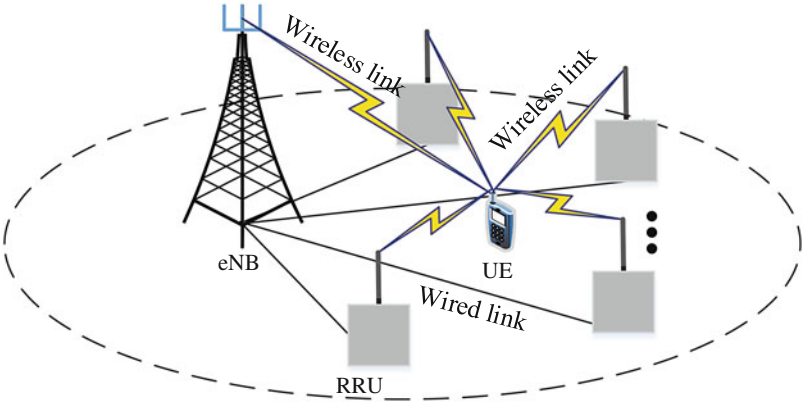

Fig. 2.3 Illustration of large-scale cooperation

coverage, a DAS is capable of significantly increasing the network's BE, even in the presence of Inter-cell Interference (ICI) [2]. This motivates researchers to identify specific scenarios as illustrated in Fig. 2.3, where the massive MIMO system associated with a distributed architecture outperforms the one relying on a co-located deployment [3, 4].

The advantage of distributed massive MIMO is plausible, because the signals arriving from the distributed antennas to each UE are subject to independent random levels of large-scale fading, thereby leading to potential capacity gains over their co-located counterpart [5]. However, it may be a challenge to achieve these gains by coordinating the intra-cell interferences, especially in scenarios having dozens or even hundreds of Remote Radio Units (RRUs) in a cell. Although full cooperation constitutes an efficient method of eliminating the intra-cell interference, it is not practical due to its high reliance on full Channel State Information (CSI) sharing. To strike an elegant trade-off between the performance attained and the overhead imposed, efficient large-scale cooperation schemes are of high importance under this scenario.

Moreover, distributed massive MIMO and small cell deployments may be viewed as being complementary rather than competitive. For example, a cooperative cellular architecture composed of a DAS and a femtocell-macrocell underlay system is proposed in [5], which may be extended to operate in conjunction with distributed massive MIMO.

2.1.2 Heterogeneous Network Scenarios

2.1.2.1 Wireless Backhaul

The HetNet with dense small cells has been regarded as a very promising design architecture in terms of energy and area BE. It typically consists of multiple types

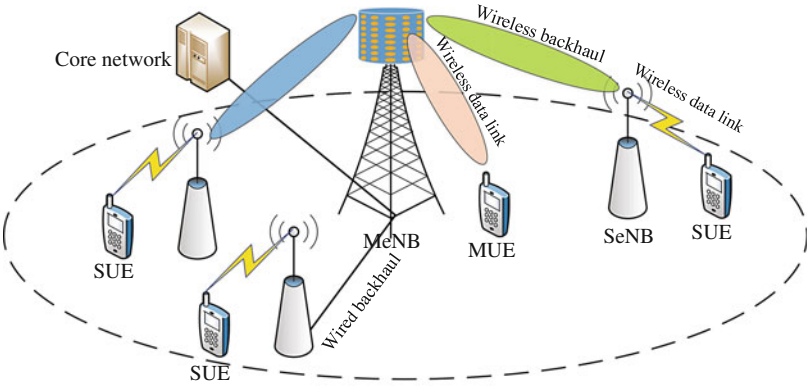

Fig. 2.4 Illustration of wireless backhaul

of radio access nodes, e.g., a Macro-cell eNB (MeNB) and multiple Small-cell eNBs (SeNBs) such as pico, femto and relay eNBs. All SeNBs need to be connected to their donor MeNBs through a wired or wireless backhaul. Generally, the wireless backhaul is preferred to instead of the wired backhaul because of easy deployment. In this scenario, a massive MIMO is used at the MeNB, which has a high DoF so to support multiple wireless backhauls in the HetNet [6].

As illustrated in Fig. 2.4, the same spectrum may be reused among wireless backhauls, access of Macro-cell UEs (MUEs) and Small-cell UEs (SUEs). In other words, SeNBs can be viewed as a special kind of UEs communicating with the MeNB via the wireless backhaul. Since the location of an eNB is usually fixed, the channel of the wireless backhaul may be quasi-static time varying. Therefore, the MeNB is capable of eliminating the interference between the wireless backhaul and MUEs through the use of precoding.

2.1.2.2 Hotspot Coverage

Statistics show that the majority of tele-traffic originates from buildings, such as super-markets, office buildings, gymnasiums and so on [7]. Therefore, high quality indoor coverage of buildings is considered as one of the key scenarios for the HetNet. Since the tele-traffic is generated at different heights in buildings, traditional AAs with a fixed Downlink (DL) tilt, which are mainly designed for UEs roaming at the street level, are no longer suitable for this scenario. A massive AA is capable of dynamically adjusting both the azimuth and elevation angles of its beam. It can transmit the beams directly to the UEs at different floors in a building, and thus significantly improves system throughput [8]. However, when the indoor coverage of the building is provided by the MeNB with a massive AA, the adjustable range of the elevation angles remains small compared to that of the SeNB, and the angular resolution cannot meet the needs of UEs, as shown in Fig. 2.5. As it is

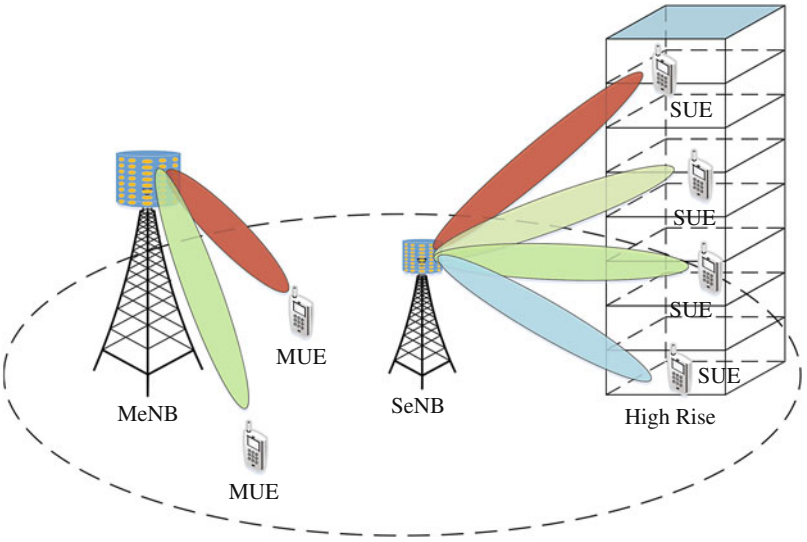

Fig. 2.5 Illustration of hotspot coverage

well known, the close distance between SeNBs and SUEs results in reduced path losses. Therefore, the SeNBs equipped with a massive AA are more appropriate for in-building coverage, providing that deployment costs are acceptable.

2.1.2.3 Dynamic Cell

Since the Reference Signal Received Power (RSRP) gleaned from the MeNB is usually higher than that from the SeNB in HetNets, more UEs are likely to be connected to the MeNB, leading to a potential unbalanced traffic distribution between the macrocell and small cells. The Cell Range Extension (CRE) technique may be used for offloading the traffic from the macro-cells to small cells [9]. However, the UEs in the extended range, which are somehow forced to access to the small cells, may experience low SINRs due to the strong interference encountering from the MeNB. This may cause the unreliable communications between them and SeNBs. In order to solve this problem, the Almost Blank Subframe (ABS) technique can be applied to reduce the interference from the MeNB through time domain coordination [10]. In other words, the Quality of Service (QoS) performances of SUEs in the extended range is improved at the expense of multiplexing gains.

With the introduction of massive AAs into SeNBs, the down tilt of the transmit signals is adjustable achieve a better received signal quality at SUEs. As illustrated in Fig. 2.6, it is helpful in adaptively expanding or shrinking the radius of small cells, i.e., *Dynamic cell*. Therefore, the UEs at the edge of the small cell may opt for adaptively connecting to the SeNB according to their received power level. It is appropriate for balancing the traffic between the macro-cell and small cells in the extended range [8, 11].

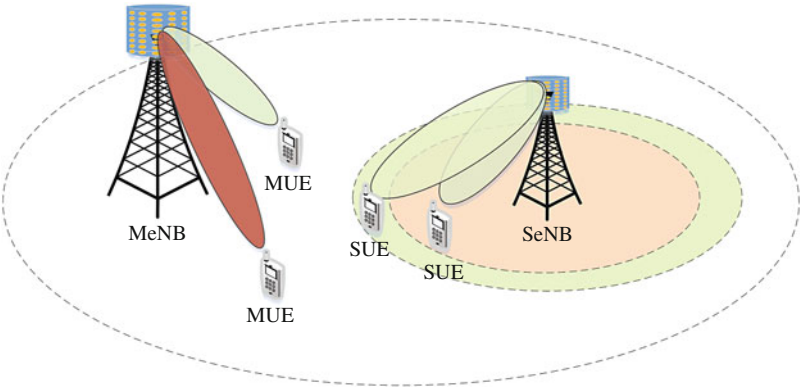

Fig. 2.6 Illustration on dynamic cell

In this section, typical application scenarios of massive MIMO are classified into two types, i.e., homogeneous and heterogeneous networks with massive MIMO. The former is with only macro-cell deployment, which includes multi-layer sectorization, adaptive beamforming and large-scale cooperation. Multi-layer sectorization is capable of increasing multiplexing gains through splitting the sectors. Adaptive beamforming focuses the radiated energy in the desired direction with the aid of an extremely narrow beam, which is able to improve the desired SINR of the UE, whilst simultaneously reducing the interference imposed on other UEs. Compared to the conventional DAS technique, large-scale cooperation, through scaling up the number of distributed antennas that are coordinated, is capable of further enhancing both coverage and achievable throughput.

There are three typical application scenarios in the case of the HomoNet with massive MIMO. Firstly, the employment of a wireless backhaul by massive MIMO between MeNB and SeNBs is more flexible and of low cost compared to its wired backhaul counterpart. Then, the SeNB with a massive AA is able to adaptively adjust both the azimuth and elevation angles in an effort to improve the coverage of indoor hotspots, e.g., in buildings. Moreover, the cell radius in HetNet is dynamically adjustable so as balance the load between MeNB and SeNBs by changing the elevation angle.

Based upon the above discussions, massive MIMO is expected to be applied in numerous scenarios to improve achievable capacity and throughput. However, extensive studies are still needed in practical network deployment.

2.2 Physical Layer Technology

When an eNB equipped with N antennas serves K ($\ll N$) single-antenna aided UEs in a single-cell environment, the performance bound of massive MIMO can be readily derived by means of information theory. The attainable multiplexing gain

equals the number of receive antennas K, and the array gain is proportional to the number of transmit antennas N [12]. However, in a practical system the realistically achievable sum rates depend on the associated coding, modulation and precoding arrangements. As massive MIMO constitutes an emerging technology, the physical layer techniques conceived for massive MIMO systems focus primarily on either TPC or on sophisticated detection arrangements [12]. Therefore, the performance of diverse massive MIMO relying on different TPCs or detectors and operating in both single-cell and multi-cell environments is discussed in this section. Both the associated theoretical and measured results indicate that the employment of simple linear TPC and detectors achieves almost the same performance as that of high-complexity non-linear TPC and detectors, at least in the single-cell scenario. Pilot contamination is the primary performance limiting factor of massive MIMO, when linear channel estimation algorithms are adopted in the multi-cell environment. Hence, solutions capable of tackling pilot contamination are also discussed. Finally, a range of non-ideal factors degrading the performance of massive MIMO are addressed.

2.2.1 Precoders/Detectors in Single-Cell Environments

2.2.1.1 Theoretical Performance

Employing the Correlation-based stochastic model (CBSM), including both the Independent and Identically Distributed (i.i.d.) Rayleigh channel model and correlated Rayleigh channel model, the performance of different TPCs or detectors designed for massive MIMO has been widely analyzed in single-cell environments [12–15], etc.

(a) i.i.d. Rayleigh channel

- **Linear precoder/detector:** When employing a linear detector, the BE performance lower bounds of the Uplink (UL) of massive MIMO systems have been studied both with perfect CSI and with the aid of realistically estimated CSI [13]. A Maximum Ratio Combining (MRC) receiver performs worse than its Zero-Forcing (ZF) and Minimum Mean Square Error (MMSE) criterion based counterparts in the high Signal-to-Noise Ratio (SNR) region [13]. However, when the SNR is low, the MRC detector outperforms the ZF and MMSE detectors, since the IUI imposed by the MRC detector falls bellow the noise level [13]. Moreover, the radiated power of the UE can be made inversely proportional to the number of Antenna Elements (AEs) at the eNB under the idealized conditions of having perfect CSI. However, in the presence of realistically estimated CSI, it is only inversely proportional to the square-root of the number of AEs [13]. The relationship between the radiated EE and BE has also been investigated. Upon increasing the BE, the EE of MRC is initially better, but beyond a crossover point it becomes worse than that of ZF [13].

Similar to [13], the BE and radiated EE recorded for the DL of massive MIMO systems are also evaluated by considering both the realistically estimated CSI and the CSI overhead imposed by the pilots [14]. The lower bounds of BE and the optimal number of UEs supported are studied for both the Maximum Ratio Transmission (MRT) based TPC as well as for ZF TPC. Based on the lower bound, the radiated EE as a function of the BE is quantified [14], which is found to be a monotonically decreasing function of the BE for both detectors. Upon increasing the BE, the EE of MRT is initially better than that of ZF, and then the opposite trend holds. In the high-EE regime, the total computational complexity of the MRT TPC may be higher than that of the ZF TPC, since its optimal number of UEs is higher. However, it may still be preferable to ZF, since MRT TPCs can be realized with the aid of a de-centralized architecture [16].

- **Non-linear precoder**: Apart from the above-mentioned linear TPCs, non-linear TPCs, such as the DPC [17], the Vector Perturbation (VP) [18] and the lattice-aided TPC methods [19] are also investigated and compared to linear precoders for transmission over the i.i.d. Rayleigh channel [12]. The performance of the ZF TPC is shown to approach that of the DPC TPC, when the number of AEs increases. Similarly, diverse non-linear detectors, such as the MMSE based Soft Interference Cancellation (MMSE-SIC) scheme [20], the Block-Iterative Generalized Decision Feedback Equalizer (BI-GDFE) [21], Tabu Search (TS) [22] and the Maximum Posterior Probability (MAP) algorithm are also evaluated in terms of the Bit Error Ratio (BER) versus complexity [12].

  Moreover, the so-called per-antenna Constant Envelope Precoding (CEP) technique implemented with the aid of a sub-optimal algorithm is also invoked for the DL of massive MIMO systems in an attempt to improve the efficiency of their Power Amplifiers (PAs) [23]. It is stated in [23] that an eNB relying on CEP needs about 4 dB lower transmit power than a conventional technique having a high Peak to Average Power Ratio (PAPR), which is an explicit benefit of using an efficient PA.

(b) Correlated Rayleigh channel

When considering both a realistic Doppler-induced correlation and imperfect CSI, the sum rates of the ZF and Regularized ZF (RZF) [24] TPCs were studied in the DL of a massive MIMO system in [25]. Since the sum rate of ZF precoding first increases and then decreases with the number of UEs, hence the optimal number of UEs is obtained in [25]. Similarly, the optimal parameters of the RZF TPC may be determined by finding the optimal sum rate. Moreover, the optimal power allocation scheme of both ZF and RZF TPCs, as well as the optimal amount of feedback required in Frequency Division Duplex (FDD) / Time-Division Duplex (TDD) systems are also determined in [25] for massive MIMO systems.

Both the ZF and Correlation Rotation (CR) aided TPC techniques in [26] are evaluated in terms of both the BE and the Symbol Error Ratio (SER), considering the effects of both transmit correlation as well as mutual coupling [15, 26]. According

to the approximate lower bounds and to the simulation results characterizing both TPCs, CR-aided precoding outperforms ZF precoding. Upon increasing the number of AEs within a given antenna dimension, the increased transmit diversity achieved dominates the attainable performance, rather than the reduction in spatial diversity imposed by shrinking the spacing among the antennas.

2.2.1.2 Measurement Performance

All the above-mentioned results are based on the use of theoretical channel models, such as the i.i.d. Rayleigh and correlated channel models. However, there exist some differences between the theoretical channel models and their practical counterparts. Therefore, the performances of different TPCs are also measured in practice.

- **Effects of correlation [27, 28]:** Both the theoretical and realistic sum-rates versus the SNRs of the DPC, RZF and MRT precoders are measured, when the eNB employs a 112-element AA in an outdoor scenario [28]. The theoretical performance bound can be derived, despite significant differences between the i.i.d. Rayleigh channel model and the realistic channel. The correlation amongst the Channel Impulse Responses (CIRs) of the different UEs decreases upon increasing the number of AEs employed at the eNB, because larger AAs are capable of resolving smaller Azimuth of Arrival (AoA) and CIR differences amongst their channels. Furthermore, when encountering different channel correlations amongst the UE channels, the measured and theoretical sum-rates of the DPC, ZF and RZF TPCs are compared in conjunction with an eNB equipped with a 128-antenna indoor cylindrical array operated in residential areas [27]. Upon increasing the number of antennas at the eNB, the channel correlation decreases, and the measured sum-rates approach their theoretical limits. When the eNB employs 20 antennas, about 98% of the sum-rate of the ideal DPC scheme is achieved for a pair of single-antenna aided UEs by the ZF or RZF TPCs [27].
- **Effects of the propagation environment [29]:** Considering realistic environments, both a 128-antenna cylindrical and a linear array are employed at the eNB [29]. Then, their realistic sum-rates are compared for both DPC and ZF TPC to the theoretical sum-rates in the i.i.d. Rayleigh channel [29]. Even for the worst combination of the cylindrical array and a dense population supported in a Line of Sight (LoS) environment, ZF precoding is capable of achieving about 55% of the DPC scheme's sum-rate in the i.i.d. Rayleigh channel, when the number of antennas exceeded 40. By contrast, in a Non Line of Sight (NLoS) environment, despite encountering a dense user population, both cylindrical and linear arrays relying on ZF TPC are capable of attaining about 80–90% of the sum-rate of the DPC scheme. Regardless of the propagation environment, most of the theoretical sum-rate of massive MIMO is achievable by linear precoding, if the eNB employs a sufficiently high number of antennas [29].

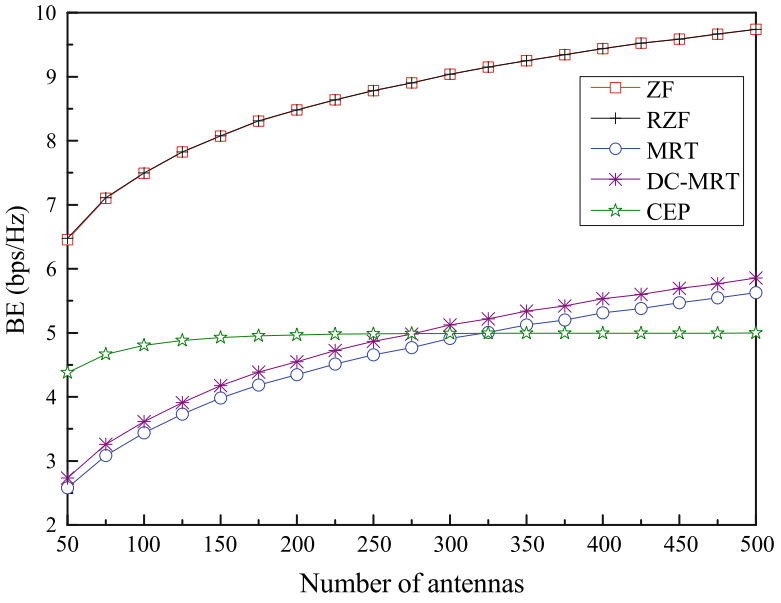

Fig. 2.7 BE of single UE versus the number of antennas in single cell scenario

- **Real time operation [16]:** To implement real-time MRT based TPC, de-centralized MRT precoding weights can be locally calculated at each antenna [16]. A prototype using a 64-antenna rectangular array is employed in [16] for simultaneously serving 15 UEs. The sum-rate of de-centralized MRT precoding is similar to that of traditional MRT precoding. Adopting 64 antennas was shown to achieve 6.7-fold sum-rate gains, while consuming only 1/64 of the transmit power compared to a single antenna [16].

2.2.1.3 Simulation Results

The quantitative results of several linear precoders are illustrated in Figs. 2.7 and 2.8. Unless otherwise specified, the default simulation configurations in this survey are as follows: (a) The number of transmit antennas is 128; (b) Equal power allocation is applied to 10 UEs; (c) The system bandwidth is 20 MHz; (d) The large-scale fading of signal propagation is modeled as $PL[\text{dB}] = 128 + 37\log_{10}d$, where d is the distance between the eNB and the given UE in kilometers, the log-normal shadow fading is also considered with the standard variance of 8 dB, and the i.i.d. Rayleigh channel is assumed for the small-scale fading; (e) The transmit power at the eNB is 14 dBm and the noise power spectral density is -174 dBm/Hz; (f) In the single-cell scenario, apart from the inner circle associated with a radius of 10 m, the UEs are uniformly distributed in hexagonal cells, whose Inter-Site Distance (ISD) is 500 m.

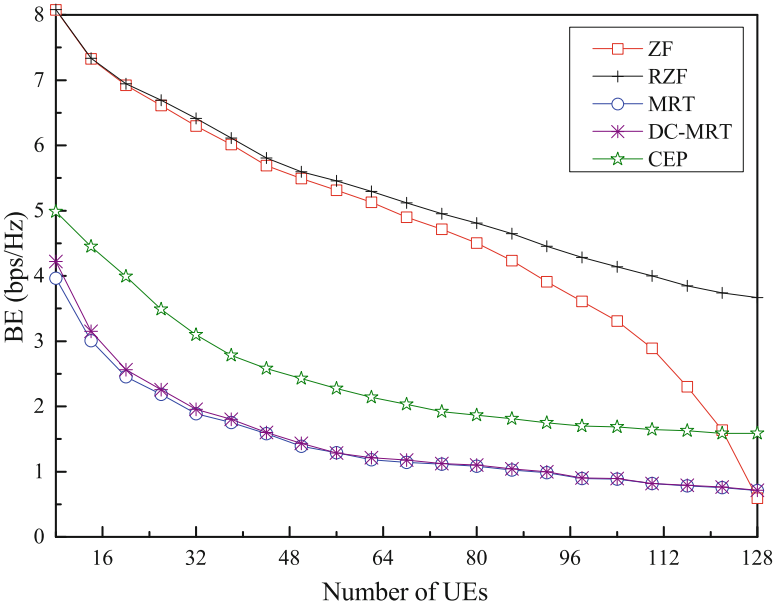

Fig. 2.8 BE of single UE versus the number of UEs in single cell scenario

As there is no performance difference between the CR precoder and the ZF precoder for transmission over the i.i.d. Rayleigh channel, only one of them has to be discussed, say the ZF precoder. As shown in Fig. 2.7, the BE per UE is improved upon increasing the number of antennas at the eNB. However, the gains of the different precoders are not the same for different numbers of antennas. On the other hand, when multiplexing a large number of UEs in the system equipped with a given number of antennas, say 128, the average array gain of each UE is reduced, which impairs the BE in Fig. 2.8. However, the total BE of all UEs is increased as a benefit of the multiplexing gains.

The properties of a variety of massive MIMO precoders and detectors operating in single-cell environments are summarized in Table 2.2. Generally, the precoders or detectors associated with a higher complexity offer an improved BE performance. Deploying more number of antennas at the eNB is capable of improving both the BE and EE. The performance of linear precoders or detectors is capable of approximating those of the high-complexity non-linear precoders or detectors. Precoders operating in realistic channels are capable of achieving a BE close to that estimated for idealized theoretical channel models. Assuming ideal CSI or estimated CSI, the transmit power of each antenna can be made inversely proportional to the number of AEs or to the square-root of the number of AEs deployed at the eNB, respectively.

Table 2.2 Precoding and detection performance of massive MIMO in single-cell

	Abbreviation	Full name	Complexity	Metrics
Precoder	– [16]	De-centralized MRT	Low	BE
	MRT [14, 16, 28]	Maximum ratio transmission	Low	BE, EE
	ZF [14, 25, 27, 29]	Zero forcing	Medium	BE, EE, SER
	RZF [25, 27, 28]	Regularized zero forcing	Medium	BE
	CR [15, 26]	Correlation rotation precoding	Medium	BE, SER
	CEP [23]	Constant envelope precoding	Medium	BE, PAPR
	DPC [12, 27–29]	Dirty paper coding	High	BE
Detector	MRC [13]	Maximum ratio combination	Low	BE, EE
	ZF [13]	Zero forcing	Medium	BE, EE
	MMSE [13]	Minimum mean-square error	Medium	BE, EE

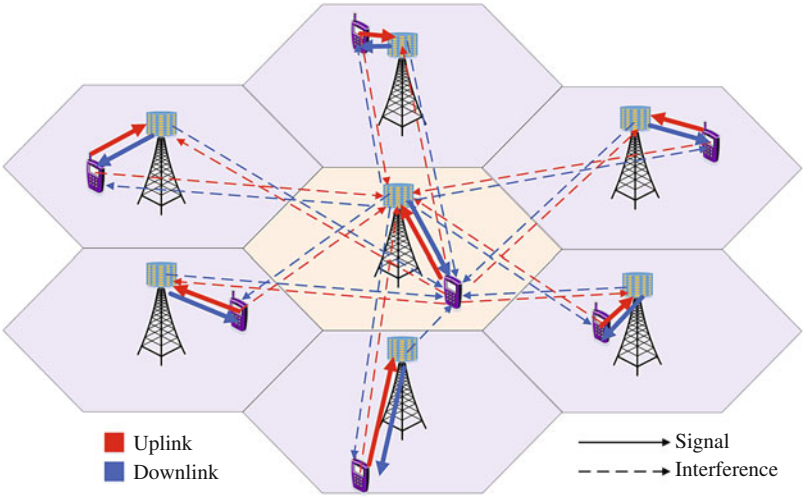

Fig. 2.9 Illustration of pilot contamination

2.2.2 Precoders/Detectors in Multi-Cell Environments

2.2.2.1 Pilot Contamination in Multi-Cell Scenarios [30–33]

This section discusses the performance of massive MIMO in non-cooperative multi-cell multi-user systems. Figure 2.9 illustrates the UL and DL interference encountered in such a multi-cell system. The affordable number of orthogonal pilots used for channel estimation is limited, because increasing the number and variety of pilots is only possible through enlarging the length of the pilot sequences, which ultimately increases the transmission overhead and/or the bandwidth. In practice the number of pilots may only be sufficient for supporting a limited number of UEs roaming in a single cell, which results in inevitable pilot reuse for the UEs

in adjacent cells. As shown in Fig. 2.9, employing the TDD mode, when the UEs of different cells send the same pilot sequence to their donor eNBs on the UL, each eNB has to rely on an interference-contaminated UL received signal, which inevitably contaminates the resultant channel estimate. Firstly, the interference-contaminated UL CSI is used for detecting the UL data. On the other hand, the DL channels may be assumed to be identical to the UL ones in the case of TDD-based reciprocity, provided that the bandwidth remains sufficiently narrow to encounter the non-frequency-selective propagation. Therefore, the UL CIR can be used by the DL transmit precoder. The precoded DL signals impinge on both the desired UEs and the UEs in other cells. Therefore, both the UL and DL sum rates are constrained by the adjacent cells interference imposed by pilot reuse. This phenomenon is known as pilot contamination and has been widely recognized as the main performance constraint of massive MIMO, as outlined below in more detail.

- **i.i.d. Rayleigh channel**: Assuming that the i.i.d. Rayleigh channel can be ideally estimated at the eNB, the performance of the ZF detector is analyzed in a UL massive MIMO system in the multi-cell scenario [32]. Both the exact closed-form and lower bound of the UL BE indicate that the system is interference-limited at high SNRs. Hence, boosting the transmit power at the UEs cannot further improve the attainable performance. The effects of interference and noise can be reduced by employing more antennas at the eNB. However, in the presence of realistically estimated CSI, the received SINRs of both the MRT precoder and of the MRC detector demonstrate that the effects of the Additive White Gaussian Noise (AWGN) and IUI disappear, and that the only remaining constraint is imposed by pilot contamination [30]. Moreover, the results in [30, 32] demonstrate that the required radiated energy per bit is reduced upon increasing the number of AEs.
- **Correlated Rayleigh channel**: Under the correlated channel model, the approximate sum rate is studied in [31], where the MRT/RZF precoder is employed for the DL or MRC/MMSE detection is adopted for the UL [31]. The BE attained depends mainly on the effective SNR as well as the DoF, which is defined as the ratio of the rank of the correlation matrix to the number of UEs. Similar conclusions in [31] can be found in [30], i.e., when the number of antennas tends to infinity, both the thermal noise and the IUI can be averaged out. Hence, pilot contamination remains the main constraint of massive MIMO, and the radiated power can be kept low. Moreover, the number of antennas required for different TPCs or detectors has to be deduced on the basis of aiming for a given percentage of the BE attained with the aid of an infinite number of antennas. The RZF/MMSE precoder/reciever is capable of achieving the same BE using a reduced number of antennas compared to the MRT/MRC schemes.
- **Dispersive multi-path channel**: The performances of both the MRC and ZF detectors are studied in the UL of a massive MIMO system in a multi-cell environment, where a dispersive multi-path channel model is assumed [33]. The lower performance bounds derived in [33] demonstrate that pilot contamination remains the dominant performance limiting factor for the massive MIMO with a

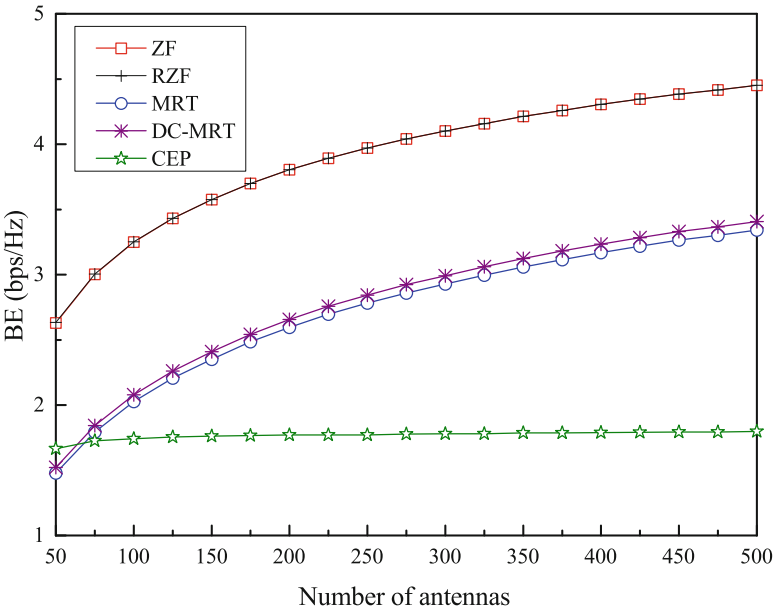

Fig. 2.10 BE of single UE versus the number of antennas over an i.i.d. Rayleigh channel in multi-cell scenario

realistic finite-dimensional channel model. The ZF receiver performs better than the MRC receiver in terms of the achievable sum-rate, when pilot contamination is not severe, and vice versa. A rich scattering propagation environment may benefit the ZF detector. However, the MRC detector performs better than ZF in poor scattering propagation environments. If the AoAs of the UEs roaming in the specific cell that uses the same pilots are not identical, pilot contamination can be completely eliminated with the aid of Bayesian channel estimation [34]. In other words, if the covariances of the desired signal and interference span different subspaces, pilot contamination can be eliminated, provided that there are an unlimited number of antennas.

In order to explicitly show the effects of pilot contamination imposed on the different precoders in the multi-cell scenario, the BE per UE under the i.i.d. Rayleigh channel is depicted in Figs. 2.10 and 2.11. The default simulation configurations are the same as those of the single-cell scenario, except that the number of cells is seven. It can be seen that the performance trends of all precoders involved in the multi-cell scenario are similar to those in the single-cell scenario. However, the BE performances are degraded due to the pilot contamination compared to those seen in single cell scenarios. Moreover, the CEP is more sensitive to pilot contamination in contrast to the other precoders.

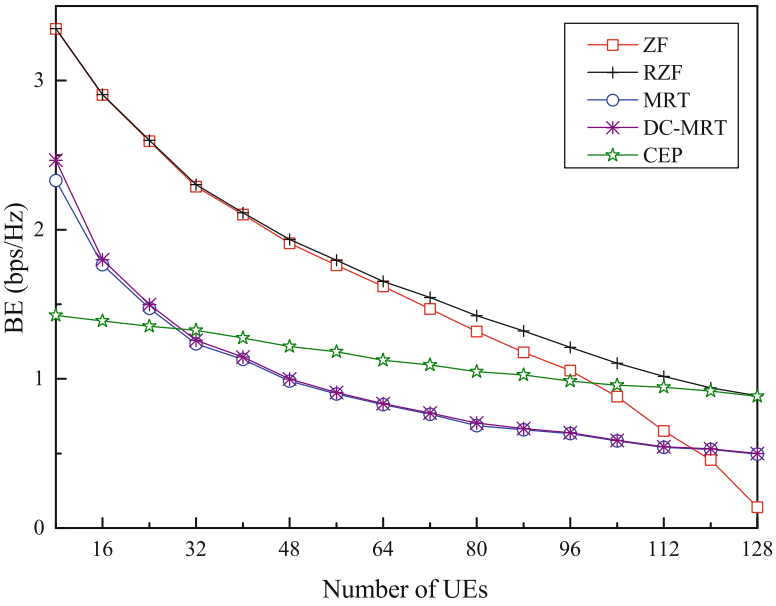

Fig. 2.11 BE of single UE versus the number of UEs over an i.i.d. Rayleigh channel in multi-cell scenario

Table 2.3 Schemes for alleviating or eliminating pilot contamination

Scheme	Channel model	Shared CSI	Shared data
Pilot design [35]	i.i.d. Rayleigh	Non	Non
Pilot allocation [36, 37]	i.i.d. Rayleigh	Overall large-scale fading	Non
	Multi-path	Overall covariances	Non
Time-shifted pilot [38]	Rice	Non	Non
Power allocation [39]		Partly large-scale fading	Non
Channel estimation [40, 41]	i.i.d. Rayleigh	Local large-scale fading	Non
Precoding [42, 43]	i.i.d. Rayleigh	Overall large-scale fading	Overall
	i.i.d. Rayleigh	Estimated channels	Non

2.2.2.2 Remedies of Pilot Contamination

As discussed before, when realistic imperfect CSI is acquired at the eNB, the pilot contamination caused by pilot reuse in multi-cell scenarios imposes the ultimate limitation on the attainable performance of massive MIMO. This subsection studies the main techniques of eliminating or at least alleviating pilot contamination. As concluded in Table 2.3, the main counter-measures can be classified as follows.

- **Pilot design**: When the classic Matched Filter (MF) is invoked for estimating the UL channel through the use of UL pilots in the i.i.d. Rayleigh channel, a specific pilot design criterion, aiming to minimize the inner product of the

pilots for different cells is proposed in [35] for mitigating pilot contamination. Based on this criterion, Chu-sequence-based pilots are designed, which makes the pilots for the UEs in the same cell orthogonal, and reuses the same pilots in the neighbouring cells after suboptimal phase shifts. Therefore, the accuracy of the estimated channels can be substantially improved and pilot contamination can be beneficially mitigated.

- **Pilot allocation**: When the eNB employs an MMSE channel estimator in the i.i.d. Rayleigh channel, pilot contamination is proved to also be the dominant constraint of BE even with the assistance of multi-cell MMSE TPC [36]. However, if we allow the UEs benefitting from low ICI to reuse the same pilots, pilot contamination may be mitigated and substantial BE improvements can be achieved [36].

  In [34, 37], a Bayesian channel estimator is first developed for the UL channel in the multi-cell scenario. Then, it is shown that pilot contamination is commensurately reduced, when using more antennas at the eNB, provided that the covariances of the desired signal and interference span different subspaces. Furthermore, a pilot allocation scheme is proposed for suppressing the pilot contamination by carefully shaping the covariance in order to satisfy this condition.
- **Frame structure**: A time-shifted frame structure is designed in [38] for mitigating pilot contamination based on MF-assisted channel estimation. In this scheme, all the cells are divided into different groups, which transmit their UL pilots in different time slots. When a specific group transmits its UL pilots, the other groups transmit their DL data. An example of the frame structure of three groups is depicted in Fig. 2.12. The theoretical proof provided in [38] shows that the ICI imposed by the different groups is gradually mitigated upon employing more antennas at the eNB. In order to efficiently suppress the ICI arriving from the inner group, optimum power allocation may be employed according to the specific received SINRs on both the UL and DL [38, 39].
- **Channel estimation**: Taking advantage of the asymptotic orthogonality of different UE channels in the i.i.d. Rayleigh channel, an eigenvalue-decomposition-based approach is proposed in [40] to improve the channel estimation accuracy.

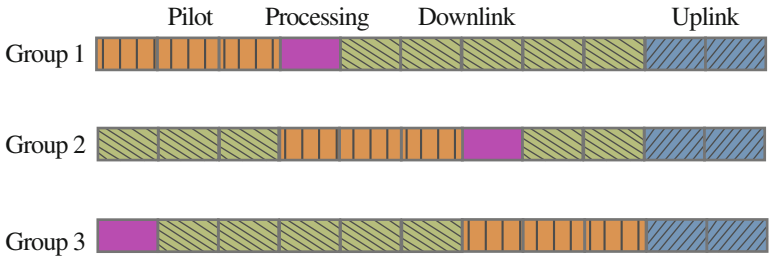

Fig. 2.12 Time-shifted frame structure with three groups [38]

Hence, the fast fading channel coefficients may be estimated with the aid of joint estimation of the channels and data by blind techniques, whilst mitigating pilot contamination [41, 44].

- **Precoding scheme**: A pilot contamination mitigating precoding scheme is designed in [42] for communicating over an i.i.d. Rayleigh channel. This two-stage precoding scheme consists of an outer multi-cell TPC arrangement based on the knowledge of large-scale fading features, and conventional inner linear TPC based on the estimated fast fading coefficients. The essential idea behind this scheme is that the eNBs linearly combine their signals intended for all the UEs by reusing the same pilots. The combined symbols are then transmitted with the aid of traditional precoding. As a result, the ICI can be completely eliminated, as shown by the theoretical derivations in [42].

  A further optimization problem is formulated in [43] to mitigate pilot contamination. The objective function used is constituted by the Mean Square Error (MSE) of the received signals of the UEs in the same cell, plus the mean-square interference power imposed on the UEs in other cells. Then, the optimal closed-form expression of precoder for this MMSE-based multi-cell precoding optimization problem is derived analytically. The proposed precoding scheme is capable of simultaneously reducing both the intra-cell and inter-cell interferences. It is implemented at each eNB without information exchange among eNBs, which has the benefit of lower overhead than the joint-multi-cell precoding in [42].

2.2.3 Non-ideal Factors Limitation of LS-MIMO

In a realistic scenario, two main types of non-ideal factors limit the attainable performance of the massive MIMO system, namely the imperfect CSI and practical hardware implementation, which are listed in Table 2.4. Naturally, realistic channel estimation is carried out at the DL receiver and its UL signalling delay results in imperfect CSI at the transmitter, whereas non-ideal hardware is attributed mainly to the deleterious effects of mutual coupling, non-linear amplification, I/Q-imbalance and phase noise, which are the widely known imperfections of practical transceivers.

Table 2.4 Non-ideal factors limiting the massive MIMO performance

Category	Non-ideal factors	Affection
Imperfect CSI	Channel estimation error [31, 42]	Pilot contamination
	Channel aging [45]	Mismatched precoding
Non-ideal hardware	Mutual coupling [46]	Energy loss
	Phase noise [47]	Phase drifts
	Amplifier non-linearities, I/Q imbalance, etc. [48]	Additive distortion noise

2.2.3.1 Imperfect CSI

- **Imperfect channel estimation**: Since in practice both the precoder and the detector have to rely on realistically estimated CSI, accurate channel estimation is vital for the performance of the massive MIMO system. Under the TDD mode, due to pilot reuse in multi-cell scenarios, the CSI obtained by linear channel estimators, such as the MMSE and MF estimators, is contaminated by interference [31, 42]. In order to eliminate or mitigate the pilot overhead, blind channel estimation is considered in [40]. Under the FDD mode, the feedback from UEs to eNBs may become overwhelming for practical systems, which can be mitigated by compressive sensing [49]. However, channel estimation for massive MIMO, such as a 100×10 element system remains a challenging problem, since the complexity of estimating or recovering 1000 channels is excessive. Therefore, non-coherent MIMO also has to be studied.
- **Channel ageing**: Adopting an autoregressive model for assessing the predictability of a realistic channel, the effect of channel ageing was investigated for massive MIMO system in [45]. Channel ageing results in a mismatch between the current channel to be encountered by the next transmission and the channel detected at the DL receiver, quantized and sent back for precoding. In order to mitigate the effects of channel ageing on the sum rate of massive MIMO, an optimal causal linear Finite Impulse Response (FIR) Wiener channel predictor is employed in [45] and as a benefit, its sum rate is substantially improved.

In a practical scenario having an imperfect CSI can be characterized for example by the correlation coefficient between the estimated CSI and the perfect CSI. At the time of writing, there are two main methods of modelling the correlation coefficient, namely the Gaussian model [50] and the Clarke model [51]. They describe the correlation coefficient as the function of Doppler frequency shift and channel delay in the form of either an exponential function or the zeroth-order Bessel function, respectively. When the correlation coefficient calculated by the Gaussian model is 0.9, the quantitative performances of the different linear precoders are shown in Figs. 2.13 and 2.14. As expected, the BE is reduced due to the inaccurate CSI compared to that seen in single cell scenarios. Therefore, advanced techniques are required for mitigating the effects of imperfect CSI.

2.2.3.2 Non-ideal Hardware

- **Mutual coupling**: Upon increasing the number of antennas at the eNB, either the spacing between the AEs is reduced, or alternatively, if the spacing is fixed, then the total AA dimension is increased. Having a reduced AE spacing leads to increased mutual coupling, which impairs the performance of massive MIMO. In order to mitigate the effects of mutual coupling, sophisticated radio-frequency matching techniques have to be employed between the AA and the radio-frequency chain. In [46], the optimal matching network is designed for circular arrays, which substantially improves attainable system capacity.

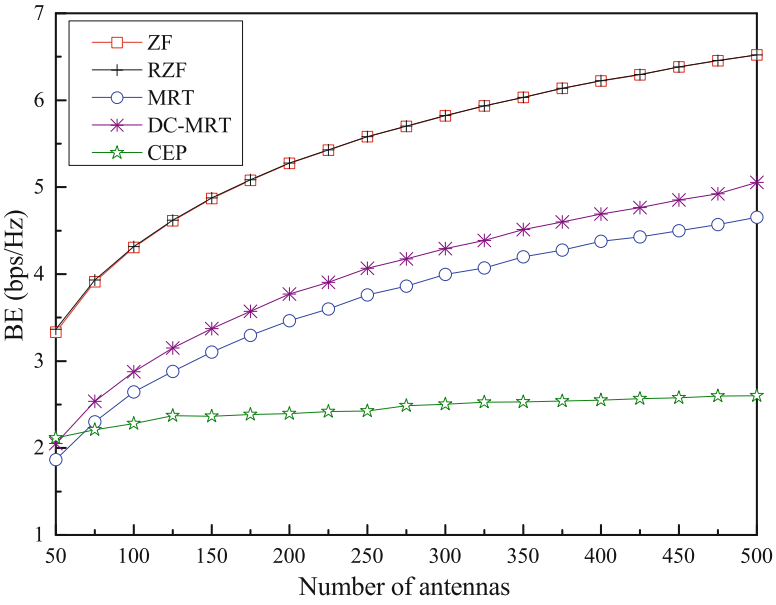

Fig. 2.13 BE of single UE versus the number of antennas with imperfect CSI in single cell scenario

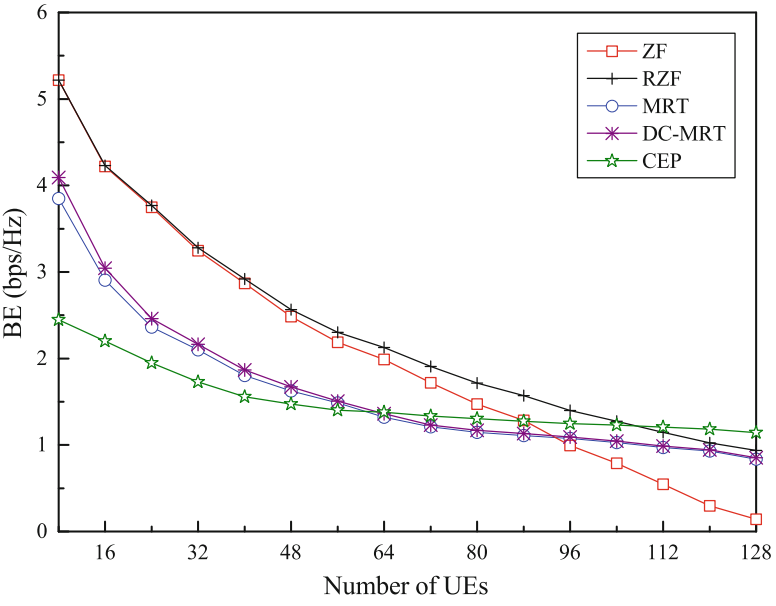

Fig. 2.14 BE of single UE versus the number of UEs with imperfect CSI in single cell scenario

- **Phase noise**: The phase noise is caused mainly by the up-conversion stage used at the transmitter and by the down-conversion circuit of the receiver. When considering the UL of a massive MIMO system, the phase noise of the UE transmitter is independent of the phase noise of all other non-cooperative UEs. By contrast, the phase noise of different antennas at the eNB is dependent on whether a single-oscillator centralized eNB or a distinct-oscillator based distributed eNB is considered. When adopting MRC detection, the lower bounds of the sum-rate found for both type of solutions suggest that the achievable array gain is proportional to the square-root of the number of antennas [47]. Due to the progressive phase noise drift at the oscillators, there exists a fundamental trade-off between the time interval used for data transmission and the sum-rate. This trade-off offers an insight into the impact of transmission parameters.
- **Additive distortion of the baseband**: The amplifier non-linearity, the I/Q imbalance and phase noise, as well as the additive distortion terms encountered at the transceivers of both the eNB and UEs were introduced into the system model in [48]. Both the channel estimation accuracy and the sum rate of UEs are predominantly limited by the distortion encountered by the UEs, not by the eNBs. Both the impact of the distortion imposed on the eNB and pilot contamination were mitigated by deploying more number of antennas in [48]. Moreover, the attainable EE can be improved by employing more number of transmit antennas, while simultaneously reducing the radiated power. Therefore, the performance degradation imposed by low-cost AEs can be mitigated by increasing the number of transmit antennas.

In this section, we mainly discussed the performance of diverse TPCs and detectors for massive MIMO systems. In the single-cell scenario, low-complexity linear precoders and detectors may perform similarly to other complex precoders and detectors in terms of their sum-rate [12, 13]. The beneficial combination of TPCs and detectors lead to the achievement of a performance close to their theoretical performance under realistic channel conditions. Both the attainable BE and EE can be improved by employing more number of antennas at the eNB. When near-perfect CSI can be acquired through channel estimation with high accuracy, the radiated power can be made inversely proportional to the number of transmit antennas at the eNB [13], but only inversely proportional to the square-root of the number of antennas in the presence of realistically estimated CSI. In the multi-cell scenario, upon employing linear channel estimation with moderate complexity, pilot contamination becomes a major obstacle to improve the BE, which is due to the limited number of available pilots. Hence, diverse counter-measures have been conceived for mitigating pilot contamination [35–43], such as specially conceived pilot design [35], power allocation [39] and pilot-decontamination precoding [42]. Finally, the performance of practical massive MIMO systems is affected by numerous non-ideal factors [42–48], including imperfect CSI [42, 45] and non-ideal hardware [46–48]. As one of major research issues, the design of non-coherent blind detection or semi-blind assisted massive MIMO systems has to be explored, which is capable of dispensing much less channel estimation information.

2.3 Networking Technology

While the underlying physical layer techniques lay the foundation of massive MIMO systems, networking techniques also play a vital role in practical systems, making them operate more efficiently, reliably and securely. Due to their crucial impact on the attainable performance of massive MIMO systems, networking techniques have gradually attracted considerable interest in both academia and industry.

The effective exploitation of radio resources is one of the main goals to be achieved by networking techniques. Towards this end, several performance indicators are considered, such as the aforementioned BE and EE. Always serving UEs which are experiencing the best channel conditions is surely capable of improving the system's BE. However, this may result in unfair resource allocation, potentially disadvantaging those UEs that suffer from poor channel conditions, such as the UEs located at cell edges. Therefore, apart from BE and EE, the networking techniques usually take into account fairness in order to guarantee a certain level of minimum performance for all UEs. In the remainder of this section, we only focus our attention on two networking techniques, i.e., Inter-cell Interference Coordination (ICIC) and radio resource scheduling, which are two most important issues in wireless networks.

2.3.1 Inter-Cell Interference Coordination

Cellular communication systems suffer from ICI at the cell boundaries, especially when all the channels are fully reused in adjacent cells. As a result, interference mitigation and coordination techniques are needed for alleviating ICI so as to well support frequency reuse. Here, we focus only on static or semi-static ICIC approaches for massive MIMO systems in different network deployments. Since dynamic ICIC can be regarded as some kind of multi-cell scheduling schemes, it is left to be discussed later.

2.3.1.1 Homogeneous Networks

ICIC techniques, such as Fractional Frequency Reuse (FFR) [52] and Soft Frequency Reuse (SFR) [53], have been widely investigated in the context of efficient radio resource management in multi-cell environments in an attempt to coordinate co-channel interference, resulting in improved cell-edge coverage, cell edge data rates and area BE. A large-scale AA provides additional spatial DoF. Therefore, ICIC for massive MIMO systems is able to exploit the spatial DoF for mitigating ICI by nulling certain spatial direction to the neighbouring cell [54].

In a massive MIMO system, each eNB is equipped with a huge number of antennas, serving its scheduled UEs with beamforming, while trading off its excess DoF against coordinating the interference to other cells within a cluster.

Compared with network MIMO, massive MIMO is preferred to because of its low costs of deploying an excessive number of antennas at the cell site [55]. Under the assumption of the same number of DoF per UE and same amount of channel estimation overhead, massive MIMO with spatial interference coordination outperforms network MIMO [56].

The 3D MIMO system, one of massive MIMO systems, has the capability to dynamically adapt the shape of the vertical beamforming pattern to the UEs at different locations. In other words, the UEs at the cell center and cell edge are covered by different vertical beamforming patterns with specific downtilt such that the received signal power for each UE is maximized. Then, cell sectorization in the 3D MIMO system can be carried out not only along the horizontal but also the vertical axis, which results in increased system throughput [57]. However, the ICI problem becomes more complicated with much more sectors per cell. Therefore, it is not straightforward whether the overall BE performance as well as the cell edge UE can be improved. The preliminary study in [58] shows that dynamic vertical beam pattern adaptation can provide BE performance gains even with either simplified or suboptimum approaches. Meanwhile, there exists some work on coordinated vertical beamforming with well-known ICIC schemes applied in Long Term Evolution (LTE) such as FFR [59]. In the literature, there is a lack of comprehensive studies on this issue to date.

2.3.1.2 Heterogeneous Networks

The HetNet is an attractive means of increasing achievable network capacity and of enhancing the coverage area and/or Quality of Experience (QoE). In a HetNet, small cells as a tier are capable of providing hotspot capacity enhancements, whereas macro cells as another tier are responsible for large area coverage in support of high mobility UEs. However, the MeNBs and SeNBs may interfere with each other, if they use the same time-frequency resources without careful coordination. Fortunately, when the MeNBs, or even the SeNBs, are equipped with a large-scale AA, the AA can provide an additional spatial DoF for multiplexing the data of several UEs onto the same time-frequency resource. Furthermore, it can concentrate the radiated energy precisely on the intended UEs, thereby reducing both the intra- and inter-tier interference. Massive MIMO systems are also capable of supporting cooperation in an implicit way between the different tiers in the HetNet for the sake of improving the overall system performance.

To satisfy ever increasing data rate demands, a two-tier TDD-based HetNet is introduced in [60], where the macro-cell tier served by the MeNBs equipped with a large-scale AA is overlaid with the small cell tier of single-antenna SeNBs. Making use of explicit benefits of channel reciprocity under the TDD mode, the MeNBs estimate the UL interference covariance matrix characterizing the interference from the overlay small cells, which can be used for DL ZF based TPC to reduce the interference to the SUEs. The MeNBs with massive MIMO can significantly

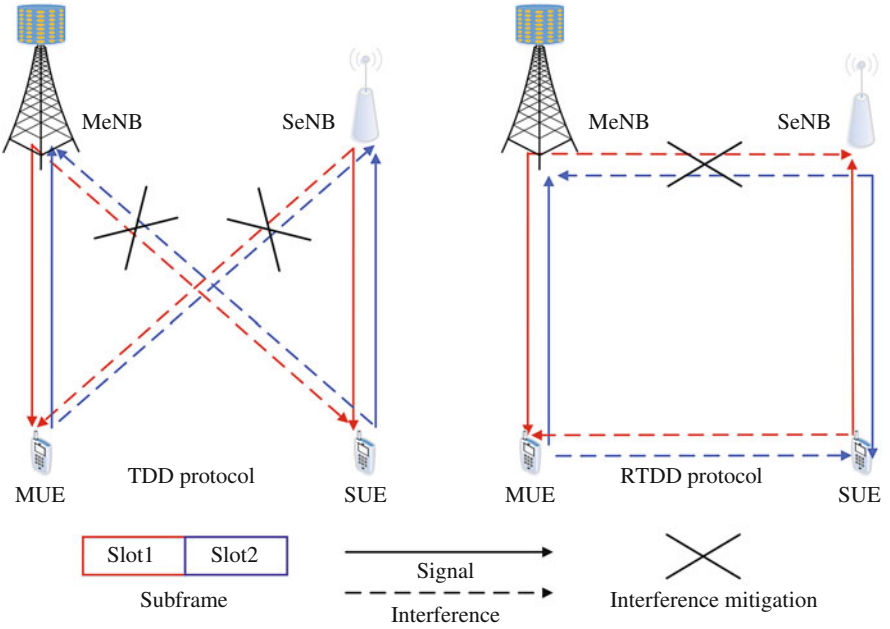

Fig. 2.15 Illustration of an example with either TDD or RTDD [62]

improve the BE of small cells at the expense of a moderate loss of the macro cell performance. Additionally, the SeNBs can also be equipped with multiple antennas if needed [61].

Recently, the so-called Reversed TDD (RTDD) protocol has been proposed for the HetNet [62]. In the RTDD protocol as shown in Fig. 2.15, the sequence of the UL and DL transmission periods in one of the tiers is reversed to the other. For example, in *Slot 1*, while the MeNB transmits the signals to MUEs in the DL, the SeNB received the signals from SUEs in the UL, and vice versa. In the traditional TDD protocol, the MeNBs and SUEs interfere with each other, and so do the SeNBs and MUEs. The channels between the eNBs and UEs potentially fluctuate rapidly thanks to UE mobility. Therefore, less interference samples are available for approximating the time-averaged interference covariance, and hence the resultant estimation errors may degrade the attainable system performance. However, the interference scenario in the HetNet is different if the RTDD protocol is applied, where the MeNB and SeNB interfere with each other, and so do the MUEs and SUEs. Since both the MeNB and SeNB are fixed in location, the interference between them are quasi-static. Hence, the estimated covariance of the channels between them are not sensitive to instantaneous channel variation. Moreover, a massive AA can be deployed at the MeNB and even at the SeNBs so that the

interference between the eNBs can be nearly eliminated by narrow beamforming. Meanwhile, the interference between UEs is usually not very serious in most cases because of the low transmission power of UEs. As a result, the RTDD protocol is more suitable for the HetNet with massive MIMO, since it readily lends itself to cooperative interference cancellation.

2.3.2 Scheduling

Based on the status of queue, channel quality, QoS requirements and so on, the eNB schedules limited radio resources across the time, frequency and spatial domains among the UEs. Different design objectives, e.g., the affordable complexity, overhead, BE, and fairness, are targeted by a variety of scheduling schemes [63]. Usually a good trade-off among all these goals is strived for practical wireless communication systems.

Given a large number of UEs and a limited number of antennas, the problem of sum capacity scaling with UE selection has been widely investigated [64, 65]. In particular, opportunistic beamforming yields significant gains by exploiting the independence of the UEs' channel fluctuation, which may be conducive to achieving multiple UE diversity. Moreover, in order to evaluate the gains of scheduling, the mutual information of the massive MIMO system may be modelled as a normal distribution under the assumption of i.i.d. Rayleigh fading channels [66]. It turns out that the variance of the channel coefficients grows slowly or even decreases with the number of transmit antennas, but increases with the number of UEs. This conclusion implies that carefully designed robust scheduling schemes would reduce the CSI-feedback rate required.

The more UE-specific and eNB-specific channel information is obtained by the scheduler, the more efficient the system can be. Nonetheless, with increased amount of required information, the overhead and computational complexity for channel information may become prohibitive. Due to the channel hardening phenomenon of massive MIMO systems, the scheduling mechanisms relying on full CSI, including large-scale and small-scale prorogation characteristics, are not cost-efficient, because no significant performance gains can be achieved compared to those requiring only partial CSI including the path loss and shadow fading. So, more attention has been paid to scheduling schemes with partial CSI instead of full CSI in massive MIMO systems, both of which are presented for comparison in this section.

2.3.2.1 Full CSI-Based Scheduling

In order to achieve the optimal network performance, the scheduler has to acquire the full and accurate knowledge of all the channels. This knowledge can be exploited to minimize the total power consumption, while satisfying the QoS and power

constraints at the eNBs in the HetNet with massive MIMO [64]. Toward this end, a spatial soft-cell approach can be taken, where each UE is dynamically assigned to access the optimal nodes, i.e., massive MIMO MeNB, conventional SeNB or both. If the system assigns a UE to an MeNB and an SeNB at the same time, multiple transmitters serve the UE through joint non-coherent multi-flow beamforming. Also, the total EE can be further improved by applying a low-complexity efficient algorithm, which exploits the hidden convexity in this problem. However, the scheduler has to know the full instantaneous CSI of all the UEs, which incurs both potentially overwhelming estimation overheads and excessive computational complexity due to the large number of AEs and UEs in a practical system. The costs of the scheduling scheme based on full CSI are likely to outweigh the gains.

2.3.2.2 Partial CSI-Based Scheduling

Fortunately, scheduling schemes with partial CSI can reduce complexity and overhead of massive MIMO systems with an acceptable performance loss.

Single-Cell Scheduling Under the single-cell scenarios, resource allocation for energy-efficient Orthogonal Frequency Division Multiple Access (OFDMA) systems with a large number of AEs was studied in [67]. Taking into account the associated circuit power dissipation, the imperfect CSI at the Transmitter (CSIT) and QoS requirements, the resources are assigned with the objective of maximizing EE. The considered parameters include the subcarrier allocation, power allocation, antenna allocation and available data rates. It is demonstrated that even though the use of a large number of transmit antennas reduces the multipath-induced fluctuation of each channel, the system performance can still benefit from the different path losses and shadow fading conditions of different UEs. Furthermore, the scheduling scheme can be updated periodically, because the path loss and shadow fading parameters vary slowly, depending on UE mobility.

The reduced-complexity probabilistic scheduling algorithms have been proposed in [65, 68, 69], where the number of AEs is quite large. Firstly, different UEs are clustered into groups based on their channel covariance matrices. Then, the UEs in each group are pre-selected randomly based on the group-specific probabilities derived from the whole system. Only the pre-selected UEs are required to transmit their training signals or CSI feedback, leading to markedly reduced overheads and complexity. Moreover, different measures have been conceived both for UE grouping and for scheduling in a FDD based massive MIMO system based on two-stage precoding, namely on inter-group precoding and intra-group precoding, which are capable of reducing the channel estimation overhead while guaranteeing fairness to the UEs [70].

Multi-Cell Scheduling Unlike the single-cell scenario, both inter-cell and intra-cell interferences have to be taken into account under the multi-cell scenario. Although fully multi-cell scheduling schemes, like the coordinated joint processing in network MIMO, can achieve large performance gains, they are not practical due to prohibitive costs. That is, not only the full CSI but also data streams intended

for different mobile users at different cells need to be shared among the eNBs [71]. Instead, another feasible solution is to improve the overall network performance by allowing beamforming vectors from different eNBs to be coordinated for the sake of implementation [72].

The main objective of applying coordinated beamforming in massive MIMO is to improve the overall system performance, while reducing the coordination overhead. There are two popular coordinated beamforming schemes, namely the hierarchical [73] and the nested structure [74, 75].

Explicitly, the BF relying on the hierarchical structure [73] at each eNB consists of an inner precoder and an outer precoder. The inner precoder supports the transmission of data to the serving UEs by exploiting the knowledge of the time-variant CSI. Meanwhile, the outer precoder exploits the remaining spatial DoF for mitigating the ICI by relying only on the knowledge of the average CSI [73]. This structure requires only a modest amount of backhaul overhead and pilots for CSI estimation. Moreover, only the knowledge of the channel's spatial correlation matrices is needed for the BF-weight optimization, which is insensitive to the backhaul latency.

By contrast, in the BF associated with the nested structure, the optimal strategy can be found recursively, where the BF weight optimization objective may be based on the fairness in power usage subject to satisfying the target SINR constraints [74], [76]. Another nested structure, whose OF focuses on Maximizing the Minimum (MAX-MIN) weighted SINR among UEs was proposed in [75, 77]. Unlike the hierarchical structure of [73], the optimal precoder of the nested structure [74], [75] is found as the solution of a joint optimization problem, which aims for striking a trade-off between providing a high SINR for the intra-cell UEs and mitigating the ICI. For instance, when this BF is applied in a massive MIMO system, all the eNBs are divided into two groups, (1) Selfish eNBs, whose UE SINRs are relative low; and (2) altruistic eNBs, whose UEs SINRs are relative high. The altruistic group may be empty; or it may use zero-forcing for eliminating the interference by imposing it on the selfish group. If the optimal ZF beamforming scheme is used in the altruistic group, each eNB in this group has to transmit less power than that in the selfish group. The precoder at each eNB uses the optimal BF parameters along with its own instantaneous CSI. Additionally, only the average CSI has to be exchanged among the eNBs.

On the other hand, different metrics can be used to indicate different system performances. Thus, it is crucial to choose an objective with an appropriate metric function for the multi-cell scheduling schemes. There are several kinds of objectives in terms of either efficiency or fairness when multi-cell scheduling is applied, e.g., (a) Minimizing the Maximum (MIN-MAX) the fairness in power consumption subject to certain SINR constraints [74, 76]: It aims to maximize the overall EE as a high priority by adjusting its coordinated beamforming scheme. A efficient solution can be obtained through Lagrange duality and random matrix theory; (b) MAX-MIN SINR subject to certain sum-rate constraints [75, 77]: It enforces the overall system fairness by guaranteeing each UE's promised SINR. In the case of non-convex optimization problems, the optimal scheme may be derived by using

nonlinear Perron-Frobenius theory; (c) Maximizing the weighted sum rate subject to some eNBs power consumption constraints: This objective can be viewed as a combination of MAX-MIN fairness and maximum sum-rate. Moreover, efficient schemes can be obtained through hidden convexity and random matrix theory [73].

In this section, a wide range of networking techniques conceived for massive MIMO systems have been investigated, with an emphasis on the associated ICIC and scheduling issues. As for ICIC, the beamforming for massive MIMO systems, which helps eliminate the ICI at the expense of computational, and 3D MIMO beamforming, which can be used for cell splitting with low complexity, have been discussed in the context of the HomoNet. The R-TDD protocol, which is helpful for interference cancellation, has also been studied in the context of the HetNet. In scheduling schemes, existing algorithms have been classified according to their requirements in terms of CSI and their different design objectives. The primary objective of scheduling is to improve the attainable system performance, while maintaining affordable implementation complexity and overhead.

2.4 Summary

This chapter provided a survey on the timely subject of massive MIMO, including application scenarios, as well as physical layer and networking techniques.

A pair of practical application scenarios were discussed, namely HomoNets and HetNets. More specifically, the cases of multi-layer sectorization, adaptive beamforming and large-scale cooperation aided HomoNets were studied, followed by the discussion on wireless backhaul design, hotspot coverage and dynamic cell in HeteNets in the specific context of massive MIMO systems. The design of sophisticated TPCs and detection schemes is vital for achieving the potential gains promised by massive MIMO systems. Therefore, both their advantages and disadvantages alongside countermeasures were summarized for both the single-cell and realistic multi-cell environments. Moreover, the effects of non-ideal hardware and imperfect CSI have also been discussed, which have to be further studied in the near future.

Associated networking solutions also attract more attention. The family of coordinated beamforming techniques relying on CSI exchange, low-complexity cell splitting and R-TDD also constitute promising design alternatives for ICIC. The channel hardening phenomenon of massive MIMO is helpful in terms of reducing the CSI overhead and supporting the development of low-complexity scheduling algorithms, albeit at the cost of limited scheduling gains. In a nutshell, an exciting era for MIMO researchers has come!

References

1. A. Saleh, A. Rustako, R. Roman, Distributed antennas for indoor radio communications. IEEE Trans. Commun. **35**(12), 1245–1251 (1987)
2. R. Heath, T. Wu, Y. H. Kwon, A. Soong, Multiuser MIMO in distributed antenna systems with out-of-cell interference. IEEE Trans. Signal Process. **59**(10), 4885–4899 (2011)
3. D. Qiao, Y. Wu, Y. Chen, Massive MIMO architecture for 5G networks: co-located, or distributed?, in *Proceedings of the 11th International Symposium on Wireless Communication Systems (ISWCS)*, Barcelona, Aug 2014, pp. 192–197
4. K. Truong, R. Heath, The viability of distributed antennas for massive MIMO systems, in *Proceedings of the 47th Asilomar Conference Signals, Systems and Computers (ASILOMAR)*, Pacific Grove, CA, Nov 2013, pp. 1318–1323
5. Z. Liu, L. Dai, A comparative study of downlink MIMO cellular networks with co-located and distributed base-station antennas. IEEE Trans. Wirel. Commun. **13**(11), 6259–6274 (2014)
6. M. Thomas, H.Yang, Dedicated LSAS for metro-cell wireless backhaul - part I: downlink. Bell Laboratories, Alcatel-Lucent, Dec 2012
7. C.V. Networking, Global mobile data traffic forecast update, 2012–2017, Cisco Visual Networking, May 2013
8. Huawei and HiSilicon, Performance evaluation of elevation beamforming in the use scenarios, 3GPP R1-131165, Apr 2013
9. Huawei and HiSilicon, Performance evaluation of cell range extension, 3GPP R1-112894, June 2011
10. A. Damnjanovic, J. Montojo, Y. Wei, T. Ji, T. Luo, M. Vajapeyam, T. Yoo, O. Song, D. Malladi, A survey on 3GPP heterogeneous networks. IEEE Trans. Wirel. Commun. **18**(3), 10–21 (2011)
11. HUAWEI and HiSilicon, Views on Rel-12 and onwards for LTE and UMTS, 3GPP RWS-120006 (2013)
12. F. Rusek, D. Persson, B.K. Lau, E. Larsson, T. Marzetta, O. Edfors, F. Tufvesson, Scaling up MIMO: opportunities and challenges with very large arrays. IEEE Signal Process. Mag. **30**(1), 40–60 (2013)
13. H.Q. Ngo, E. Larsson, T. Marzetta, Energy and spectral efficiency of very large multiuser MIMO systems. IEEE Trans. Commun. **61**(4), 1436–1449 (2013)
14. H. Yang, T. Marzetta, Performance of conjugate and zero-forcing beamforming in large-scale antenna systems. IEEE J. Sel. Areas Commun. **31**(2), 172–179 (2013)
15. C. Masouros, M. Sellathurai, T. Ratnarajah, Large-scale MIMO transmitters in fixed physical spaces: the effect of transmit correlation and mutual coupling. IEEE Trans. Commun. **61**(7), 2794–2804 (2013)
16. C. Shepard, H. Yu, N. Anand, E. Li, T. Marzetta, R. Yang, L. Zhong, Argos: practical many-antenna base stations, in *Proceedings of the ACM International Conference Mobile Computing and Network*, Istanbul, Aug 2012, pp. 53–64
17. C.B. Peel, On dirty-paper coding. IEEE Signal Process. Mag. **20**(3), 112–113 (2003)
18. B. Hochwald, C. Peel, A. Swindlehurst, A vector-perturbation technique for near-capacity multiantenna multiuser communication-part II: perturbation. IEEE Trans. Commun. **53**(3), 537–544 (2005)
19. C. Windpassinger, R.F.H. Fischer, J. Huber, Lattice-reduction-aided broadcast precoding. IEEE Trans. Commun. **52**(12), 2057–2060 (2004)
20. Y.-C. Liang, E.Y. Cheu, L. Bai, G. Pan, On the relationship between MMSE-SIC and BI-GDFE receivers for large multiple-input multiple-output channels. IEEE Trans. Signal Process. **56**(8), 3627–3637 (2008)
21. Y.-C. Liang, S. Sun, C. K. Ho, Block-iterative generalized decision feedback equalizers for large MIMO systems: algorithm design and asymptotic performance analysis. IEEE Trans. Signal Process. **54**(6), 2035–2048 (2006)

22. H. Zhao, H. Long, W. Wang, Tabu search detection for MIMO systems, in *Proceedings of the IEEE International Symposium on Personal, Indoor and Mobile Radio Communications (PIMRC)*, Athens, Sept 2007, pp. 1–5
23. S. Mohammed, E. Larsson, Per-antenna constant envelope precoding for large multi-user MIMO systems. IEEE Trans. Commun. **61**(3), 1059–1071 (2013)
24. C. Peel, B. Hochwald, A. Swindlehurst, A vector-perturbation technique for near-capacity multiantenna multiuser communication-part I: channel inversion and regularization. IEEE Trans. Commun. **53**(1), 195–202 (2005)
25. S. Wagner, R. Couillet, M. Debbah, D.T.M. Slock, Large system analysis of linear precoding in correlated MISO broadcast channels under limited feedback. IEEE Trans. Inf. Theory **58**(7), 4509–4537 (2012)
26. C. Masouros, Correlation rotation linear precoding for MIMO broadcast communications. IEEE Trans. Signal Process. **59**(1), 252–262 (2011)
27. X. Gao, O. Edfors, F. Rusek, F. Tufvesson, Linear pre-coding performance in measured very-large MIMO channels, in *Proceedings of the IEEE 74th Vehicular Technology Conference (VTC-Fall)*, San Francisco, CA, Sept 2011, pp. 1–5
28. J. Hoydis, C. Hoek, T. Wild, S. ten Brink, Channel measurements for large antenna arrays, in *Proceedings of the International Symposium on Wireless Communication Systems (ISWCS)*, Pairs, Aug 2012, pp. 811–815
29. X. Gao, F. Tufvesson, O. Edfors, F. Rusek, Measured propagation characteristics for very-large MIMO at 2.6 GHz, in *Proceedings of the 46th Asilomar Conference on Signals, Systems and Computers (ASILOMAR)*, Pacific Grove, CA, Nov 2012, pp. 295–299
30. T. Marzetta, Noncooperative cellular wireless with unlimited numbers of base station antennas. IEEE Trans. Wirel. Commun. **9**(11), 3590–3600 (2010)
31. J. Hoydis, S. ten Brink, M. Debbah, Massive MIMO in the UL/DL of cellular networks: how many antennas do we need? IEEE J. Sel. Areas Commun. **31**(2), 160–171 (2013)
32. H.Q. Ngo, T. Duong, E. Larsson, Uplink performance analysis of multicell MU-MIMO with zero-forcing receivers and perfect CSI, in *Proceedings of the IEEE Swedish Communication Technologies Workshop*, Stockholm, Oct 2011, pp. 40–45
33. H. Ngo, E. Larsson, T. Marzetta, The multicell multiuser MIMO uplink with very large antenna arrays and a finite-dimensional channel. IEEE Trans. Commun. **61**(6), 2350–2361 (2013)
34. H. Yin, D. Gesbert, M. Filippou, Y. Liu, A coordinated approach to channel estimation in large-scale multiple-antenna systems. IEEE J. Sel. Areas Commun. **31**(2), 264–273 (2013)
35. A. Hu, T. Lv, H. Gao, Y. Lu, E. Liu, Pilot design for large-scale multi-cell multiuser MIMO systems, in *Proceedings of the IEEE International Conference on Communications*, Budapest, June 2013, pp. 5381–5385
36. H. Wang, Y. Huang, S. Jin, F. Yu, L. Yang, Performance analysis on precoding and pilot scheduling in very large MIMO multi-cell systems, in *Proceedings of the IEEE Wireless Communication and Networking Conference*, Shanghai, Apr 2013, pp. 2722–2726
37. H. Yin, D. Gesbert, M.C. Filippou, Y. Liu, Decontaminating pilots in massive MIMO systems, in *Proceedings of the IEEE International Conference on Communications (ICC)*, Budapest, June 2013, pp. 3170–3175
38. F. Fernandes, A. Ashikhmin, T. Marzetta, Inter-cell interference in noncooperative TDD large scale antenna systems. IEEE J. Sel. Areas Commun. **31**(2), 192–201 (2013)
39. F. Fabio, A. Alexei, M. Thomas, Interference reduction on cellular networks with large antenna arrays, in *Proceedings of the IEEE International Conference on Communication (ICC)*, Ottawa, May 2012
40. H.Q. Ngo, E. Larsson, EVD-based channel estimation in multicell multiuser MIMO systems with very large antenna arrays, in *Proceedings of the IEEE International Conference on Acoustics, Speech and Signal Processing (ICASSP)*, Kyoto, May 2012, pp. 3249–3252
41. R.R. Müller, M. Vehkaperä, L. Cottatellucci, Blind pilot decontamination, in *Proceedings of the 17th ITG Workshop on Smart Antennas*, Stuttgart, Mar 2013, pp. 1–6

42. A. Ashikhmin, T. Marzetta, Pilot contamination precoding in multi-cell large scale antenna systems, in *Proceedings of the International Symposium on Information Theory (ISIT)*, Cambridge, July 2012, pp. 1137–1141
43. J. Jose, A. Ashikhmin, T. Marzetta, S. Vishwanath, Pilot contamination and precoding in multi-cell TDD systems. IEEE Trans. Wirel. Commun. **10**(8), 2640–2651 (2011)
44. E.G. Larsson, F. Tufvesson, O. Edfors, T.L. Marzetta, Massive MIMO for next generation wireless systems. IEEE Commun. Mag. **52**(2), 186–195 (2014)
45. K. Truong, R. Heath, Effects of channel aging in massive MIMO systems. J. Commun. Netw. **15**(4), 338–351 (2013)
46. P. Taluja, B. Hughes, Diversity limits of compact broadband multi-antenna systems. IEEE J. Sel. Areas Commun. **31**(2), 326–337 (2013)
47. A. Pitarokoilis, S.K. Mohammed, E.G. Larsson, Uplink performance of time-reversal MRC in massive MIMO systems subject to phase noise. IEEE Trans. Wirel. Commun. **15**(99), 1 (2014)
48. E. Björnson, J. Hoydis, M. Kountouris, M. Debbah, Massive MIMO systems with non-ideal hardware: energy efficiency, estimation, and capacity limits. IEEE Trans. Inf. Theory **60**(11), 7112–7139 (2014)
49. X. Rao, V. Lau, Distributed compressive CSIT estimation and feedback for FDD multi-user massive MIMO systems. IEEE Trans. Signal Process. **62**(12), 3261–3271 (2014)
50. Y. Ma, D. Zhang, A. Leith, Z. Wang, Error performance of transmit beamforming with delayed and limited feedback. IEEE Trans. Wirel. Commun. **8**(3), 1164–1170 (2009)
51. J. Zhang, M. Kountouris, J. Andrews, R. Heath, Multi-mode transmission for the MIMO broadcast channel with imperfect channel state information. IEEE Trans. Wirel. Commun. **59**(3), 803–814 (2011)
52. T.D. Novlan, R.K. Ganti, A. Ghosh, J.G. Andrews, Analytical evaluation of fractional frequency reuse for OFDMA cellular networks. IEEE Trans. Wirel. Commun. **10**(12), 4294–4305 (2011)
53. X. Mao, A. Maaref, K.H. Teo, Adaptive soft frequency reuse for inter-cell interference coordination in SC-FDMA based 3GPP LTE uplinks, in *Proceedings of the IEEE GLOBECOM*, New Orleans, Nov 2008, pp. 1–6
54. A. Adhikary, E. Al Safadi, G. Caire, Massive MIMO and inter-tier interference coordination, in *Information Theory and Applications Workshop (ITA)*, San Diego, Feb 2014, pp. 1–10
55. S. Ramprashad, G. Caire, Cellular vs. network MIMO: a comparison including the channel state information overhead, in *Proceedings of the International Symposium on Personal, Indoor and Mobile Radio Communications (PIMRC)*, Tokyo, Sept 2009, pp. 878–884
56. K. Hosseini, W. Yu, R. Adve, Large-scale MIMO versus network MIMO for multicell interference mitigation. IEEE J. Sel. Top. Signal Process. **8**(5), 930–941 (2014)
57. C.-S. Lee, M.-C. Lee, C.-J. Huang, T.-S. Lee, Sectorization with beam pattern design using 3D beamforming techniques, in *Proceedings of the Asia-Pacific Signal Information Processing Association Annual Summit and Conference (APSIPA)*, Kaohsiung, Oct 2013, pp. 1–5
58. H. Halbauer, S. Saur, J. Koppenborg, C. Hoek, Interference avoidance with dynamic vertical beamsteering in real deployments, in *Proceedings of the IEEE Wireless Communications and Networking Conference Workshops (WCNCW)*, Paris, Apr 2012, pp. 294–299
59. V. D'Amico, C. Botella, J. Giese, R. Fritzsche, H. Halbauer, J. Holfeld, P. Marsch, S. Saur, T. Svensson, T. Wild, W. Zirwas, Advanced interference management in ARTIST4G: interference avoidance, in *Proceedings of the European Wireless Technology Conference (EUWIT)*, Pairs, Sept 2010, pp. 21–24
60. M. Kountouris, N. Pappas, Hetnets and massive MIMO: modeling, potential gains, and performance analysis, in *Proceedings of the IEEE-APS Topical Conference on Antennas and Propagation in Wireless Communications*, Torino, Sept 2013, pp. 1319–1322.
61. J. Hoydis, K. Hosseini, S.T. Brink, M. Debbah, Making smart use of excess antennas: massive MIMO, small cells, and TDD. Bell Labs Tech. J. **18**(2), 5–21 (2013)
62. K. Hosseini, J. Hoydis, S. ten Brink, M. Debbah, Massive MIMO and small cells: how to densify heterogeneous networks, in *Proceedings of the IEEE International Conference on Communications (ICC)*, Budapest, June 2013, pp. 5442–5447

63. F. Capozzi, G. Piro, L. Grieco, G. Boggia, P. Camarda, Downlink packet scheduling in LTE cellular networks: key design issues and a survey. IEEE Commun. Surveys Tutor. **15**(2), 678–700 (2013)
64. E. Bjornson, M. Kountouris, M. Debbah, Massive MIMO and small cells: improving energy efficiency by optimal soft-cell coordination, in *Proceedings of the IEEE International Conference on Communications (ICC)*, Casablanca, June 2013, pp. 1–5
65. H. Papadopoulos, G. Caire, S.A. Ramprashad, Achieving large spectral efficiencies from MU-MIMO with tens of antennas: location-adaptive TDD MU-MIMO design and user scheduling, in *Proceedings of the IEEE Asilomar Conference on Signals, Systems, and Computers*, Pacific Grove, Nov 2010, pp. 636–643
66. B. Hochwald, T. Marzetta, V. Tarokh, Multiple-antenna channel hardening and its implications for rate feedback and scheduling. IEEE Trans. Inf. Theory **50**(9), 1893–1909 (2004)
67. D. Ng, E. Lo, R. Schober, Energy-efficient resource allocation in OFDMA systems with large numbers of base station antennas. IEEE Trans. Wirel. Commun. **11**(9), 3292–3304 (2012)
68. J. Nam, A. Adhikary, J.-Y. Ahn, G. Caire, Joint spatial division and multiplexing: opportunistic beamforming, user grouping and simplified downlink scheduling. IEEE J. Sel. Top. Signal Process. **8**(5), 876–890 (2014)
69. H. Huh, A.M. Tulino, G. Caire, Network MIMO with linear zero-forcing beamforming: large system analysis, impact of channel estimation, and reduced-complexity scheduling. IEEE Trans. Inf. Theory **58**(5), 2911–2934 (2012)
70. Y. Xu, G. Yue, S. Mao, User grouping for massive MIMO in FDD systems: new design methods and analysis. IEEE Access **2**, 947–959 (2014)
71. P. de Kerret, D. Gesbert, Degrees of freedom of the network MIMO channel with distributed CSI. IEEE Trans. Inf. Theory **58**(11), 6806–6824 (2012)
72. Y. Yang, B. Bai, W. Chen, L. Hanzo, A low-complexity cross-layer algorithm for coordinated downlink scheduling and robust beamforming under a limited feedback constraint. IEEE Trans. Veh. Technol. **63**(1), 107–118 (2014)
73. A. Liu, V. Lau, Hierarchical interference mitigation for massive MIMO cellular networks. IEEE Trans. Signal Process. **62**(18), 4786–4797 (2014)
74. R. Zakhour, S. Hanly, Min-max fair coordinated beamforming via large systems analysis, in *Proceedings of the 8th International Symposium on Wireless Communication Systems (ISWCS)*, Aachen, Nov 2011, pp. 1990–1994
75. Y. Huang, C.W. Tan, B.D. Rao, Multicell network duality with instantaneous and statistical channel information: a nonlinear Perron-Frobenius characterization, in *Proceedings of the Conference on Information Sciences and Systems (CISS)*, Princeton, Mar 2012, pp. 1–6
76. R. Zakhour, S. Hanly, Min-max power allocation in cellular networks with coordinated beamforming. IEEE J. Sel. Areas Commun. **31**(2), 287–302 (2013)
77. Y. Huang, C.W. Tan, B. Rao, Joint beamforming and power control in coordinated multicell: max-min duality, effective network and large system transition. IEEE Trans. Wirel. Commun. **12**(6), 2730–2742 (2013)

Chapter 3
Massive MIMO-Aided Millimeter Communication Technology

Heterogeneous and Small Cell Networks (HetSNets) can increase the SE and throughput with the hierarchical deployment of low power nodes as well as the macro nodes. In order to meet the increasing capacity requirements of future 5G wireless networks, much more number of low power nodes needs to be deployed if no new frequency resources becomes available, which may cause the serious interference between nodes. Then, the introduction of mm-wave communications with massive MIMO provides unprecedented spectral resources for HetSNets in 5G. However, major challenges remain for implementing mm-wave massive MIMO in HetSNets. To this end, we introduce several typical deployment scenarios for HetSNets with mm-wave massive MIMO. A frame structure based on TDD is proposed and discussed then in details. Next, the challenges and possible solutions relating to both physical, MAC and network layers are studied. Finally, system-level simulations are implemented to evaluate the system performance of HetSNets with mm-wave massive MIMO.

3.1 Background

The traffic load of wireless communications networks with various QoS requirements has been increasing rapidly recently due to the widespread use of mobile Internet applications by smart terminals. This trend continues, requiring emerging wireless networks to be designed to meet these requirements. The 5G cellular communications system is expected to be standardized around 2020 [1]. The overarching goal of 5G is to achieve 10–100 times higher user data rates such that in dense urban environments the typical user data rate will range from 1 to 10 Gbps while supporting 10–100 times more connected devices. Also, the energy efficiency of low-power massive machine communications will be improved 10 times so that sensors will have a battery life of nearly a decade. Moreover, end-to-end latency will

L. Zhao et al., *Massive MIMO in 5G Networks: Selected Applications*,
SpringerBriefs in Electrical and Computer Engineering,
https://doi.org/10.1007/978-3-319-68409-3_3

be less than 5 ms providing ultra-fast application response times. As a result, novel technologies are demanded to realize such ambitious goals. Generally speaking, there are several means to improve network capacity. The first one is to increase the utilized bandwidth, e.g., through carrier aggregation, cognitive radios, and so on. The second way is to increase geographic spectrum reusability, such as small cell techniques. The third but not the least one is to improve spectral efficiency, such as MIMO and Non-Orthogonal Multiple Access (NOMA) techniques. However, there is no clear roadmap on how to achieve the so-far defined 5G performance targets. Breakthrough technologies are thus needed in the near future [2].

The low frequency bands have almost been used up in recent years, and it is difficult to find sufficient frequency bands in the micro-wave range for 5G. By contrast, there are still a large number of unused frequency bands in mm-wave radio, which may be of potential use to mobile cellular communications given recent advances in hardware and electronic components. At present, mm-wave communications have already had numerous indoor and outdoor applications such as in residential, business, public, and commercial places. It is well suited for not only in-home applications like audio/video transmission, desktop connections and portable devices, but also outdoor point-to-point applications. Mm-wave communications can play an increasingly significant role as wireless backhaul for outdoor small cells, thanks to its low construction costs, quick deployment, and flexibility in providing access. Besides these benefits, the eNB in a small cell may provide high system throughout through mm-wave communications. The propagation characteristics of mm-wave communications are characterized by high levels of oxygen absorption and rain attenuation, especially in outdoor environments. This limits the range and cell coverage of mm-wave radio as opposed to micro-wave radio. On the other hand, mm-wave communications systems facilitate the integration with the increasingly popular massive MIMO technologies [3]. This is because the wavelength of mm-wave radio is small enough so that the physical size of a massive antenna array can be greatly reduced for easy deployment at small-cell eNBs. Apart from improving spectral efficiency, massive MIMO is also an effective technique to compensate for the severe propagation loss of mm-wave radio [4]. Recently, beamforming/precoding techniques with massive MIMO in mm-wave have been widely studied in IEEE standards, such as IEEE 802.15.3c (TG3c) for Wireless Personal Area Networks (WPAN), IEEE 802.11ad (TGad) and Wireless Gigabit Alliance (WiGig). Meanwhile, massive MIMO with 3D beamforming is becoming a burning topic in Release-12 of the 3GPP Long Term Evolution (LTE) [5]. Therefore, the HetSNets with mm-wave massive MIMO will play a very important role in future 5G cellular networks. However, there are lots of problems related to the implementation of HetSNets with mm-wave communications capabilities.

The scope of this chapter is thus to study where and how mm-wave communications can possibly work well with the micro-wave communications in HetSNets with the assistance of massive MIMO. Section 3.2 briefly discusses typical deployment scenarios for the HetSNet with mm-wave massive MIMO to

show application feasibility. Also, the TDD frame structure in line with 3GPP LTE systems is designed, which can support multi-hop transmission with wireless backhaul. Section 3.3 presents the physical-layer feasibility of mm-wave massive MIMO, including both CSI acquisition and beamforming scheme. In Sect. 3.4, the challenges and solutions are discussed for HetSNets with mm-wave massive MIMO from the viewpoint of MAC layer. Section 3.5 presents preliminary performances of mm-wave communications with massive MIMO. Finally, conclusions are drawn in Sect. 3.6.

3.2 Deployment of Millimeter-Wave Communications

HetSNets typically consist of multiple types of radio access nodes in a 3GPP LTE network, e.g., a MeNB and several SeNBs such as pico, femto and relay eNBs. In such a network, each SeNB combines its backhaul data with that received from other nodes in the network before forwarding it to the MeNB. The SeNBs are supposed to be separated by short distance, e.g., 100–200 m, which helps mitigate the severe propagation loss. Coverage within the small cells (i.e., user access) may also be provided by mm-wave radio, reducing the level of interference experienced on the sub-3 GHz frequency bands used for traditional mobile communications.

3.2.1 Typical Deployment Scenarios

With the introduction of mm-wave communications into the HetSNet, there are several potential deployment scenarios, where mm-wave communications are used for either backhaul or user access links. Some of typical scenarios are illustrated in Fig. 3.1.

Scenario 1 Traditionally, an SeNB is connected to its donor MeNB through wired backhaul such as an optical fiber. All UEs are served by either the MeNB or SeNBs in the micro-wave band. Under this scenario, interference coordination schemes have to be carefully designed so as to avoid the interference between the MeNB and SeNBs.

Scenario 2 Compared with Scenario 1, the UEs communicating with the MeNB work in the micro-wave band, whereas the UEs served by the SeNBs use mm-wave radio. The SeNBs are connected to the MeNB via a wired backhaul. No interference coordination is needed between the MeNB and SeNBs under this scenario. However, the UEs should support dual bands for smooth handover between the MeNB and SeNBs, thus increasing the costs of the UEs.

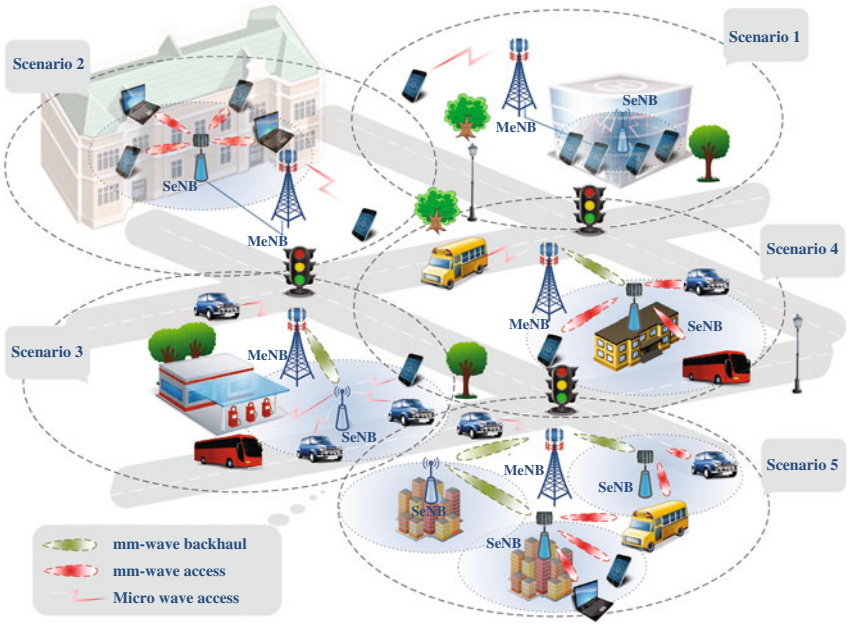

Fig. 3.1 Illustration of typical deployment scenarios

Scenario 3 In lieu of wired backhaul, the mm-wave band is employed for backhaul transmission between the MeNB and SeNBs. For the sake of implementation, only single-hop is permitted for backhaul transmission with mm-wave radio. Through such deployment, only network facilities need to be upgraded while the UEs remain unchanged. This is helpful for the quick deployment of the SeNBs. Similar to Scenario 1, advanced interference coordination schemes are necessary between the MeNB and SeNBs.

Scenario 4 Mm-wave communications are adopted for single-hop wireless backhaul for the SeNBs in Scenario 4. Moreover, the SeNBs serve the UEs in a small cell via mm-wave radio, which can significantly increase network capacity because of the tremendous bandwidth offered by the mm-wave band.

Scenario 5 Increasing geographic spectrum reusability is another means to improve network capacity, resulting in dense small cell deployment. Then, multi-hop wireless backhaul is a good way to connect dense SeNBs with the MeNB. In this scenario, the SeNBs can cooperate with each other and communicate with their donor MeNB via mm-wave radio. Also, the access links between the SeNBs and their served UEs work in the mm-wave band. This scenario is much more flexible and can provide high capacity, in which most key techniques for HetSNets with mm-wave communications may be applicable.

3.2.2 Frame Structure

The propagation characteristics of mm-wave communication bands are quite different from those of micro-wave communications, such as Doppler frequency shift and multipath delay. The Orthogonal Frequency Division Multiplexing (OFDM) parameters for micro-wave communications in 3GPP LTE systems cannot be applied to mm-wave communication without any change. On the other hand, much more frequency bandwidth is available in mm-wave communication bands, which means the bandwidth per subcarrier needs to be enlarged keeping the size and thereby complexity of Fast Fourier Transform (FFT) unchanged. Moreover, the back-compatibility with 3GPP LTE systems must be considered when the mm-wave communication is introduced into HetSNets. Therefore, a new frame structure has to be designed for mm-wave communications co-exist with micro-wave communications in HetSNets.

Assuming that 28 GHz band with 1 GHz in bandwidth is used for mm-wave communications due to its availability and being widely-investigation [6]. Measurement results show that the delay spread is not severe if Transmitter-Receiver (Tx-Rx) separation is less 200 m at 28 GHz in the urban environment. In the case of LOS, there are too few multipaths to determine the Root Mean Squared (RMS) delay spread, while in the case of NLOS, most measured multipath components have an RMS delay spreads below 0.2 μs. Thus, OFDM-based mm-wave wireless systems need to tolerate an RMS delay of less than 0.2 μs. The guard interval for mm-wave communications is expected to be much larger than the RMS delay in order to alleviate Inter-Symbol Interference (ISI). Besides this, backwards compatibility with micro-wave communications has to be taken into consideration. Therefore, the guard period of 0.469 μs is selected, because this value is not only two times more than the RMS delay but also one tenth of the guard period in micro-wave communications. As we know, a symbol period of 66.67 μs is selected in 3GPP LTE, which is 66.67/4.69 times larger than the guard period. Correspondingly, a useful symbol duration of 6.667 μs can be chosen for mm-wave communications and the subcarrier spacing is computed as the inverse of the OFDM useful symbol duration, i.e., 150 kHz. Then, the basic mm-wave frame has 10 subframes, each subframe of 0.1 ms consisting of 14 OFDM symbols. The frame structure and main parameters are depicted in Fig. 3.2 as one possible TDD solution to HetSNets with mm-wave communications.

When wireless backhaul is adopted in HetSNets with mm-wave communications, the mm-wave subframe configuration is able to support the multi-hop transmission. Each mm-wave subframe can be used for single-hop transmission. Figure 3.3 illustrates an example configuration for multi-hop transmission. In the first mm-wave subframe, the MeNB transmits backhaul signals to the nearby SeNB 1# in the 1st-hop transmission, and SeNB 2# far from the MeNB sends information to its SUEs simultaneously. Subsequently, the MeNBs remain silent in the second mm-wave subframe, and SeNB 1# transmit signals to SeNB 2# and their SUEs,

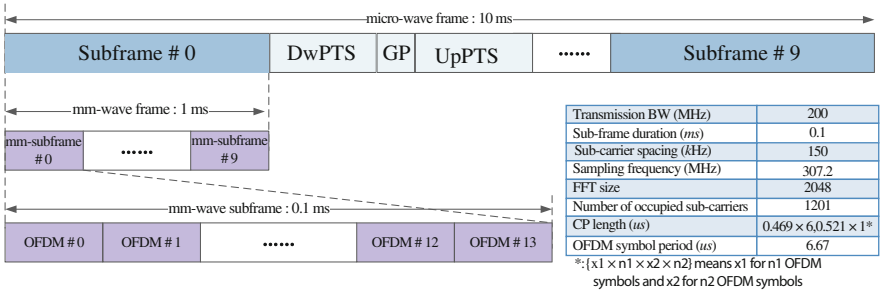

Fig. 3.2 Modified TDD frame structure for mm-wave communications

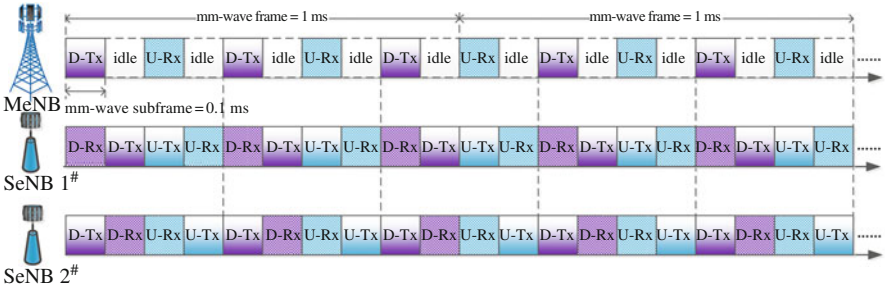

Fig. 3.3 Mm-wave subframe configuration for multi-hop communications

taking advantage of spatial multiplexing. The uplink procedure is similar to that of the downlink. Moreover, in order to reduce the Rx/Tx switch, several mm-wave subframes can be grouped together as the radio resources for a single-hop.

3.3 Physical Layer Challenges and Solutions

In order to implement the mm-wave communication system for both indoor and outdoor environments, advanced physical-layer techniques have to be first developed. Given the current CSI information estimated by pilots, there are some other factors affecting the gain of precoding or beamforming, which can not be neglected in mm-wave communications compared with micro-wave communications.

3.3.1 CSI Acquisition

Compared with micro-wave communication systems, there is usually a much larger number of antennas in HetSNets especially using mm-wave bands. Therefore, how to acquire accurate CSI is one of the most important challenges in mm-wave

communication systems. Accurate CSI is essential for both precoding at the transmitter and detection at the receiver, which determines physical-layer performances.

3.3.1.1 Pilot Scarcity Problem

In OFDM-based mm-wave communication systems, the number of available orthogonal pilot subcarriers is limited, e.g., the space between pilot subcarriers is no more than the coherent time or bandwidth of the channel. However, many pilot subcarriers are needed for downlink channel estimation because there are a large number of antennas at the eNB. In other words, it is almost impossible to allocate each antenna with orthogonal pilot subcarriers for downlink channel estimation. The effect of pilot scarcity depends on the deployment of HetSNets, and can be dealt with by different ways.

Macrocell with Micro-Wave Communications In a TDD system, an eNB can estimate uplink CSI through uplink pilots, and then use them for downlink transmission based upon channel reciprocity. Since the number of antennas at the UE is much smaller than that at the eNB, there is no limitation for the number of pilot subcarriers on the uplink. By this way, no channel estimation with dedicated pilots on the downlink is needed. However, since the uplink pilot subcarrier are reused between the neighboring cells, imperfect CSI is estimated through linear estimation algorithms, e.g., MF and MMSE, in multi-cell environments. Therefore, pilot contamination becomes the performance bottleneck for micro-wave communications with massive MIMO [4].

Small Cell with mm-Wave Communications The UEs can deploy a larger number of antennas due to the smaller space between adjacent antennas as opposed to micro-wave communications, which aggravates the issue of pilot scarcity. On the contrary, the number of UEs served by each small cell decreases with the increasing in the density of small cells, which alleviates the use of orthogonal pilots. However, pilot scarcity will become severe for the wireless backhaul links between multiple SeNBs and the MeNB of the denser small cells.

3.3.1.2 Solutions

The performance of mm-wave communications is dependent highly on the accuracy of CSI. In order to acquire accurate CSI with a reasonable pilot overhead, several state-of-the-art channel estimation methods have been proposed as follows.

Compressed-Sensing-Based Channel Estimation According to compressed sensing theory, the resources occupied by each pilot sequence can be significantly reduced owing to the sparsity of multipath, AoAs, Doppler, etc. [7]. Employing relevant algorithms, the receiver can estimate a channel efficiently with less resources-occupied pilots compared with the current system. Therefore, the

maximum number of orthogonal pilot sequences can be increased given the coherent time and bandwidth, which can resolve the issue of pilot starvation radically.

Space Reuse Pilot When the UEs reusing the same pilot sequence are distributed in different positions, the signals of these UEs can be distinguished by both the AoAs and Elevation angle of Arrivals (EoAs). If the receiver can filter the signals in the spatial domain, the UE channels can be estimated precisely. Tolerating pilot reuse among different UEs or cells, this method can improve the accuracy of channel estimation owing to space information [8].

Statistic-Based Channel Estimation Another efficient scheme is blind channel estimation, which can acquire the channel through some prior information, such as large-scale fading. The statistic of large-scale fading information generally requires less training, which helps reduce the use of the limited number of pilot sequences compared with the estimation of a fast-fading channel. Assuming i.i.d. Rayleigh fading, a fast-fading channel can be acquired via eigenvalue decomposition [9].

Moreover, some solutions are also given to eliminate the effect of imperfect CSI caused by pilot reuse but not to improve the accuracy of CSI, such as the method of pilot contamination precoding [10].

3.3.2 Beamforming Schemes

Mm-wave communication can use a plenty of spectral resources. However, it induces a severer path loss compared to the systems using low-frequency bands; and the additional loss may be incurred due to rain and oxygen absorption. Therefore, mm-wave communications require a large antenna gain to compensate for the loss, and therefore guarantees coverage and reliable communications. On the other hand, multiple antennas can be deployed in a small area in mm-wave communications. Hence, it is straightforward to employ massive MIMO in mm-wave communications.

3.3.2.1 Problems of Beamforming/Precoding

Beamforming has been widely studied in IEEE standards. However, there are several problems for the beamforming or precoding schemes, which needs to be solved before being applied in mm-wave communications. Firstly, the beam alignment and blockage between the eNB and UEs have to be dealt with in the LoS environments. As the beam width of mm-wave is extremely narrow with massive antennas, the vibration of the eNB caused by the wind flow or UE movement may adversely impact on the gain of beamforming [11]. Moreover, narrow beams are easily obscured by people or other objects at the UEs, which needs adaptive processing algorithms and advanced techniques similar to those used in traditional phones [2]. Secondly, the issue of outdated precoding arises due to the varying channel in both

the NLoS and LoS environments, i.e., the channel used for precoding mismatches the current propagation channel [8]. In a broad sense, both problems are attributed to channel aging due to the variation of the eNBs, UEs, surrounding environment and so on.

3.3.2.2 Solutions

Effective beamforming or precoding for MU-MIMO is essential for enhancing coverage and SE in HetSNets. The aforementioned problems can be mitigated according to the following methods with different gains and complexities.

Channel Prediction Channel prediction is one of vital techniques that can improve the performance radically, at the expense of system complexity. According to the older samples of the channel, channel variation can be modeled as a function of time, and thereby subsequent channels can be predicted through the use of some efficient algorithms. However, channel prediction is only applicable when the channels are correlated in the time dimension, which is mainly used for channel variation induced by the environment, etc.

Beam Calibration In IEEE standards, beamforming is mainly dependent on training samples to calibrate the direction of the current beam at both the eNB and UEs for indoor scenarios, which can be extended to the FDD mode in mm-wave communications. In order to overcome the wind flow or UE movements for outdoor environments, adaptive subspace sampling and hierarchical beam codebooks are studied in detail. However, this scheme induces some overhead and time delay, which deteriorates system QoS [11].

Position Estimation Compared with channel prediction and calibration, the movement tendency or speed estimation of UEs is another option to track the positions of UEs, which has been studied widely in short-range communications. Given the UE position information, the beam can be made adaptively point to the UE. This scheme can improve the performance at the expense of complexity, thanks to the position estimation algorithm. A practical system should balance between the performance improvement and system complexity sensibly.

Robust Precoding Robust precoding is a concessive scheme compared with the aforementioned ideas. It properly extends the width of the beam in order to cover the moving UEs or fit for array swaying, which helps enhance the targeted ratio at the cost of the beam gain. There exists a trade-off between the gain and targeted ratio. The beam width can be adaptively adjusted according to the targeted ratio or other prior information. Although the array gain is impaired by the wider beam, the overhead and complexity are reduced sharply compared with the foregoing schemes. In addition to CSI acquisition and deficient beamforming/precoding, some other problems, such as antenna array design and initial access of UEs, are vital for practical HetSNets, which need further discussion in the near future.

3.4 MAC and Networking Design

The use of highly directional beamforming raises a number of new issues in network design. We focus only on MAC layers and the networking in this section. Thanks to the dense deployment of small cell using narrow beamform with large gains at mm-wave communication bands, the multi-hop transmission is possibly implemented in HetSNets. Then, the routing scheme with the specific metric under the constraints of the delay and reasonable control overhead becomes very important in the MAC layer of HetSNets with mm-wave communications. Different from interference coordination in micro-wave communications, i.e., mainly either in time domain or in frequency domain, the spatial interference coordination is paid more attention in mm-wave communications and thereby discussed in this section. Moreover, due to the limited coverage of mm-wave communications, the control channels are implemented in micro-wave communication band while data channels are transmitted in mm-wave communication band for the sake of the connectivity and mobility management.

3.4.1 Routing in Multi-Hop HetSNets

In dense urban areas, a large number of small cells may be deployed closely in HetSNets. There are backhaul connections among the SeNBs via mm-wave radio. The backhaul between the SeNBs and their donor MeNB can be via either mm-wave radio or wired links, depending on the deployment scenarios. In such a network, the nodes can cooperate with each other, providing improved reliability, enhanced coverage, and reduced equipment costs. Compared with mobile ad hoc networks, route recovery or energy efficiency is not a major concern for multi-hop HetSNets due to limited mobility and the existence of power supply at the eNBs. Moreover, there is almost no interference between mm-wave signals due to the narrow beamform with large gains. In other words, the channels for connecting the SeNBs can be regarded as orthogonal so that no channel assignment is needed. However, each channel has its own propagation characteristics, and the network topology is determined by the deployment scenario. Therefore, how to design an efficient routing protocol becomes one of the key challenges in multi-hop HetSNets.

When designing the routing scheme, there are several objectives that need to be taken into account, e.g., increasing system throughput, decreasing the end-to-end delay, achieving a good load balance and so on. Thus, much attention is paid to how to obtain a reliable quantitative routing metric, which can link several factors (such as system throughput, end-to-end delay, and connectivity) with the quality of the routing scheme. In general, we can define such a metric as a function of N influence factors I_j, i.e., $\gamma = f(I_1, I_2, \cdots, I_N)$. For example, there are two QoS factors that mainly affect the routing performance, i.e., the end-to-end delay τ and the packet loss rate η of the path. Then, the routing metric can be defined as a linear

weighted sum of the influence factors, i.e., $\gamma = (1-\beta)\tau + \beta\eta$, which determines the importance of the delay relative to the loss rate and where β is the weighting coefficient.

Most existing routing algorithms are based on the minimum hop count, which is not of interest in this section. Instead, through guaranteeing some end-to-end QoS requirements, QoS routing algorithms with specific routing metrics become much more promising in future broadband wireless communications networks. Queue theory is a good theoretical tool to solve QoS related problems. In a multi-hop wireless network, not only the traffic arrival process but also the variation of the wireless channel can be modelled by a completed tandem queuing framework [12]. The queuing dynamics of nodes in a given path determines the end-to-end QoS metrics including the delay and the loss rate, which have to be measured timely in order to enable the routing algorithm to adapt to the changes of the network in time. The end-to-end delay is the sum of the delays that any packet experiences in all the queues and links along its routing path. Packets may be lost due to buffer overflow in one of the queues in tandem.

As shown in Fig. 3.2, a number of consecutive time slots form a fixed-sized time frame, where the time slots in each time frame are periodically allocated to some transmission links. Representing one hop, each link may be allocated time slots in each time frame with different spatial orthogonal channels formed by mm-wave beamforming signals. Figure 3.4 presents an example of a possible path from an SeNB to the MeNB and its corresponding tandem queue. Data traffic entering each queue may come from different connections. Traffic from connections other than the considered connection may come and leave the tandem system in any queue. In other words, in each queue of the tandem system (except for *Queue* 1), either new or forwarding traffic arrives, while the buffered traffic is leaving. There are K single queues along the route. The arrival traffic to each queue is from the previous queue of the tandem system and from other connections traversing the corresponding link (except for *Queue* 1). Given the allocated radio resources for each link along the tandem system, we can determine the service rate. Thus, if the arrival probability for the aggregate traffic is determined, the queuing performance measures for each queue in the tandem system can be calculated.

Assume that all the end-to-end performance measures for a general tandem system of queues with an arbitrary number of hops can be found. Then, the tandem queuing model can be applied to find a path of connections from a source node to its desired destination node so that the end-to-end QoS requirements for the connection can be satisfied. Given an optimization objective, e.g., minimizing the end-to-end delay, the best feasible route can be possibly found by exhaustive search over all the possible routes. However, this approach results in a very large amount of signaling overhead and prohibitively high computational complexity. Therefore, investigating new routing schemes with the tandem queuing model in consideration of feasible implementation complexity becomes one of the challenges in the study of the multi-hop HetSNets with mm-wave communications.

Moreover, the route information of HetSNets can be updated periodically in the control channel to keep track of the changes in the topology and traffic load of the

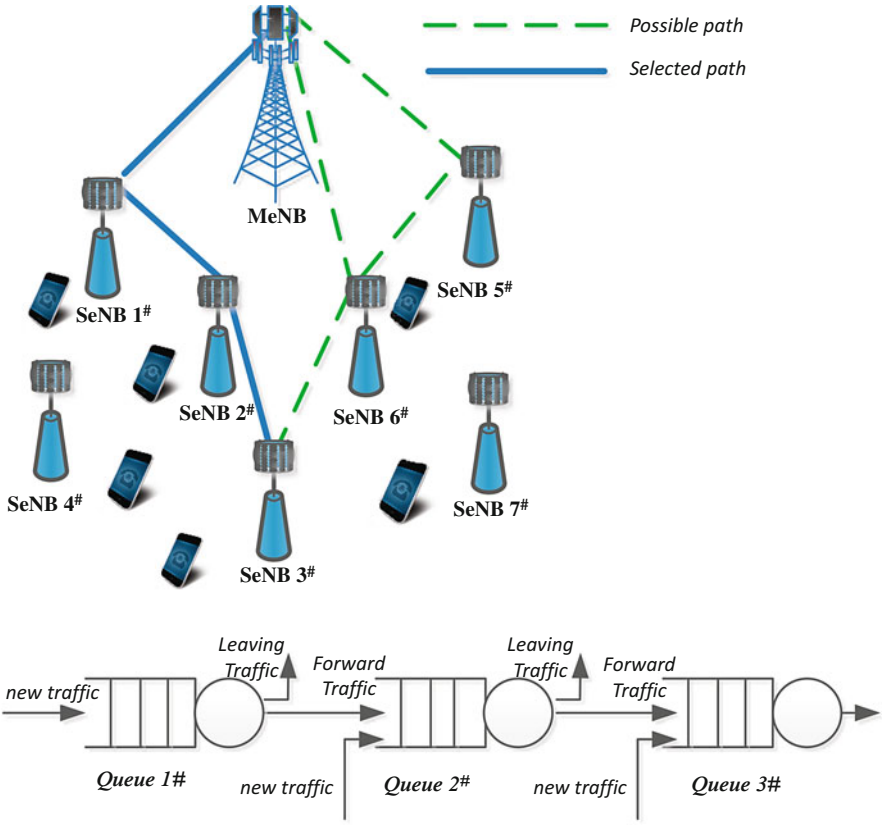

Fig. 3.4 A routing example in multi-hop HetSNets

network. To reduce the control overhead and delay, hierarchical routing schemes may be applied in HetSNets. Several neighboring SeNBs can be grouped together into a cluster. Then, the routing can be performed either intra-cluster or inter-cluster, depending on service requirements.

3.4.2 Access Control and Interference Coordination

Thanks to the narrow beam in massive MIMO with mm-wave radio, spectral resources can be easily reused spatially. The interference among various links and cells in HetSNets with mm-wave communications becomes much simpler than that with only micro-wave radio. However, since multi-hop transmission is allowed and each eNB works in the half-duplex mode, the interference between the downlink and uplink has to be first avoided via interference coordination among the eNBs in the time domain. Since the signal strength deteriorates rapidly in the mm-wave

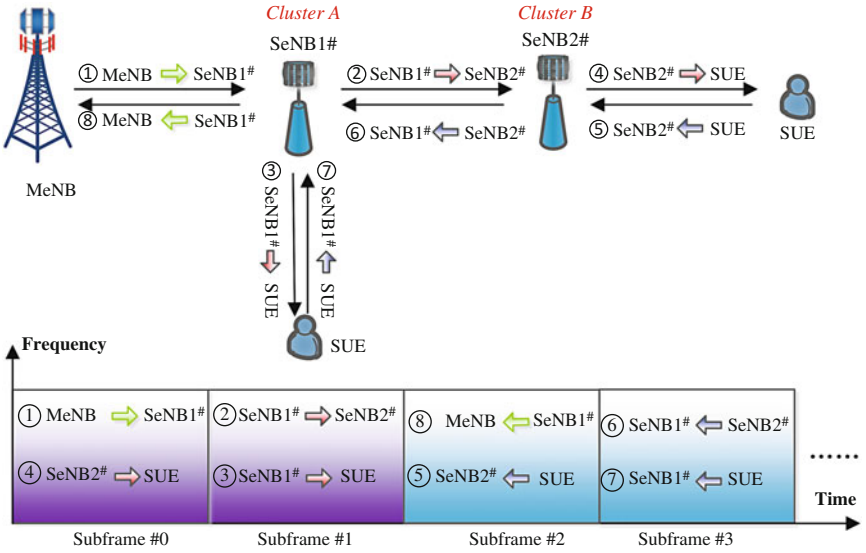

Fig. 3.5 Illustration of radio resources allocation in multi-hop HetSNets

band, more than one eNB can transmit simultaneously if they are not very close to each other. Thus, all the SeNBs are grouped into clusters according to the distances not only between themselves but also to their donor MeNB. The eNBs in the same cluster cannot transmit simultaneously, whereas those in different clusters can if the distance between the clusters is large enough. As illustrated in Fig. 3.5, the MeNB and SeNB 1# belong to *Cluster A*, while SeNB 2# is in *Cluster B* because it is a little far from the MeNB. Assuming that the configuration in Fig. 3.3 is adopted in the system, the MeNB establishes downlink backhaul transmission with SeNB 1# in subframe 0, while SeNB 2# serves its SUEs also in this subframe. In subframe 1, SeNB1 transmits signals to both its SUEs and SeNB 2# distinguished by narrow beams, while MeNB remains silent. A similar procedure is performed in subframes 2 and 3. Thus, by properly grouping all the SeNBs, the interference can be avoid between the downlink and uplink in the HetSNet with mm-wave communications.

Since the interference between the eNBs can be nearly eliminated through beamforming, neither intra-cell nor inter-cell coordination is necessary on the downlink. In other words, each eNB can reuse all the spectral resources. As shown in Fig. 3.5, due to the limitation of SUEs, distinguishing uplink signals cannot rely only on the spatial domain. In subframe 2, there is almost no interference between the access link from SUE to SeNB 2# and the backhaul link from SeNB 1# to MeNB due to spatial reuse. However, the signals from SUEs without beamforming arrive at SeNB 1# simultaneously in subframe 3 as well as the wireless backhaul signal sent from SeNB 2#. They may interfere with each other if no action is taken. A feasible way to avoid possible interference is to make the signals orthogonal in the frequency domain. Since the beamformer with large gains can still be used for the backhaul

link, much less spectral resources are needed for the backhaul link of SeNB 2# to SeNB 1# than the access link from SUEs to SeNB 1#. Moreover, if there are more than one SeNB in Cluster A, the uplink interference between the access links of the small cells can be coordinated by specific soft-frequency reuse schemes.

3.4.3 Mm-Wave Softcell Concept

Although dense small cells can facilitate geographic spectrum reusability, their small cell size may cause overly frequent handover. Consequently, it is imperative to introduce mechanisms for mobility management in HetSNets with mm-wave radio. Motivated by the soft cell concept [5], the control channels are provided by the MeNB with micro-wave communications, while high date rate services are supported by the SeNBs with mm-wave communications in the small cells simultaneously, i.e., separated C-plane/U-plane configuration. Also, the MeNB mainly ensures wide-area coverage so as to maintain good connectivity and mobility. One of the carriers in the micro-wave bands is selected as the anchor carrier, in which the system and control signaling information are sent by the MeNB. When the control channels in the anchor carrier work normally, the SeNBs do not send cell-specific signals/channels, such as Primary/Secondary Synchronization Signals (PSS/SSS), Cell Specific Reference Signals (CRS), etc. However, the resources for the control channels are reserved in the small cells and become active in the event of emergency, which is managed by the MeNB under the master-slave mode. Usually, the Radio Resource Control (RRC) connection procedures such as channel establishment and release between the SUEs and the SeNBs are controlled by the MeNB through the anchor carrier.

One of the most important benefits of the separation between C-plane and U-plane lies in its robustness to handover. There is no handover when a UE moves from one small cell to another within the coverage of the MeNB. Meanwhile, the requirements on the RRC messages can be relaxed because of the low handover probability between the macro cells. Also, energy efficiency can be improved by the separated C-plane/U-plane configuration in a massive deployment of small cells. For example, some SeNBs can be turned off when there are no serving SUEs. However, this requires new features of the UEs. Dual transmit channels and MAC entities in both the micro-wave and mm-wave carriers have to be supported in the UEs. Then, all the carriers can be measured and discovered rapidly.

3.5 Performance and Discussions

System-level simulations are carried out to evaluate the system performance of HetSNets with mm-wave communication in the downlink in this section. Detailed simulation parameters including the channel model and system assumptions are

Table 3.1 Parameters assumption in HetSNets with mm-wave communication

Parameters		Values
Carrier frequency /bandwidth (micro-wave)		2 GHz/ 10 MHz
Carrier frequency /bandwidth (mm-wave)		28 GHz/ 200 MHz
MeNB inter-site distance (ISD)		500 m
Cellular layout		Hexagonal grid/19 sites/3 sectors per sites
Small cell deployment		2, 4, 10 SeNBs per sector
UE density		60 UEs per site
Total MeNB Tx power		46 dBm
Total SeNB Tx power		37 dBm
MeNB antenna configuration		2
SeNB antenna configuration		10×8 area array
UE antenna configuration		1
Noise figure at UE		9 dB
Thermal noise density		-174 dBm/Hz
Penetration loss (mm-wave)		100 dB
Shadowing standard deviation		8 dB micro-wave / 12 dB mm-wave
Pathloss	Micro-wave	$128.1 + 37.6 \log(R)$, R in km
	mm-wave	$157.4 + 32 \log(R)$, R in km [4]

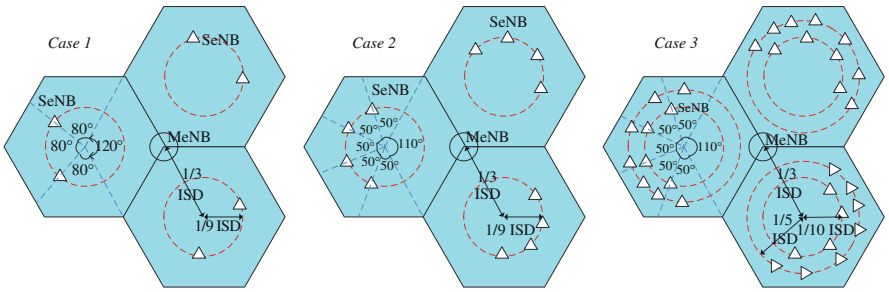

Fig. 3.6 SeNB deployment

summarized in Table 3.1, most of which are defined in the 3GPP specifications [13]. All the UEs are evenly distributed in circular areas around each eNB.

As shown in Fig. 3.6, we consider densely populated areas, where there are multiple SeNBs deployed in each sector. How to place the SeNBs may significantly affect the performances of the HetSNets. Usually the SeNBs are placed as close as possible to the cell edge, while a qualified backhaul link can be maintained by a high-gain beam. Also, enough distances between each SeNB should be maintained in order to avoid too much interference among each other. Then, in our simulations for *Case 1* and *Case 2*, i.e., 2 or 4 SeNBs per sector, respectively, as illustrated in Fig. 3.6, the SeNBs are placed on the circles around the centers of the hexagons with a radius of 1/9 ISD in consideration of the cell edge priority. In *Case 3*, i.e., 10 SeNBs per sector, the SeNBs are placed in two two-tier circles, with radius

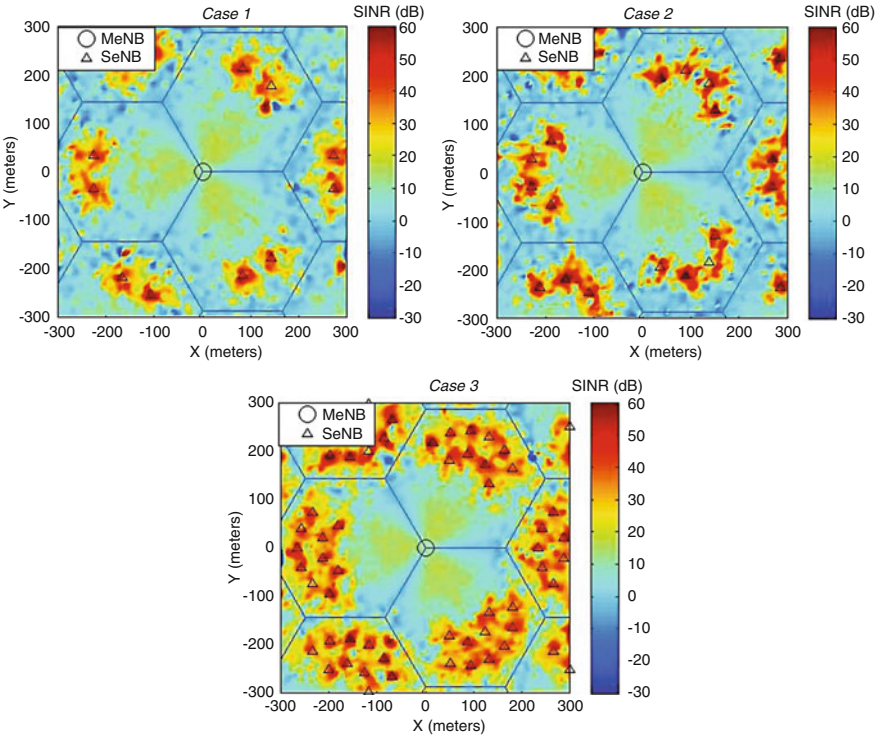

Fig. 3.7 SeNB deployment

of 1/10 ISD and 1/5 ISD for the inner and outer circle, respectively. Each SeNB can independently schedule its connected UEs according to certain channel-aware scheduling algorithm on the mm-wave frequency band. A small number of SUEs may occupy the entire mm-wave frequency band, resulting in very high data rate transmission.

Figure 3.7 presents the spatial characteristics of the SINR of HetSNets under different cases. Different colors represent different throughput values; e.g., the area with the red color has higher SINR than that with the green or blue color. It is clear that there are much more areas with the red color in *Case 2* and *Case 3* than that in *Case 1*. So the SINR performances are dramatically increased by deploying more number of SeNBs. However, such improvement is more obvious in *Case 2* than in *Case 3*. When a large number of SeNBs with full frequency reuse among cells are deployed, e.g., 10, the close distance between the SeNBs may cause interference and decrease the SINR even with the narrow beam transmission in the mm-wave frequency band.

The performances including the average SUE throughput and the aggregate throughput of small cells in the networks under different cases are compared in Table 3.2. In *Case 1*, only 21.7% of all UEs are served by the SeNBs with the

Table 3.2 Performance comparisons in HetSNets under difference cases

	Average throughput per SUE (Mbps)	Average number of SUEs per cell	Ratio of SUEs/all UEs	Total cell throughput (Gbps)
Case 1	333.50	13	21.7%	4.34
Case 2	544.59	23	38.8%	7.67
Case 3	427.94	32	53.3%	13.69

average throughput per SUE of 333.5 Mbps due to the sparse deployment. With the increase of SeNBs deployed, more UEs choose to connect to the SeNBs with single or multihop transmission, i.e., 38.8% and 53.3% of all UEs in *Case 2* and *Case 3*, respectively, since there is shorter distance between SeNBs and UEs. Meanwhile, more small cells means that the same frequency resources can be more frequently reused with the aid of beamforming techniques. So, not only the average throughput per SUE but also the total throughput are rapidly increased. Moreover, in this way, more severe co-channel interference due to close distance is caused while a higher frequency reuse factor is adopted. So, the average throughput per SUE is little decreased in *Case 3* than that in *Case 2*. However, because much more UEs may access the network through their nearby SeNBs in *Case 3* than in *Case 2*, the total throughput performance continues to be improved when the number of SeNBs increase from 4 to 10, i.e., 13.69 Gbps, almost double of that in *Case 2*.

3.6 Summary

HetSNets with mm-wave massive MIMO will be integral to meeting the requirements of future 5G wireless communications. Due to the vast spectral resources of mm-wave radios, users will enjoy unprecedented services with almost wire-like user experience. We thus investigated the feasibility of mm-wave communications with massive MIMO in HetSNets under various deployment scenarios, and proposed backwards-compliant frame structures. This allowed us to address several of the important challenges related to mm-wave communications, and achieve total cell throughput of almost 14 Gbps, i.e., an order of magnitude more than the current Gbps-design [14].

With the development of physical layer techniques of mm-wave communication with massive MIMO, the fundamental knowledge about mm-wave communication become more solid. Then, future research on HetSNets with mm-wave communications will be conducted based on a tight coupling of the unique characteristics of mm-wave communications, massive MIMO and wireless heterogeneous networks. Specifically, the loss due to propagation characteristics at the mm-wave band should be compensated for at an acceptable cost with massive MIMO. In addition, radio resources management in HetSNets has to be adjusted to make use of the high-gain and narrow beamforming in mm-wave communications.

References

1. Scenarios, requirements and KPIs for 5G mobile and wireless system, Tech. Rep. ICT-317669-METIS/D1.1 (2013)
2. F. Boccardi, J.R.W. Heath, A. Lozano, T.L. Marzetta, P. Popovski, Five disruptive technology directions for 5G. IEEE Commun. Mag. **52**(2), 74–80 (2014)
3. E.G. Larsson, F. Tufvesson, O. Edfors, T.L. Marzetta, Massive MIMO for next generation wireless systems. IEEE Commun. Mag. **52**(2), 186–195 (2014)
4. Z. Pi, F. Khan, A millimeter-wave massive MIMO system for next generation mobile broadband, in *IEEE Signals, Systems and Computers (ASILOMAR)*, 2012, pp. 693–698
5. D. Astely, E. Dahlman, G. Fodor, S. Parkvall, J. Sachs, LTE release 12 and beyond. IEEE Commun. Mag. **51**(7), 154–160 (2013)
6. T.S. Rappaport, S. Sun, R. Mayzus, H. Zhao, Y. Azar, K. Wang, G.N. Wong, J.K. Schulz, M. Samimi, F. Gutierrez, Millimeter wave mobile communications for 5G cellular: it will work! IEEE Trans. Commun. **1**, 335–349 (2013)
7. C.E. Yonina, K. Gitta, *Compressed Sensing: Theory and Applications* (Cambridge University Press, New York, 2012)
8. H. Yin, D. Gesbert, M. Filippou, Y. Liu, A coordinated approach to channel estimation in large-scale multiple-antenna systems. IEEE J. Sel. Areas Commun. **31**(2), 264–273 (2013)
9. H.Q. Ngo, E.G. Larsson, EVD-based channel estimations for multicell multiuser MIMO with very large antenna arrays, in *Proceedings of IEEE International Conference on Acoustics, Speed and Signal Processing (ICASSP)*, Kyoto, 2012, pp. 3249–3252
10. A. Ashikhmin, T.L. Marzetta, Pilot contamination precoding in multi-cell large scale antenna systems, in *Proceedings of IEEE International Symposium on Information Theory (ISIT)*, Cambridge, MA, July 2012, pp. 1137–1141
11. S. Hur, T. Kim, D.J. Love, J.V. Krogmeier, T.A. Thomas, A. Ghosh, Millimeter-wave beamforming for wireless backhaul and access in small cell networks. IEEE Trans. Commun. **61**(10), 4391–4403 (2013)
12. L. Le, E. Hossain, Tandem queue models with applications to QoS routing in multihop wireless networks. IEEE Trans. Mobile Comput. **7**(8), 1025–1040 (2008)
13. Evolved universal terrestrial radio access (E-UTRA), Tech. Rep. 3GPP TR 36.814, V9.0.0 (2010)
14. P. Blasco, L. Giupponi, A. Galindo-Serrano, M. Dohler, Aggressive joint access and backhaul design for distributed-cognition 1Gbps/km2 system architecture, in *Proceedings of International Conference on Wired/Wireless Internet Communications (WWIC)*, Lulea (2010), pp. 1–3

Chapter 4
Massive MIMO-Assisted Energy Transfer Technology

This chapter considers a downlink massive MIMO system, where the base station simultaneously sends information and energy to information users and energy users, respectively. The aim is to maximize the minimum harvested energy among the energy users while meeting the rate requirements of information users. With perfect CSI, the problem is solved by obtaining the asymptotically optimal power allocation of information users and the combination coefficients of the energy precoder. For the CSI estimation in time-division duplex systems, orthogonal pilot sequences are employed by information users during the uplink, and one common pilot sequence is shared by all energy users. It is shown that the energy harvesting performance of such a shared pilot scheme is always better than that of the orthogonal pilot scheme. Further, exploiting the inter-cell interference in multi-cell systems, a joint precoder is proposed for cooperative energy transfer, for which both the centralized and distributed implementations are given. Results indicate that the cooperative energy transfer always outperforms the non-cooperative scheme with either perfect or estimated CSI.

4.1 Background

Wireless energy transfer has been studied for several decades, and can be classified into three types, namely the near-field coupling based on inductive coils, laser beaming and the long-distance transfer based on Radio-Frequency (RF) [1–3]. The first type operates within a distance on the order of wavelength and can achieve an efficiency up to 70% [1, 2]. Some technological obstacles still prevent the practical applications of the second type [2]. The third type is considered as a promising technique for prolonging the lifetime of users' batteries and also for cutting the last mile limiting the "true wireless" communications [3]. There are two RF-based energy transfer scenarios. One is that ambient energy is opportunistically harvested

L. Zhao et al., *Massive MIMO in 5G Networks: Selected Applications*,
SpringerBriefs in Electrical and Computer Engineering,
https://doi.org/10.1007/978-3-319-68409-3_4

and the other is that a dedicated energy source transfers energy to charge users' batteries [1, 3]. The latter together with the wireless information transmission constitute the Hybrid information and Energy Transfer (HIET), which is the focus of this chapter.

Currently, there are four main HIET schemes, namely power splitting, time switching, FDMA and Spatial Division Multiple Access (SDMA) [4–7]. They transfer information and energy by exploiting different types of resources, such as power, time, frequency and space, respectively. Power splitting and time switching are receiver techniques to separate energy and information, and can be considered as complimentary to FDMA and SDMA schemes. Considering the scarcity of frequency resources, the SDMA scheme is more practical for future HIET systems and is considered in this work. SDMA based on MIMO technology has been realized in practical communication systems [8], which can significantly improve the spectrum efficiency, energy efficiency and reliability [9]. In order to scale up these advantages, massive MIMO with hundreds of antennas has been proposed [10–13]. As the extremely narrow beam of massive MIMO can focus energy on the targeted users, the efficiency or distance of energy transfer can potentially be significantly increased [2, 9, 14]. For example, it has been reported that the 20000-antenna COTA system could provide 1 W power to users that are about 10 m away [15].

Assuming that the uplink information transmission is powered by the downlink harvested energy, an energy efficiency optimization problem was treated under the massive MIMO setup in [16]. Taking the interval of uplink pilot transmission into account, the allocation of time slots for uplink pilot transmission, downlink energy transfer and uplink information transmission was studied to maximize the throughput of uplink information transmission in [7]. In order to estimate the channels of users at the Base Station (BS), orthogonal pilot sequences are typically employed by different energy users in existing works [7, 15–18]. However, this will reduce the number of information users in the system, as the total number of orthogonal pilot sequences is fixed [10, 12, 13]. Moreover, although the inter-cell interference can benefit the energy harvesting in the multi-cell scenario [19], how to efficiently exploit the interference for energy transfer is less studied compared with the information transmission.

In this chapter, we consider a downlink HIET system with massive MIMO, where the BS simultaneously transmits information and energy to information users and energy users, respectively. With the total power constraint, the goal is to maximize the minimum harvested energy among energy users, while meeting the rate requirements of information users. The MF precoder is employed for both information and energy transfer, since it is asymptotically optimal with massive MIMO. As the energy users only harvest energy and do not demodulate the received signals, the same symbol can be transmitted to all energy users. Then, the optimal energy precoder becomes the linear combination of the channels of energy users. Therefore, with perfect CSI, we solve the problem by obtaining the power allocation for information users and the combination coefficients for energy precoder. Further, in order to construct the energy precoder with estimated CSI in the TDD system, the BS only needs to estimate the combination channel of energy users. Therefore,

the same pilot sequence can be shared by all energy users during the uplink (By contrast, orthogonal pilot sequences are still transmitted by different information users). The combination coefficients of energy precoder determine the downlink power allocation for energy users and are indirectly controlled by the pilot power of uplink. Therefore, apart from the power allocation for information users, the pilot power of uplink is derived for the care of estimated CSI. Results indicate the energy harvesting performance of such a shared pilot scheme is always better than that of the orthogonal pilot scheme. Moreover, we also consider the multi-cell scenario, and design both centralized and distributed energy precoders to exploit the inter-cell interference for cooperative energy transfer. Compared with the non-cooperative scheme, the cooperative scheme significantly improves the efficiency of energy transfer with either perfect or estimated CSI.

4.2 Downlink Hybrid Information and Energy Transfer

4.2.1 Downlink HIET System Model

Consider a downlink HIET system, as shown in Fig. 4.1, where one BS employing M antennas simultaneously sends information to K_{I} single-antenna information users and sends energy to K_{E} single-antenna energy users. The total number of users is

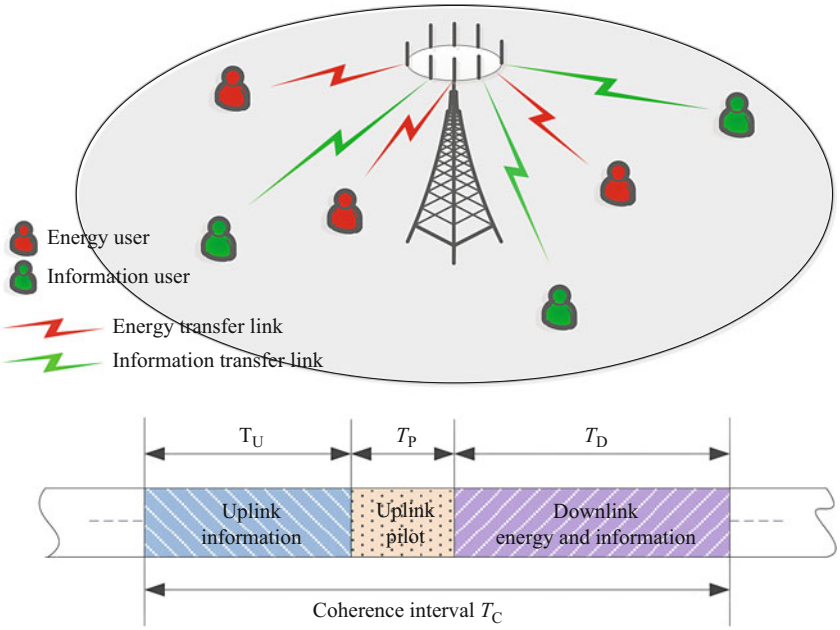

Fig. 4.1 System model of downlink hybrid information and energy transfer

$K = K_{\mathrm{E}} + K_{\mathrm{I}}$. The system operates in a TDD mode due to the shortage of pilot sequences for the downlink in FDD mode [9]. On the uplink, the users send data and pilot sequences to the BS during intervals T_{U} and T_{P}, respectively. Then, the uplink channels can be estimated at the BS. By channel reciprocity, the BS obtains the downlink channels and then forms the precoders for information and energy transmission during the interval T_{D} of downlink.

4.2.1.1 Channel Model

Denote $\mathbf{g}_{\psi k} = \theta_{\psi k}^{1/2}\mathbf{h}_{\psi k} \in \mathbb{C}^{M\times 1}$ $\left(k = 1, 2, \cdots, K_{\psi}; \psi \in \{\mathrm{E}, \mathrm{I}\}\right)$ as the channel vector from the kth ψ user to the BS, where $\theta_{\psi k}$ is the large-scale fading coefficient that incorporates the path loss and the shadowing effect, and $\mathbf{h}_{\psi k} = \left[h_{\psi k1}, h_{\psi k2}, \cdots, h_{\psi kM}\right]^{\mathrm{T}}$ contains the fast fading variables. All fast fading variables are i.i.d. complex Gaussian random variables with mean 0 and variance 1, namely $h_{\psi km} \overset{\text{i.i.d.}}{\sim} \mathbb{CN}(0, 1)$.

4.2.1.2 Transmitter

The MF precoders are asymptotically optimal for information users and thus employed in the massive MIMO downlink [10, 13], namely $\mathbf{W}_{\mathrm{I}} = [\mathbf{w}_{\mathrm{I}1}, \cdots, \mathbf{w}_{\mathrm{I}K_{\mathrm{I}}}]$ with

$$\mathbf{w}_{\mathrm{I}k} = \frac{\mathbf{g}_{\mathrm{I}k}^{*}}{\left\|\mathbf{g}_{\mathrm{I}k}^{*}\right\|}, \ k = 1, 2, \cdots, K_{\mathrm{I}}. \tag{4.1}$$

Given the symbol vector $\mathbf{s}_{\mathrm{I}} = [s_{\mathrm{I}1}, \cdots, s_{\mathrm{I}K_{\mathrm{I}}}]^{\mathrm{T}} \in \mathbb{C}^{K_{\mathrm{I}}\times 1}$ with $\mathbb{E}\left[\mathbf{s}_{\mathrm{I}}\mathbf{s}_{\mathrm{I}}^{\mathrm{H}}\right] = \mathbf{I}_{K_{\mathrm{I}}}$, the transmitted signal for the information users is given by

$$\mathbf{x}_{\mathrm{I}} = \mathbf{W}_{\mathrm{I}}\mathrm{diag}^{1/2}\left\{\frac{\mathbf{p}}{M}\right\}\mathbf{s}_{\mathrm{I}}, \tag{4.2}$$

where the power allocation vector $\frac{\mathbf{p}}{M} = \frac{1}{M}[p_1, p_2, \cdots, p_{K_{\mathrm{I}}}]^{\mathrm{T}}$ and thus the total power for information users $\frac{p_{\mathrm{I}}}{M} = \frac{1}{M}\mathbf{1}^{\mathrm{T}}\mathbf{p}$. Keeping p_{I} constant, the denominator M ensures that the power of received signal is constant and does not tend to infinity with increasing M [10, 11].

On one hand, the MF precoder is the optimal precoder for energy transfer [5, 7]. On the other hand, the energy users only harvest energy and do not demodulate the received signals, therefore different energy users can share the same symbol s_{E} with $|s_{\mathrm{E}}| = 1$. Then the precoder for energy transfer can be written as

$$\mathbf{w}_{\mathrm{E}} = \sum_{k=1}^{K_{\mathrm{E}}} \alpha_k \mathbf{g}_{\mathrm{E}k}^{*}, \tag{4.3}$$

where $[\alpha_1, \alpha_2, \cdots, \alpha_{K_\mathrm{E}}]^\mathrm{T} \triangleq \boldsymbol{\alpha}$ contains the combination coefficients such that $\|\mathbf{w}_\mathrm{E}\| = 1$. The transmitted signal for the energy users is then given by

$$\mathbf{x}_\mathrm{E} = \mathbf{w}_\mathrm{E} \sqrt{\frac{p_\mathrm{E}}{M}} s_\mathrm{E}, \tag{4.4}$$

where $\frac{p_\mathrm{E}}{M}$ is the total power for energy users and the denominator M is used to keep the power of received signal constant.

4.2.1.3 Receiver

The received signal by the kth ψ user can be written as

$$y_{\psi k} = \mathbf{g}_{\psi k}^\mathrm{T} (\mathbf{x}_\mathrm{E} + \mathbf{x}_\mathrm{I}) + n_{\psi k}, \ k = 1, 2, \cdots, K_\psi, \tag{4.5}$$

where $n_{\psi k}$ is the i.i.d. additive white Gaussian noise with mean 0 and variance σ_ψ^2.

The harvested energy by the kth energy user is given by

$$\mathscr{E}_k (p_\mathrm{E}, \mathbf{p}, \boldsymbol{\alpha}) = \eta T_\mathrm{D} \mathbb{E} \left[\left| \mathbf{g}_{\mathrm{E}k}^\mathrm{T} \mathbf{x}_\mathrm{E} \right|^2 + \left| \mathbf{g}_{\mathrm{E}k}^\mathrm{T} \mathbf{x}_\mathrm{I} \right|^2 + |n_{\mathrm{E}k}|^2 \right], \tag{4.6}$$

where $\eta \in [0, 1]$ denotes the energy conversion efficiency that depends on the rectification process and the energy harvesting circuit [20, 21].

Note that since a constant symbol is transmitted for all energy users and is known to the information users, then $\mathbf{x}_\mathrm{E}$ in (4.5) can be subtracted from $y_{\mathrm{I}k}$ through interference cancellation [22]. The ergodic rate of the kth information user is then given by

$$r_k (\mathbf{p}, \boldsymbol{\alpha}) = \mathbb{E} \left\{ \log_2 \left[1 + \rho_k (\mathbf{p}, \boldsymbol{\alpha}) \right] \right\}, \tag{4.7}$$

where ρ_k is the signal-to-interference-plus-noise ratio (SINR) of the kth information user, given by

$$\rho_k = \frac{\frac{p_k}{M} \left| \mathbf{g}_{\mathrm{I}k}^\mathrm{T} \frac{\mathbf{g}_{\mathrm{I}k}^*}{\|\mathbf{g}_{\mathrm{I}k}^*\|} \right|^2}{\sum\limits_{l=1, \neq k}^{K_\mathrm{I}} \frac{p_l}{M} \left| \mathbf{g}_{\mathrm{I}k}^\mathrm{T} \frac{\mathbf{g}_{\mathrm{I}l}^*}{\|\mathbf{g}_{\mathrm{I}l}^*\|} \right|^2 + \sigma_\mathrm{I}^2}. \tag{4.8}$$

Recall that $\mathbf{g}_{\mathrm{I}k} = \sqrt{\theta_{\mathrm{I}k}} \mathbf{h}_{\mathrm{I}k}$. In the sequel, we will make use of ρ_k^{-1}, given by

$$\rho_k^{-1} = \frac{M}{p_k} \left(\sum_{l=1, \neq k}^{K_\mathrm{I}} \frac{p_l}{M} \left| \frac{\mathbf{h}_{\mathrm{I}k}^\mathrm{T}}{\|\mathbf{h}_{\mathrm{I}k}^\mathrm{T}\|} \frac{\mathbf{h}_{\mathrm{I}l}^*}{\|\mathbf{h}_{\mathrm{I}l}^*\|} \right|^2 + \frac{2\sigma_\mathrm{I}^2}{\theta_{\mathrm{I}k}} \frac{1}{2 \|\mathbf{h}_{\mathrm{I}k}^\mathrm{T}\|^2} \right). \tag{4.9}$$

According to [23–25], we have the following distributions

$$\left| \frac{\mathbf{h}_{\mathrm{I}k}^{\mathrm{T}}}{\left\| \mathbf{h}_{\mathrm{I}k}^{\mathrm{T}} \right\|} \frac{\mathbf{h}_{\mathrm{I}l}^{*}}{\left\| \mathbf{h}_{\mathrm{I}l}^{*} \right\|} \right|^2 \sim \beta \left(1, M-1\right), \ l \neq k, \tag{4.10}$$

$$\frac{1}{2\left\| \mathbf{h}_{\mathrm{I}k}^{\mathrm{T}} \right\|^2} \sim \chi^{-1}\left(2M\right), \tag{4.11}$$

and they are independent of each other.

4.2.2 Power Allocation Problem for HIET Systems

Given the total transmit power $\frac{p_{\mathrm{T}}}{M}$ at the BS, our aim is to guarantee the data rates of information users and in the meantime transfer energy to the energy users fairly. Assuming that the average rate requirements of all information users are $\bar{\mathbf{r}} = [\bar{r}_1, \bar{r}_2, \cdots, \bar{r}_{K_{\mathrm{I}}}]^{\mathrm{T}}$, we have the following problem

$$\begin{aligned} &\max_{p_{\mathrm{E}}, \mathbf{p}, \boldsymbol{\alpha}} \min_{k} \left\{ \mathscr{E}_k \left(p_{\mathrm{E}}, \mathbf{p}, \boldsymbol{\alpha}\right) \right\} \\ \text{s.t.} \ \ &r_k \left(\mathbf{p}, \boldsymbol{\alpha}\right) \geq \bar{r}_k, \ k = 1, 2, \cdots, K_{\mathrm{I}}, \\ &\mathbf{1}^{\mathrm{T}}\mathbf{p} + p_{\mathrm{E}} \leq p_{\mathrm{T}}. \end{aligned} \tag{4.12}$$

As the CSI affects both the information rate and the harvested energy, we will solve this problem under perfect CSI and estimated CSI, respectively, in the following two sections.

4.3 Power Allocation of Single Cell Scenario

4.3.1 Power Allocation with Perfect CSI

According to (4.7)–(4.8), the ergodic rates of information users are not affected by the signals for energy users. Therefore we solve the problem in (4.12) in two steps. First, we allocate power to information users based on their rate requirements. Then, the residual power is allocated to energy users.

4.3.1.1 Power Allocation for Information Users

As the function $\log_2(1+1/x)$ is convex, using Jensen's inequality [26], we can lower bound the rate in (4.7) as

$$r_k \geq \log_2\left(1+\frac{1}{\mathbb{E}\left[\rho_k^{-1}\right]}\right) \triangleq r_k^{\mathrm{L}}. \tag{4.13}$$

Substituting the expectations $\mathbb{E}[\beta(1,M-1)] = \frac{1}{M}$ and $\mathbb{E}\left[\chi^{-1}(2M)\right] = \frac{1}{2M-2}$ into (4.9), we obtain

$$\mathbb{E}\left[\rho_k^{-1}\right] = \frac{1}{p_k}\left(\frac{p_{\mathrm{I}}-p_k}{M}+\frac{M}{M-1}\frac{\sigma_{\mathrm{I}}^2}{\theta_{\mathrm{I}k}}\right). \tag{4.14}$$

Note that, when $M\to\infty$, we have $\mathbb{E}\left[\rho_k^{-1}\right]\to\frac{\sigma_{\mathrm{I}}^2}{p_k\theta_{\mathrm{I}k}}$. On the other hand, for $M\to\infty$ [27, 28]:

$$\frac{1}{M}\mathbf{h}_{\mathrm{I}k}^{\mathrm{T}}\mathbf{h}_{\mathrm{I}l}^{*}\to 0, l\neq k, \tag{4.15}$$

$$\frac{1}{M}\left\|\mathbf{h}_{\mathrm{I}k}\right\|^2\to 1. \tag{4.16}$$

Hence for $M\gg 1$, using (4.15)–(4.16) in (4.9), we have

$$\begin{aligned}\rho_k^{-1} &= \sum_{l=1,\neq k}^{K_{\mathrm{I}}}\frac{p_l}{p_k}\frac{M}{\left\|\mathbf{h}_{\mathrm{I}k}^{\mathrm{T}}\right\|^2}\left|\frac{\mathbf{h}_{\mathrm{I}k}^{\mathrm{T}}\mathbf{h}_{\mathrm{I}l}^{*}}{M}\right|^2\frac{M}{\left\|\mathbf{h}_{\mathrm{I}l}^{*}\right\|^2}+\frac{\sigma_{\mathrm{I}}^2}{p_k\theta_{\mathrm{I}k}}\frac{M}{\left\|\mathbf{h}_{\mathrm{I}k}^{\mathrm{T}}\right\|^2}\\ &\to\frac{\sigma_{\mathrm{I}}^2}{p_k\theta_{\mathrm{I}k}}=\mathbb{E}\left[\rho_k^{-1}\right].\end{aligned} \tag{4.17}$$

That is, (4.13) is tight when the number of antennas M is large.

In order to meet the information users' rate requirements, we let $r_k^{\mathrm{L}}\geq\bar{r}_k$, i.e.,

$$p_k\geq\frac{p_{\mathrm{I}}+\frac{M^2}{M-1}\frac{\sigma_{\mathrm{I}}^2}{\theta_{\mathrm{I}k}}}{M\left(2^{\bar{r}_k}-1\right)^{-1}+1}, \tag{4.18}$$

then $r_k\geq r_k^{\mathrm{L}}\geq\bar{r}_k$. Taking advantage of $\sum_{k=1}^{K_{\mathrm{I}}}p_k = p_{\mathrm{I}}$, the total power for information users is given by

$$\frac{p_{\mathrm{I}}}{M}\geq\frac{M}{M-1}\frac{\sum_{k=1}^{K_{\mathrm{I}}}\frac{\sigma_{\mathrm{I}}^2}{\theta_{\mathrm{I}k}}\left[M\left(2^{\bar{r}_k}-1\right)^{-1}+1\right]^{-1}}{1-\sum_{k=1}^{K_{\mathrm{I}}}\left[M\left(2^{\bar{r}_k}-1\right)^{-1}+1\right]^{-1}}, \tag{4.19}$$

and the residual power for energy users is $\frac{1}{M}p_{\mathrm{E}}\leq\frac{1}{M}(p_{\mathrm{T}}-p_{\mathrm{I}})$.

Therefore, the problem (4.12) can be simplified into

$$\max_{\boldsymbol{\alpha}} \min_{k} \{\mathscr{E}_k(\boldsymbol{\alpha})\} \tag{4.20}$$
$$\text{s.t.} \quad \|\mathbf{w}_{\mathrm{E}}\|^2 = 1.$$

4.3.1.2 Power Allocation for Energy Users

Theorem 1 *Under the perfect CSI assumption, the optimal combination coefficients for the energy transfer precoder, i.e., the solution to problem (4.20) is given by*

$$\alpha_k = \frac{1}{M}\sqrt{\frac{1}{\theta_{\mathrm{E}k}p_{\mathrm{E}}}\left[\frac{Mp_{\mathrm{E}}+K_{\mathrm{E}}p_{\mathrm{T}}}{\theta_{\mathrm{E}k}}\left(\sum_{k=1}^{K_{\mathrm{E}}}\frac{1}{\theta_{\mathrm{E}k}}\right)^{-1}-p_{\mathrm{T}}\right]} \tag{4.21}$$

$$= \frac{1}{\theta_{\mathrm{E}k}}\sqrt{\frac{1}{M}\left(\sum_{k=1}^{K_{\mathrm{E}}}\frac{1}{\theta_{\mathrm{E}k}}\right)^{-1}+\mathscr{O}\left(\frac{1}{M}\right)}, k=1,2,\cdots,K_{\mathrm{E}}. \tag{4.22}$$

Hence for large M, the coefficient α_k is inversely proportional to the large-scale factor $\theta_{\mathrm{E}k}$, i.e., $\alpha_k \propto \frac{1}{\theta_{\mathrm{E}k}}$. And the harvested energies of all energy users are equal, given by

$$\mathscr{E} = \eta T_{\mathrm{D}}\left[\left(p_{\mathrm{E}}+\frac{K_{\mathrm{E}}}{M}p_{\mathrm{T}}\right)\left(\sum_{k=1}^{K_{\mathrm{E}}}\frac{1}{\theta_{\mathrm{E}k}}\right)^{-1}+\sigma_{\mathrm{E}}^2\right] \tag{4.23}$$

$$= \eta T_{\mathrm{D}}\left[p_{\mathrm{E}}\left(\sum_{k=1}^{K_{\mathrm{E}}}\frac{1}{\theta_{\mathrm{E}k}}\right)^{-1}+\sigma_{\mathrm{E}}^2\right]+\mathscr{O}\left(\frac{1}{M}\right). \tag{4.24}$$

Proof Making use of $\mathbb{E}\left[\left\|\mathbf{h}_{\mathrm{E}k}^{\mathrm{T}}\right\|^2\right] = M$, $\mathbb{E}\left[\left\|\mathbf{h}_{\mathrm{E}k}^{*}\right\|^4\right] = M(M+1)$ and $\mathbb{E}\left[\left|\frac{\mathbf{h}_{\mathrm{E}k}^{\mathrm{T}}}{\left\|\mathbf{h}_{\mathrm{E}k}^{\mathrm{T}}\right\|}\frac{\mathbf{h}_{\mathrm{E}i}^{*}}{\left\|\mathbf{h}_{\mathrm{E}i}^{*}\right\|}\right|^2\right] = \frac{1}{M}$, the first term in (4.6) can be written as

$$\mathbb{E}\left[\left|\mathbf{g}_{\mathrm{E}k}^{\mathrm{T}}\mathbf{x}_{\mathrm{E}}\right|^2\right] = p_{\mathrm{E}}\theta_{\mathrm{E}k}\left[\alpha_k^2\theta_{\mathrm{E}k}(M+1)+\sum_{i=1,\neq k}^{K_{\mathrm{E}}}\alpha_i^2\theta_{\mathrm{E}i}\right]. \tag{4.25}$$

Since for large M, $\frac{1}{M}\left\|\mathbf{h}_{\mathrm{E}k}^{*}\right\|^{2}=1=\frac{1}{M}\mathbb{E}\left[\left\|\mathbf{h}_{\mathrm{E}k}^{*}\right\|^{2}\right]$, we have

$$\left\|\mathbf{w}_{\mathrm{E}}\right\|^{2}=\mathbb{E}\left[\left\|\mathbf{w}_{\mathrm{E}}\right\|^{2}\right]=M\sum_{k=1}^{K_{\mathrm{E}}}\alpha_{k}^{2}\theta_{\mathrm{E}k}=1, M\gg 1. \tag{4.26}$$

Substituting (4.26) into (4.25) leads to

$$\mathbb{E}\left[\left|\mathbf{g}_{\mathrm{E}k}^{\mathrm{T}}\mathbf{x}_{\mathrm{E}}\right|^{2}\right]=p_{\mathrm{E}}\theta_{\mathrm{E}k}\left(\alpha_{k}^{2}\theta_{\mathrm{E}k}M+\frac{1}{M}\right). \tag{4.27}$$

In the same way, the second term in (4.6) can be derived as

$$\begin{aligned}\mathbb{E}\left[\left|\mathbf{g}_{\mathrm{E}k}^{\mathrm{T}}\mathbf{x}_{\mathrm{I}}\right|^{2}\right]&=\left(\frac{\theta_{\mathrm{E}k}}{2}\mathbb{E}\left[2\left\|\mathbf{h}_{\mathrm{E}k}^{\mathrm{T}}\right\|^{2}\right]\sum_{i=1}^{K_{\mathrm{I}}}\frac{p_{i}}{M}\mathbb{E}\left[\left|\frac{\mathbf{h}_{\mathrm{E}k}^{\mathrm{T}}}{\left\|\mathbf{h}_{\mathrm{E}k}^{\mathrm{T}}\right\|}\frac{\mathbf{h}_{\mathrm{I}i}^{*}}{\left\|\mathbf{h}_{\mathrm{I}i}^{*}\right\|}\right|^{2}\right]\right)\\&=\frac{\theta_{\mathrm{E}k}}{M}\sum_{i=1}^{K_{\mathrm{I}}}p_{i}=\frac{\theta_{\mathrm{E}k}p_{\mathrm{I}}}{M}.\end{aligned} \tag{4.28}$$

Substituting (4.27) and (4.28) into (4.6), we have

$$\mathscr{E}_{k}\left(\alpha_{k}\right)=\eta T_{\mathrm{D}}\left(M\alpha_{k}^{2}\theta_{\mathrm{E}k}^{2}p_{\mathrm{E}}+\frac{1}{M}\theta_{\mathrm{E}k}p_{\mathrm{T}}+\sigma_{\mathrm{E}}^{2}\right). \tag{4.29}$$

Next, since the optimization problem (4.20) employs the max-min criterion [29], the combination coefficients should satisfy

$$\mathscr{E}_{1}\left(\alpha_{1}\right)=\mathscr{E}_{2}\left(\alpha_{2}\right)=\cdots=\mathscr{E}_{K_{\mathrm{E}}}\left(\alpha_{K_{\mathrm{E}}}\right)\triangleq\mathscr{E}. \tag{4.30}$$

According to (4.29) and (4.30), the combination coefficients can be written as

$$\alpha_{k}^{2}=\frac{1}{M\theta_{\mathrm{E}k}p_{\mathrm{E}}}\left[\frac{1}{\theta_{\mathrm{E}k}}\left(\frac{\mathscr{E}}{\eta T_{\mathrm{D}}}-\sigma_{\mathrm{E}}^{2}\right)-\frac{p_{\mathrm{T}}}{M}\right], k=1,2,\cdots,K_{\mathrm{E}}. \tag{4.31}$$

Substituting (4.31) into (4.26), we obtain (4.23). Further, substituting (4.23) into (4.31) leads to (4.21).

4.3.1.3 Tradeoff Between Harvested Energy and Information Rate

Let the number of antennas $M\rightarrow\infty$ in (4.19) and assume the required rates of all information users are the same, namely $\bar{r}_{k}=\bar{r}$ $(k=1,2,\cdots,K_{\mathrm{I}})$, the allocated

power for information users becomes $p_{\mathrm{I}} = \sigma_{\mathrm{I}}^2 \left(2^{\bar{r}} - 1\right) \sum_{k=1}^{K_{\mathrm{I}}} \theta_{\mathrm{I}k}^{-1}$. Based on (4.24), the theoretical tradeoff between the harvested energy and information rate is given as follows under perfect CSI,

$$\mathscr{E}(\bar{r}) = \eta T_{\mathrm{D}} \left\{ \left[p_{\mathrm{T}} - \left(2^{\bar{r}} - 1\right) \sum_{k=1}^{K_{\mathrm{I}}} \frac{\sigma_{\mathrm{I}}^2}{\theta_{\mathrm{I}k}} \right] \left(\sum_{k=1}^{K_{\mathrm{E}}} \frac{1}{\theta_{\mathrm{E}k}} \right)^{-1} + \sigma_{\mathrm{E}}^2 \right\}, \tag{4.32}$$

which indicates the harvested energy decreases with the increasing information rate.

4.3.2 Power Allocation with Estimated CSI

When all users send pilot sequences to the BS during the interval T_{P} (cf. Fig. 4.1), the received signals can be given by

$$\mathbf{Y} = \mathbf{G}\mathbf{Q}^{1/2}\boldsymbol{\Phi}^{\mathrm{H}} + \mathbf{N}, \tag{4.33}$$

where $\mathbf{G} = [\mathbf{g}_{\mathrm{E}1}, \cdots, \mathbf{g}_{\mathrm{E}K_{\mathrm{E}}}, \mathbf{g}_{\mathrm{I}1}, \cdots, \mathbf{g}_{\mathrm{I}K_{\mathrm{I}}}]$, $\mathbf{Q} = \mathrm{diag}\left\{\left[\mathbf{q}_{\mathrm{E}}^{\mathrm{T}}, \mathbf{q}_{\mathrm{I}}^{\mathrm{T}}\right]\right\}$, $\mathbf{q}_{\psi} = \left[q_{\psi 1}, q_{\psi 2}, \cdots, q_{\psi K_{\psi}}\right]^{\mathrm{T}}$ contains the pilot powers of all ψ users and with constraint $0 \leq q_{\psi k} \leq q_{\psi}$. The matrix $\boldsymbol{\Phi} = [\boldsymbol{\Phi}_{\mathrm{E}}, \boldsymbol{\Phi}_{\mathrm{I}}] \in \mathbb{C}^{L \times K}$ contains the pilot sequences, $\boldsymbol{\Phi}_{\psi} = \left[\boldsymbol{\phi}_{\psi 1}, \boldsymbol{\phi}_{\psi 2}, \cdots, \boldsymbol{\phi}_{\psi K_{\psi}}\right] \in \mathbb{C}^{L \times K_{\psi}}$ $(L \geq K)$ and the column vector $\boldsymbol{\phi}_{\psi k} = \left[\phi_{\psi k1}, \phi_{\psi k2}, \cdots, \phi_{\psi kL}\right]^{\mathrm{T}}$ with $\boldsymbol{\phi}_{\psi k}^{\mathrm{H}} \boldsymbol{\phi}_{\psi k} = 1$. $\mathbf{N} \in \mathbb{C}^{M \times L}$ denotes the noise matrix and its elements are i.i.d. complex Gaussian random variables with mean 0 and variance σ_{BS}^2.

The information users transmit orthogonal pilot sequences, i.e., $\boldsymbol{\phi}_{\mathrm{I}k}^{\mathrm{H}} \boldsymbol{\phi}_{\mathrm{I}l} = 0\,(l \neq k)$. On the other hand, there are two piloting schemes for energy users:

- Orthogonal pilot: orthogonal pilot sequences are sent by different energy users, namely

$$\boldsymbol{\phi}_{\mathrm{E}k}^{\mathrm{H}} \boldsymbol{\phi}_{\mathrm{E}l} = 0\,(l \neq k)\,, \boldsymbol{\phi}_{\mathrm{E}k}^{\mathrm{H}} \boldsymbol{\phi}_{\mathrm{I}l} = 0. \tag{4.34}$$

- Shared pilot: different energy users share the same pilot sequence, namely

$$\boldsymbol{\phi}_{\mathrm{E}k} = \boldsymbol{\phi}_{\mathrm{E}}\,(k = 1, 2, \cdots, K_{\mathrm{E}})\,, \boldsymbol{\phi}_{\mathrm{E}}^{\mathrm{H}} \boldsymbol{\phi}_{\mathrm{I}l} = 0. \tag{4.35}$$

As before, we solve the problem in (4.12) in two steps.

4.3.2.1 Power Allocation for Information Users

The estimated channels of information users can be expressed as

$$\hat{\mathbf{g}}_{\mathrm{I}k} = \frac{1}{\sqrt{q_{\mathrm{I}k}}}\mathbf{Y}\boldsymbol{\phi}_{\mathrm{I}k} = \mathbf{g}_{\mathrm{I}k} + \frac{1}{\sqrt{q_{\mathrm{I}k}}}\bar{\mathbf{n}}_{\mathrm{I}k}, \tag{4.36}$$

where $\bar{\mathbf{n}}_{\mathrm{I}k} = \mathbf{N}\boldsymbol{\phi}_{\mathrm{I}k} \overset{\text{i.i.d.}}{\sim} \mathbb{CN}\left(0, \sigma_{\mathrm{BS}}^2\mathbf{I}_M\right)(k = 1, 2, \cdots, K_{\mathrm{I}})$.

Replacing $\mathbf{g}_{\mathrm{I}k}^*$ in (4.8) by $\hat{\mathbf{g}}_{\mathrm{I}k}^*$ and using the properties that $\frac{1}{M}\mathbf{g}_{\mathrm{I}k}^{\mathrm{T}}\hat{\mathbf{g}}_{\mathrm{I}l}^* \to 0\,(k \neq l)$, $\frac{1}{M}\mathbf{g}_{\mathrm{I}k}^{\mathrm{T}}\bar{\mathbf{n}}_{\mathrm{I}k}^* \to 0$ and $\frac{1}{M}\left\|\mathbf{g}_{\mathrm{I}k}\right\|^2 \to \theta_{\mathrm{I}k}$ for large M, the SINR of the kth information user becomes

$$\rho_k = \frac{\theta_{\mathrm{I}k}}{\theta_{\mathrm{I}k} + \frac{\sigma_{\mathrm{BS}}^2}{q_{\mathrm{I}k}}}\frac{p_k\theta_{\mathrm{I}k}}{\sigma_{\mathrm{I}}^2}, M \gg 1. \tag{4.37}$$

Therefore, to meet its rate requirement $\bar{r}_k$, the allocated power for the kth information user can be expressed as

$$\frac{p_k}{M} \geq \frac{1}{M}\frac{\theta_{\mathrm{I}k} + \frac{\sigma_{\mathrm{BS}}^2}{q_{\mathrm{I}k}}}{\theta_{\mathrm{I}k}}\frac{\sigma_{\mathrm{I}}^2}{\theta_{\mathrm{I}k}}\left(2^{\bar{r}_k} - 1\right), \tag{4.38}$$

and the residual power for energy users is given by

$$\frac{p_{\mathrm{E}}}{M} = \frac{p_{\mathrm{T}} - p_{\mathrm{I}}}{M} \leq \frac{p_{\mathrm{T}}}{M} - \frac{1}{M}\sum_{k=1}^{K_{\mathrm{I}}}\frac{\theta_{\mathrm{I}k} + \frac{\sigma_{\mathrm{BS}}^2}{q_{\mathrm{I}k}}}{\theta_{\mathrm{I}k}}\frac{\sigma_{\mathrm{I}}^2}{\theta_{\mathrm{I}k}}\left(2^{\bar{r}_k} - 1\right). \tag{4.39}$$

4.3.2.2 Power Allocation for Energy Users

Under the orthogonal pilot scheme, the estimated channel of the kth energy user can be written as

$$\hat{\mathbf{g}}_{\mathrm{E}k} = \frac{1}{\sqrt{q_{\mathrm{E}k}}}\mathbf{Y}\boldsymbol{\phi}_{\mathrm{E}k} = \mathbf{g}_{\mathrm{E}k} + \frac{1}{\sqrt{q_{\mathrm{E}k}}}\bar{\mathbf{n}}_{\mathrm{E}k}, \tag{4.40}$$

where $\bar{\mathbf{n}}_{\mathrm{E}k} = \mathbf{N}\boldsymbol{\phi}_{\mathrm{E}k} \overset{\text{i.i.d.}}{\sim} \mathbb{CN}\left(0, \sigma_{\mathrm{BS}}^2\mathbf{I}_M\right)(k = 1, \cdots, K_{\mathrm{E}})$ and are independent of $\bar{\mathbf{n}}_{\mathrm{I}k}\,(k = 1, \cdots, K_{\mathrm{I}})$.

When the precoder for energy users is formed based on (4.40), using $\frac{1}{M}\left\|\mathbf{g}_{\mathrm{E}k}^{*}\right\|^{2}=\theta_{\mathrm{E}k}$ and $\frac{1}{M}\left\|\bar{\mathbf{n}}_{\mathrm{E}k}^{*}\right\|^{2}=\sigma_{\mathrm{BS}}^{2}$ for large M, we have

$$\begin{aligned}\left\|\mathbf{w}_{\mathrm{E}}\right\|^{2}&=\sum_{k=1}^{K_{\mathrm{E}}}\alpha_{k}^{2}\left(\left\|\mathbf{g}_{\mathrm{E}k}^{*}\right\|^{2}+\frac{1}{q_{\mathrm{E}k}}\left\|\bar{\mathbf{n}}_{\mathrm{E}k}^{*}\right\|^{2}\right)\\&=M\sum_{k=1}^{K_{\mathrm{E}}}\alpha_{k}^{2}\left(\theta_{\mathrm{E}k}+\frac{\sigma_{\mathrm{BS}}^{2}}{q_{\mathrm{E}k}}\right)=1, M\gg 1.\end{aligned}\tag{4.41}$$

Replacing $\mathbf{g}_{\mathrm{E}k}^{*}$ in (4.6) by $\hat{\mathbf{g}}_{\mathrm{E}k}^{*}$, and making use of $\frac{1}{M}\mathbf{g}_{\mathrm{E}k}^{\mathrm{T}}\hat{\mathbf{g}}_{\mathrm{E}l}^{*}=0\,(k\neq l)$, $\frac{1}{M}\mathbf{g}_{\mathrm{E}k}^{\mathrm{T}}\hat{\mathbf{g}}_{ll}^{*}=0$, $\frac{1}{M}\mathbf{g}_{\mathrm{E}k}^{\mathrm{T}}\bar{\mathbf{n}}_{\mathrm{E}l}^{*}=0$ and $\frac{1}{M}\left\|\mathbf{g}_{\mathrm{E}k}\right\|^{2}=\theta_{\mathrm{E}k}$ for large M, the harvested energy by the kth energy user becomes

$$\mathscr{E}_{k}^{\mathrm{OP}}(\alpha_{k})=\eta T_{\mathrm{D}}\left(M\alpha_{k}^{2}\theta_{\mathrm{E}k}^{2}p_{\mathrm{E}}+\sigma_{\mathrm{E}}^{2}\right)+\mathscr{O}\left(\frac{1}{M}\right), M\gg 1.\tag{4.42}$$

Following the similar derivation as in the proof of Theorem 1, i.e., letting $\mathscr{E}_{k}^{\mathrm{OP}}(\alpha_{k})=\mathscr{E}^{\mathrm{OP}}\ (k=1,2,\cdots,K_{\mathrm{E}})$, expressing α_{k} in terms of $\mathscr{E}^{\mathrm{OP}}$ and substituting them into (4.41), we obtain

$$\alpha_{k}=\frac{1}{\theta_{\mathrm{E}k}}\sqrt{\frac{1}{M}\left(\sum_{k=1}^{K_{\mathrm{E}}}\frac{\theta_{\mathrm{E}k}+\frac{\sigma_{\mathrm{BS}}^{2}}{q_{\mathrm{E}k}}}{\theta_{\mathrm{E}k}^{2}}\right)^{-1}}, M\gg 1.\tag{4.43}$$

Substituting (4.43) into (4.42) gives rise to the same harvested energy of all energy users, namely

$$\mathscr{E}^{\mathrm{OP}}=\eta T_{\mathrm{D}}\left[p_{\mathrm{E}}\left(\sum_{k=1}^{K_{\mathrm{E}}}\frac{\theta_{\mathrm{E}k}+\frac{\sigma_{\mathrm{BS}}^{2}}{q_{\mathrm{E}k}}}{\theta_{\mathrm{E}k}^{2}}\right)^{-1}+\sigma_{\mathrm{E}}^{2}\right], M\gg 1.\tag{4.44}$$

When the shared pilot scheme is adopted, only a linear combination of the channels of energy users can be estimated, given by

$$\hat{\mathbf{g}}_{\mathrm{E}}=\mathbf{Y}\boldsymbol{\phi}_{\mathrm{E}}=\sum_{k=1}^{K_{\mathrm{E}}}\sqrt{q_{\mathrm{E}k}}\mathbf{g}_{\mathrm{E}k}+\bar{\mathbf{n}}_{\mathrm{E}},\tag{4.45}$$

where $\bar{\mathbf{n}}_{\mathrm{E}}=\mathbf{N}\boldsymbol{\phi}_{\mathrm{E}}\sim\mathbb{CN}\left(0,\sigma_{\mathrm{BS}}^{2}\mathbf{I}_{M}\right)$ and is independent of $\bar{\mathbf{n}}_{\mathrm{I}k}\,(k=1,2,\cdots,K_{\mathrm{I}})$. Therefore, the precoder for energy users is then given by

$$\mathbf{w}_{\mathrm{E}}=\frac{\hat{\mathbf{g}}_{\mathrm{E}}^{*}}{\left\|\hat{\mathbf{g}}_{\mathrm{E}}^{*}\right\|}=\sum_{k=1}^{K_{\mathrm{E}}}\frac{\sqrt{q_{\mathrm{E}k}}}{\left\|\hat{\mathbf{g}}_{\mathrm{E}}^{*}\right\|}\mathbf{g}_{\mathrm{E}k}^{*}+\frac{\bar{\mathbf{n}}_{\mathrm{E}}^{*}}{\left\|\hat{\mathbf{g}}_{\mathrm{E}}^{*}\right\|}.\tag{4.46}$$

Substituting (4.46) into (4.6), the harvested energy is only determined by the power of uplink pilot, thus (4.12) can be transformed into the following max-min formulation,

$$\max_{\mathbf{q}_\mathrm{E}} \min_{k} \left\{ \mathscr{E}_k^{\mathrm{SP}} (\mathbf{q}_\mathrm{E}) \right\} \tag{4.47}$$

$$\text{s.t. } 0 \le q_{\mathrm{E}k} \le q_\mathrm{E}, \quad k = 1, 2, \cdots, K_\mathrm{E}. \tag{4.48}$$

Theorem 2 *With estimated CSI under the shared pilot scheme, the optimal pilot power for the energy transfer precoder is given by*

$$q_{\mathrm{E}k} = \frac{\theta_{\mathrm{E}k_\mathrm{m}}^2}{\theta_{\mathrm{E}k}^2} q_\mathrm{E}, k = 1, 2, \cdots, K_\mathrm{E}, \tag{4.49}$$

where $k_\mathrm{m} = \arg\min_k \{\theta_{\mathrm{E}k}\}$. *The same harvested energy of all energy users is given by*

$$\mathscr{E}^{\mathrm{SP}} = \eta T_\mathrm{D} \left[p_\mathrm{E} \left(\sum_{k=1}^{K_\mathrm{E}} \frac{1}{\theta_{\mathrm{E}k}} + \frac{\sigma_{\mathrm{BS}}^2}{\theta_{\mathrm{E}k_\mathrm{m}}^2 q_\mathrm{E}} \right)^{-1} + \sigma_\mathrm{E}^2 \right], M \gg 1, \tag{4.50}$$

and the equivalent combination coefficients are given by

$$\tilde{\alpha}_k = \frac{\sqrt{q_{\mathrm{E}k}}}{\left\| \hat{\mathbf{g}}_\mathrm{E}^* \right\|} = \frac{1}{\theta_{\mathrm{E}k}} \sqrt{\frac{1}{M} \left(\sum_{k=1}^{K_\mathrm{E}} \frac{1}{\theta_{\mathrm{E}k}} + \frac{\sigma_{\mathrm{BS}}^2}{\theta_{\mathrm{E}k_\mathrm{m}}^2 q_\mathrm{E}} \right)^{-1}}, M \gg 1. \tag{4.51}$$

Proof Substituting $\mathbf{w}_\mathrm{E}$ into (4.6) and making use of $\frac{1}{M} \mathbf{g}_{\mathrm{E}k}^\mathrm{T} \hat{\mathbf{g}}_{\mathrm{I}k}^* = 0$, $\frac{1}{M} \mathbf{g}_{\mathrm{E}k}^\mathrm{T} \hat{\mathbf{g}}_\mathrm{E}^* = q_{\mathrm{E}k} \theta_{\mathrm{E}k}$ and $\frac{1}{M} \left\| \hat{\mathbf{g}}_\mathrm{E}^* \right\|^2 = \sum_{k=1}^{K_\mathrm{E}} q_{\mathrm{E}k} \theta_{\mathrm{E}k} + \sigma_{\mathrm{BS}}^2$ for large M, the harvested energy of the kth energy user becomes

$$\mathscr{E}_k^{\mathrm{SP}} (\mathbf{q}_\mathrm{E}) = \eta T_\mathrm{D} \left(\frac{q_{\mathrm{E}k} \theta_{\mathrm{E}k}^2 p_\mathrm{E}}{\sum_{k=1}^{K_\mathrm{E}} q_{\mathrm{E}k} \theta_{\mathrm{E}k} + \sigma_{\mathrm{BS}}^2} + \sigma_\mathrm{E}^2 \right) + \mathscr{O}\left(\frac{1}{M} \right), M \gg 1. \tag{4.52}$$

Then, (4.47) can be rewritten as follows

$$\min_{\mathbf{q}_\mathrm{E}} \max_{k} \left\{ \frac{1}{q_{\mathrm{E}k} \theta_{\mathrm{E}k}^2} \sum_{k=1}^{K_\mathrm{E}} q_{\mathrm{E}k} \theta_{\mathrm{E}k} + \frac{\sigma_{\mathrm{BS}}^2}{q_{\mathrm{E}k} \theta_{\mathrm{E}k}^2} \right\} \text{ s.t. (4.48)}, \tag{4.53}$$

which can be split into two subproblems, namely

$$\min_{\mathbf{q}_\mathrm{E}} \max_{k} \left\{ \frac{\sigma_\mathrm{BS}^2}{q_{\mathrm{E}k}\theta_{\mathrm{E}k}^2} \right\} \text{ s.t. (4.48)}, \tag{4.54}$$

and

$$\min_{\mathbf{q}_\mathrm{E}} \max_{k} \left\{ \frac{1}{q_{\mathrm{E}k}\theta_{\mathrm{E}k}^2} \sum_{k=1}^{K_\mathrm{E}} q_{\mathrm{E}k}\theta_{\mathrm{E}k} \right\} \text{ s.t. (4.48)}. \tag{4.55}$$

Therefore, if there is an intersection of solutions to (4.54) and (4.55), then it is the solution to (4.47). We next solve the two subproblems.

As $\theta_{\mathrm{E}k_\mathrm{m}}^2 \leq \theta_{\mathrm{E}k}^2$ $(k \neq k_\mathrm{m})$, the solution set to (4.54) is given by

$$\left\{ q_{\mathrm{E}k_\mathrm{m}} = q_\mathrm{E}, q_{\mathrm{E}k} \in \left[\frac{\theta_{\mathrm{E}k_\mathrm{m}}^2}{\theta_{\mathrm{E}k}^2} q_\mathrm{E}, q_\mathrm{E} \right], k \neq k_\mathrm{m} \right\}. \tag{4.56}$$

Denote $\alpha_k^2 = \frac{q_{\mathrm{E}k}}{\sum_{k=1}^{K_\mathrm{E}} q_{\mathrm{E}k}\theta_{\mathrm{E}k}}$, (4.55) is similar to (4.20). Following the same line as in the proof of Theorem 1, the solution set to (4.55) is $\{\alpha_1^2\theta_{\mathrm{E}1}^2 = \alpha_2^2\theta_{\mathrm{E}2}^2 = \cdots = \alpha_{K_\mathrm{E}}^2\theta_{\mathrm{E}K_\mathrm{E}}^2,$ $0 \leq q_{\mathrm{E}k} \leq q_\mathrm{E}\}$, namely

$$\left\{ q_{\mathrm{E}1}\theta_{\mathrm{E}1}^2 = q_{\mathrm{E}2}\theta_{\mathrm{E}2}^2 = \cdots = q_{\mathrm{E}K_\mathrm{E}}\theta_{\mathrm{E}K_\mathrm{E}}^2, q_{\mathrm{E}k} \in [0, q_\mathrm{E}] \right\}. \tag{4.57}$$

There is a unique intersection point of (4.56) and (4.57), i.e. (4.49), which is the optimal solution to (4.47). Substituting (4.49) into (4.52) and (4.46), respectively, gives rise to (4.50) and (4.51).

4.3.2.3 Comparison of Two Piloting Schemes

Assuming the same uplink pilot power in both schemes, i.e., $q_{\mathrm{E}k}$ in (4.44) is the same as that in (4.49). Then, for large M and ignorable noise power, the ratio between the harvested energies of the two piloting schemes is given by

$$\frac{\mathscr{E}^\mathrm{SP}}{\mathscr{E}^\mathrm{OP}} = \frac{p_\mathrm{E}\left[\sum_{k=1}^{K_\mathrm{E}} \left(\frac{1}{\theta_{\mathrm{E}k}} + \frac{1}{K_\mathrm{E}} \frac{\sigma_\mathrm{BS}^2}{\theta_{\mathrm{E}k_\mathrm{m}}^2 q_\mathrm{E}} \right)\right]^{-1} + \sigma_\mathrm{E}^2}{p_\mathrm{E}\left[\sum_{k=1}^{K_\mathrm{E}} \left(\frac{1}{\theta_{\mathrm{E}k}} + \frac{\sigma_\mathrm{BS}^2}{\theta_{\mathrm{E}k_\mathrm{m}}^2 q_\mathrm{E}} \right)\right]^{-1} + \sigma_\mathrm{E}^2} \approx \frac{\sum_{k=1}^{K_\mathrm{E}} \left(\frac{1}{\theta_{\mathrm{E}k}} + \frac{\sigma_\mathrm{BS}^2}{\theta_{\mathrm{E}k_\mathrm{m}}^2 q_\mathrm{E}} \right)}{\sum_{k=1}^{K_\mathrm{E}} \left(\frac{1}{\theta_{\mathrm{E}k}} + \frac{1}{K_\mathrm{E}} \frac{\sigma_\mathrm{BS}^2}{\theta_{\mathrm{E}k_\mathrm{m}}^2 q_\mathrm{E}} \right)} \to \begin{cases} 1, & q_\mathrm{E} \to \infty, \\ K_\mathrm{E}, & q_\mathrm{E} \to 0. \end{cases} \tag{4.58}$$

Hence the shared pilot scheme leads to higher harvested energy.

Another advantage of the shared pilot scheme is that the total number of pilot sequences is $K_{\mathrm{I}}+1$, as opposed to $K=K_{\mathrm{I}}+K_{\mathrm{E}}$ for the orthogonal pilot scheme. To ensure the orthogonality of the pilot sequences, the lengths of the pilot sequences are therefore $K_{\mathrm{I}}+1$ and $K=K_{\mathrm{I}}+K_{\mathrm{E}}$ under the two pilot schemes, respectively. Hence, the shared pilot scheme can use shorter pilot sequences and reduce the uplink pilot interval T_{P} in Fig. 4.1, and correspondingly increase the downlink interval T_{D}. This way, the shared pilot scheme results in even higher harvested energy, given by

$$\tilde{\mathscr{E}}^{\mathrm{SP}}=\left(T_{\mathrm{C}}-T_{\mathrm{U}}-\frac{K_{\mathrm{I}}+1}{K}T_{\mathrm{P}}\right)\frac{1}{T_{\mathrm{D}}}\mathscr{E}^{\mathrm{SP}}\geq\mathscr{E}^{\mathrm{SP}}\geq\mathscr{E}^{\mathrm{OP}}. \tag{4.59}$$

4.3.3 Performance Evaluation

In the simulations, the large-scale fading variable $\theta_{\psi k}=\varphi_{\psi}d_{\psi k}^{-\alpha_{\psi}}\xi_{\psi k}$ $(\psi\in\{\mathrm{E},\mathrm{I}\})$, where φ_{ψ} is a constant related to the antenna gain and carrier frequency, α_{ψ} represents the path loss exponent, $d_{\psi k}$ is the distance between the kth ψ user and the BS, and $\xi_{\psi k}$ denotes the shadow fading with the distribution $10\log_{10}\xi_{\psi k}\overset{\text{i.i.d.}}{\sim}\mathbb{N}\left(0,\sigma_{\mathrm{SF}}^2\right)$. The noise power $\sigma_{\psi}^2=N_{\psi}B$ and $\sigma_{\mathrm{BS}}^2=\sigma_{\mathrm{I}}^2$, where N_{ψ} and B are the noise power spectral density and the system bandwidth, respectively. In the single-cell scenario, the ψ users are uniformly distributed on a disc with the inner radius R_{ψ}^0 and the outer radius R_{ψ}. The related parameters are listed in Table 4.1. In the following figures, all results are the average of 10^5 realizations of user distribution in the cell. We set the energy conversion efficiency $\eta=0.8$ [21]. The harvested energy is normalized by the downlink interval, i.e., $\frac{\mathscr{E}}{T_{\mathrm{D}}}$, and the unit is milli-Joule per second (mJ/s). "PCSI" and "ECSI" represent the results with perfect CSI and estimated CSI, respectively.

4.3.3.1 Information Rate

Adopting the equal power allocation for information users, Fig. 4.2 shows the rates of information users versus different system parameters. When the number

Table 4.1 Simulation parameters of downlink HIET system

Parameters	Values
Constant φ_{E}=φ_{I}	1E−3
Path loss exponent α_{E} (α_{I})	3 (3.8)
S.t.d. variance of shadow fading σ_{SF}	8 dB
Noise power spectrum density N_{E} (N_{I})	−124(−120) dBm/Hz
System bandwidth B	100 kHz
Radiuses of information users R_{I} (R_{I}^0)	100 (10) m
Radiuses of energy users R_{E} (R_{E}^0)	10 (1) m

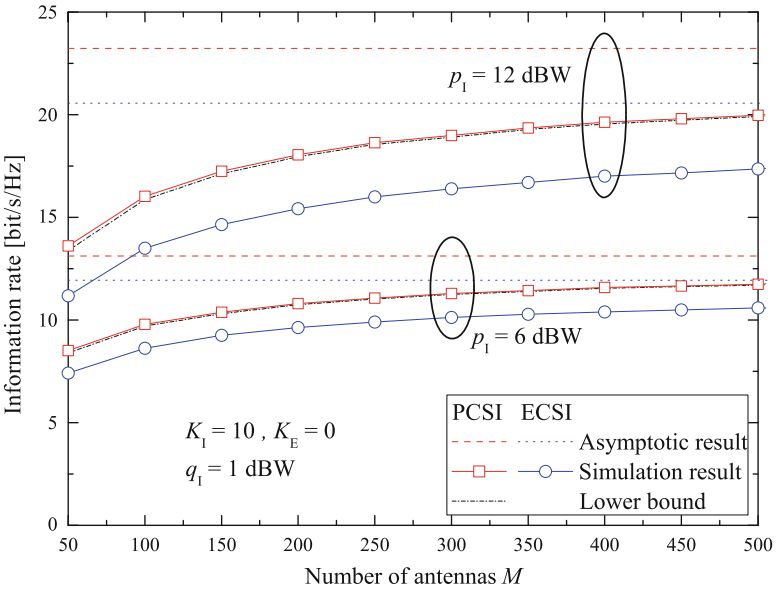

Fig. 4.2 Information rate versus the number of antennas

of antennas is infinite, the asymptotic results with PCSI and ECSI are given by (4.17) and (4.37), respectively. The lower bound of information rate with PCSI is calculated by (4.13). In Fig. 4.2, for both PCSI and ECSI, the simulation results tend to the asymptotic results when the number of antennas increases. The lower bound of information rate is tight for PCSI. Boosting the downlink transmitted power can improve the information rates. However, the gap between the asymptotic result and simulation result increases due to the higher inter user interference.

4.3.3.2 Harvested Energy

Considering only the energy users, Fig. 4.3 depicts the minimum harvested energy versus the maximum pilot power. For PCSI, the theoretical results with $M = 300$ and the asymptotic results with infinite M are given by (4.23) and (4.24), respectively. The asymptotic results with ECSI and infinite M are given by (4.44) and (4.50) for the orthogonal pilot scheme and the shared pilot scheme, respectively. From Fig. 4.3, the energy harvesting performance of the shared pilot scheme is always better than that of the orthogonal pilot scheme, corroborating the discussions in Sect. 4.3.2.3. With the increasing pilot power, the harvested energies of both schemes increase and eventually approach to those of PCSI. The results with $M = 300$ approximate the asymptotic results. With different numbers of antennas, the ratios of the harvested energies between the two piloting schemes are shown in Fig. 4.4. Deploying more antennas and serving more energy users can increase the

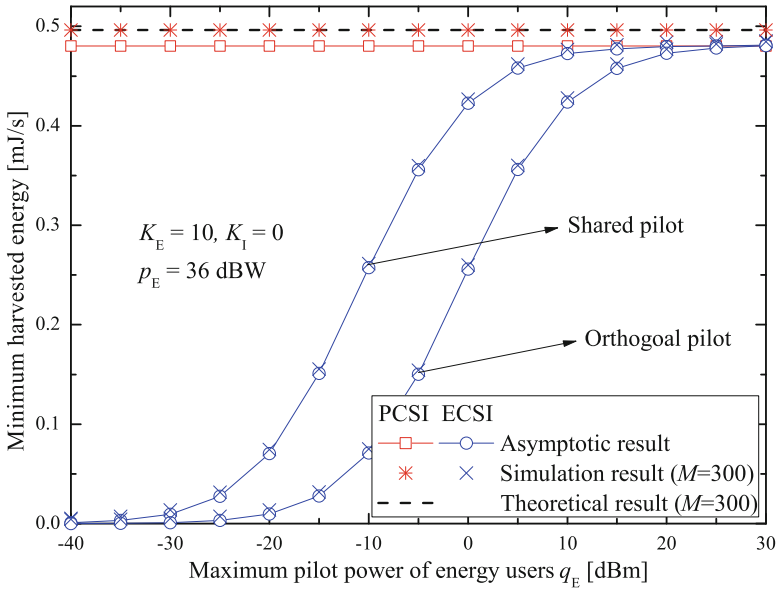

Fig. 4.3 Minimum harvested energy versus maximum pilot power

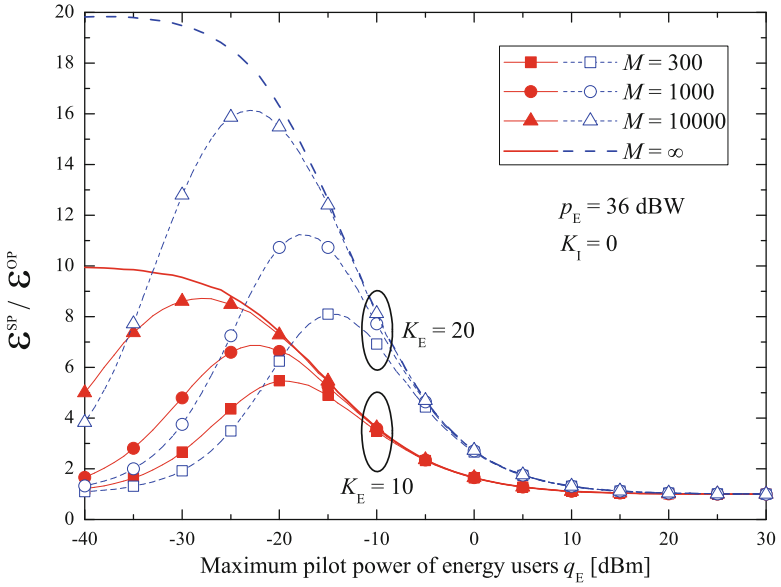

Fig. 4.4 Ratio of the harvested energy by the shared pilot scheme to that by the orthogonal pilot scheme

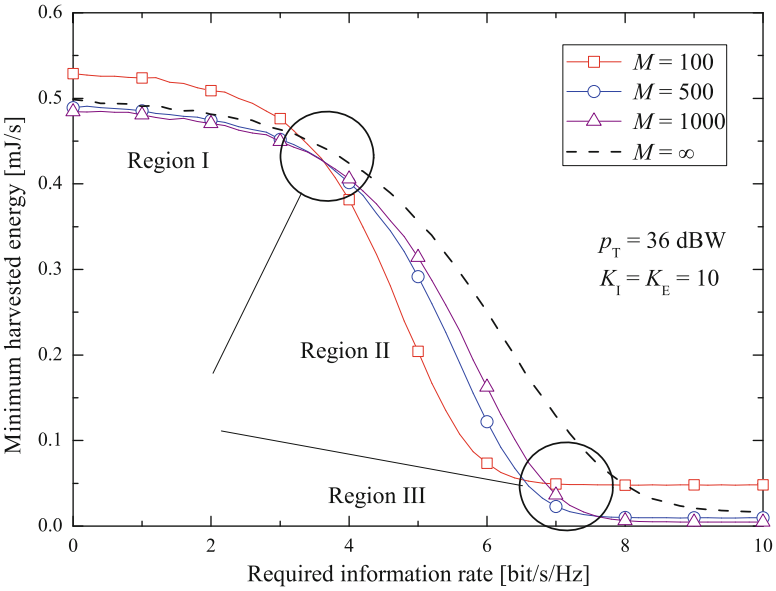

Fig. 4.5 Minimum harvested energy versus required information rate with PCSI

performance gain of the shared pilot scheme over the orthogonal pilot scheme. With infinite number of antennas, when the maximum pilot power decreases, the ratio approaches to the number of energy users, which is the maximum possible.

4.3.3.3 Tradeoff Between Information Rate and Harvested Energy

Assuming the required information rate $\bar{r}_k = \bar{r}\,(k = 1, 2, \cdots, K_\mathrm{I})$, Figs. 4.5 and 4.6 show the minimum harvested energy of energy users versus the required rates of information users. With PCSI and finite M in Fig. 4.5, overall, the harvested energy decreases with the increasing information rate, however there are three different regions. In region I with low information rate, when M increases, the harvested energy decreases because of harvesting less interference power based on (4.19) and (4.23). As increasing M can improve the information rate, more downlink power is saved for energy transfer, which results in region II. When the required rate is large enough, little power is left for energy users and thereby the interference power dominates the harvested energy. Eventually, region III becomes similar to region I. With ECSI and infinite M in Fig. 4.6, the trade-off between the minimum harvested energy and the required information rate becomes better with more pilot power, and tends to the trade-off with PCSI. Moreover, the trade-off with the shared pilot scheme outperforms that with the orthogonal pilot scheme.

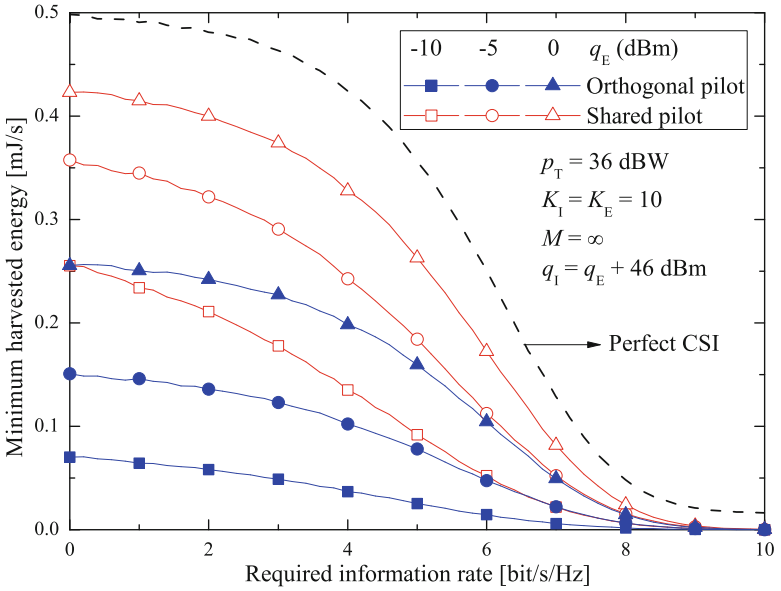

Fig. 4.6 Minimum harvested energy versus required information rate with ECSI

4.4 Cooperative Energy Transfer of Multi-Cell Scenario

We now consider the multi-cell scenario, where there are L cells and the BS in each cell transmits information and energy to the information users and energy users, respectively, in its cell. With estimated CSI, pilot contamination can be eliminated for information users by joint encoding [30]. On the other hand, due to the asymptotic orthogonality of channel vectors in different cells, there is no difference between single-cell and multi-cell for information users with perfect CSI. Therefore, in multi-cell case, information users are treated the same way as in the single-cell case, and the power allocations with perfect CSI and estimated CSI are given by (4.18) and (4.38), respectively.

In the non-cooperative energy transfer, the BS in each cell independently implements the single-cell precoding methods for its energy users, as discussed in Sects. 4.3.1 and 4.3.2. Due to the asymptotic orthogonality of the channel vectors in different cells, the inter-cell interference vanishes and therefore the results of harvested energy are also the same as those for single cell. In particular, with perfect CSI, the energy precoder in each cell is given by (4.3) and (4.22), with the harvested energy in each cell given by (4.24). With estimated CSI under the shared pilot scheme, the energy precoder in each cell is given by (4.46) and (4.49), and the harvested energy in each cell is given by (4.50).

However, note that an energy user can potentially harvest energy from BS transmissions in other cells, which is not exploited by the above non-cooperative

approach. In the cooperative approach, we will design the energy precoders of all cells jointly. Here the harvested energy from the signals of information users vanishes due to the asymptotic orthogonality between the channel vectors of information users and energy users. Therefore in what follows we only focus on the energy users.

4.4.1 System Model of Cooperative Energy Transfer

Suppose there are K_j energy users in cell j. Denote $\mathbf{g}_{j,(l,k)} = \theta_{j,(l,k)}^{1/2}\mathbf{h}_{j,(l,k)} \in \mathbb{C}^{M\times 1}$ as the uplink channel from energy user k in cell l to the BS in cell j, where $\theta_{j,(l,k)}$ and $\mathbf{h}_{j,(l,k)}$ are defined similarly as in the single-cell case. In cooperative energy transfer, the energy precoder in cell j is the linear combination of the uplink channels of all energy users in all cells, namely

$$\mathbf{w}_j = \sum_{l=1}^{L}\sum_{k=1}^{K_l}\alpha_{lk}\mathbf{g}_{j,(l,k)}^{*}. \tag{4.60}$$

Denoting $\mathbf{w} = \left[\mathbf{w}_1^{\mathrm{T}}, \mathbf{w}_2^{\mathrm{T}}, \cdots, \mathbf{w}_L^{\mathrm{T}}\right]^{\mathrm{T}}$ as the global precoder, the combination coefficients $\{\alpha_{lk}\}$ should meet $\|\mathbf{w}\| = 1$.

Assuming $\frac{p}{M}$ is the overall power of all BSs for energy users and the same symbol s is transmitted for all energy users with $|s| = 1$, then the transmitted signal for energy users is $\mathbf{x}_j = \sqrt{\frac{p}{M}}\mathbf{w}_j s$ in cell j. Further, the received signal of the kth energy user in cell l is given by

$$y_{lk} = \sum_{j=1}^{L}\mathbf{g}_{j,(l,k)}^{\mathrm{T}}\mathbf{x}_j + n_{lk}, \tag{4.61}$$

where $n_{lk} \overset{\text{i.i.d.}}{\sim} \mathbb{CN}\left(0, \sigma^2\right)$ is the additive white Gaussian noise. And the harvested energy is

$$\mathscr{E}_{lk}\left(\{\alpha_{lk}\}\right) = \eta T_{\mathrm{D}}\mathbb{E}\left[\left|\sum_{j=1}^{L}\mathbf{g}_{j,(l,k)}^{\mathrm{T}}\mathbf{x}_j\right|^2 + |n_{lk}|^2\right]. \tag{4.62}$$

Considering both a centralized way and a distributed way to construct the energy precoder, we next solve the max-min energy harvesting problem in Sects. 4.4.2 and 4.4.3, respectively.

4.4.2 Centralized Energy Precoder

The max-min energy harvesting problem is formulated as follows,

$$\max_{\{\alpha_{lk}\}} \min_{\{l,k\}} \{\mathscr{E}_{lk}(\{\alpha_{lk}\})\} \tag{4.63}$$

$$\text{s.t.} \quad \|\mathbf{w}\|^2 = 1. \tag{4.64}$$

4.4.2.1 Perfect CSI

Recall that $\frac{1}{M}\left\|\mathbf{g}_{j,(l,k)}\right\|^2 = \theta_{j,(l,k)}$ and $\frac{1}{M}\mathbf{g}_{j,(l,k)}^{\mathrm{T}}\mathbf{g}_{j,(b,i)}^{*} = 0$ $(l \neq b \text{ or } k \neq i)$ for large M, the harvested energy of the kth energy user in cell l is

$$\mathscr{E}_{lk} = \eta T_{\mathrm{D}}\left[pM\alpha_{lk}^2\left(\sum_{j=1}^{L}\theta_{j,(l,k)}\right)^2 + \sigma^2\right] + \mathscr{O}\left(\frac{1}{M}\right). \tag{4.65}$$

Letting $\mathscr{E}_{lk} = \mathscr{E}$, expressing α_{lk} in terms of $\mathscr{E}$ and taking advantage of

$$\|\mathbf{w}\|^2 = M\sum_{l=1}^{L}\sum_{k=1}^{K_l}\alpha_{lk}^2\sum_{j=1}^{L}\theta_{j,(l,k)} = 1, M \gg 1, \tag{4.66}$$

the combination coefficient of the kth energy user in cell l is

$$\alpha_{lk} = \left(\sum_{j=1}^{L}\theta_{j,(l,k)}\right)^{-1}\sqrt{\frac{1}{M}\left[\sum_{l=1}^{L}\sum_{k=1}^{K_l}\left(\sum_{j=1}^{L}\theta_{j,(l,k)}\right)^{-1}\right]^{-1}}, M \gg 1. \tag{4.67}$$

Recall that for a non-cooperative case, $\alpha_{lk} \propto \frac{1}{\theta_{l,(l,k)}}$; whereas we have $\alpha_{lk} \propto \frac{1}{\sum_{j=1}^{L}\theta_{j,(l,k)}}$ for the cooperative case.

Substituting (4.67) into (4.65), we obtain the harvested energies of all energy users, given by

$$\mathscr{E} = \eta T_{\mathrm{D}}\left\{p\left[\sum_{l=1}^{L}\sum_{k=1}^{K_l}\left(\sum_{j=1}^{L}\theta_{j,(l,k)}\right)^{-1}\right]^{-1} + \sigma^2\right\}, M \gg 1. \tag{4.68}$$

4.4.2.2 Estimated CSI

Similar to the single-cell case, we employ the shared pilot scheme, where all energy users in cooperative cells share the same pilot sequence for uplink channel estimation. Thus the jth BS only can estimate the combination channel of all energy users, given by

$$\hat{\mathbf{g}}_j = \sum_{l=1}^{L} \sum_{k=1}^{K_l} \sqrt{q_{lk}} \mathbf{g}_{j,(l,k)} + \bar{\mathbf{n}}_j, \tag{4.69}$$

where q_{lk} is the pilot power of the kth energy user in cell l and with constraint $q_{lk} \leq q$, $\bar{\mathbf{n}}_j \overset{\text{i.i.d.}}{\sim} \mathbb{CN}\left(0, \sigma_{\text{BS}}^2 \mathbf{I}_M\right)$ is the equivalent noise vector.

Substituting $\mathbf{w}_j = \frac{\hat{\mathbf{g}}_j^*}{\left\|\left[\hat{\mathbf{g}}_1^{\text{H}}, \hat{\mathbf{g}}_2^{\text{H}}, \cdots, \hat{\mathbf{g}}_L^{\text{H}}\right]\right\|}$ into (4.62), for large M, making use of $\frac{1}{M}\mathbf{g}_{j,(l,k)}^{\text{T}} \hat{\mathbf{g}}_j^* = q_{lk}\theta_{j,(l,k)}$ and

$$\frac{1}{M}\left\|\left[\hat{\mathbf{g}}_1^{\text{H}}, \hat{\mathbf{g}}_2^{\text{H}}, \cdots, \hat{\mathbf{g}}_L^{\text{H}}\right]\right\|^2 = \sum_{j=1}^{L}\left(\sum_{l=1}^{L}\sum_{k=1}^{K_l} q_{lk}\theta_{j,(l,k)} + \sigma_{\text{BS}}^2\right), \tag{4.70}$$

the harvested energy of the kth energy user in cell l is given by

$$\mathscr{E}_{lk} = \eta T_{\text{D}}\left[\frac{pq_{lk}\left(\sum_{j=1}^{L}\theta_{j,(l,k)}\right)^2}{\sum_{j=1}^{L}\left(\sum_{l=1}^{L}\sum_{k=1}^{K_l} q_{lk}\theta_{j,(l,k)} + \sigma_{\text{BS}}^2\right)} + \sigma^2\right] + \mathscr{O}\left(\frac{1}{M}\right), M \gg 1. \tag{4.71}$$

Following the derivation as in the proof of Theorem 2, we obtain

$$q_{lk} = q\left(\sum_{j=1}^{L}\theta_{j,(l,k)}\right)^{-2} \min_{l,k}\left\{\left(\sum_{j=1}^{L}\theta_{j,(l,k)}\right)^2\right\}. \tag{4.72}$$

Therefore, the harvested energy of each energy user is

$$\mathscr{E} = \eta T_{\text{D}} p\left[\sum_{l=1}^{L}\sum_{k=1}^{K_l}\frac{1}{\sum_{j=1}^{L}\theta_{j,(l,k)}} + \frac{L}{\min_{l,k}\left\{\left(\sum_{j=1}^{L}\theta_{j,(l,k)}\right)^2\right\}}\frac{\sigma_{\text{BS}}^2}{q}\right]^{-1} + \eta T_{\text{D}}\sigma^2, M \gg 1, \tag{4.73}$$

and the equivalent combination coefficient is

$$\tilde{\alpha}_{lk}=\frac{1}{\sum\limits_{j=1}^{L}\theta_{j,(l,k)}}\sqrt{\frac{1}{M}\left[\sum_{l=1}^{L}\sum_{k=1}^{K_l}\frac{1}{\sum\limits_{j=1}^{L}\theta_{j,(l,k)}}+\frac{L\frac{\sigma_{\mathrm{BS}}^2}{q}}{\min\limits_{l,k}\left\{\left(\sum\limits_{j=1}^{L}\theta_{j,(l,k)}\right)^2\right\}}\right]^{-1}},\ M\gg 1. \tag{4.74}$$

4.4.2.3 Comparison Between Non-cooperative and Cooperative Schemes

For non-cooperative energy transfer, we set the transmission power $\frac{p_l}{M}=\frac{1}{L}\frac{p}{M}$ and the harvested energy of each energy user is $\mathscr{E}_l$ in the lth cell. With perfect CSI and estimated CSI, $\mathscr{E}_l$ can be calculated by (4.24) and (4.50), respectively. As the max-min criterion is adopted, we compare $\min\limits_{l}\{\mathscr{E}_l\}$ with the harvested energy of cooperative energy transfer as follows.

- Perfect CSI: Due to $\theta_{l,(l,k)}\le\theta_{l,(l,k)}+\sum\limits_{j=1,\neq l}^{L}\theta_{j,(l,k)}$, then

$$\sum_{l=1}^{L}\sum_{k=1}^{K_l}\left(\sum_{j=1}^{L}\theta_{j,(l,k)}\right)^{-1}\le\sum_{l=1}^{L}\sum_{k=1}^{K_l}\frac{1}{\theta_{l,(l,k)}}\le L\max_{l}\left\{\sum_{k=1}^{K_l}\frac{1}{\theta_{l,(l,k)}}\right\}. \tag{4.75}$$

  Hence the harvested energy in (4.68) is larger than $\min\limits_{l}\{\mathscr{E}_l\}$.
- Estimated CSI: Due to (4.75) and

$$\min_{l,k}\left\{\left(\sum_{j=1}^{L}\theta_{j,(l,k)}\right)^2\right\}\ge\min_{l,k}\left\{\theta_{l,(l,k)}^2\right\}, \tag{4.76}$$

  the harvested energy in (4.73) is larger than $\min\limits_{l}\{\mathscr{E}_l\}$.

Hence the cooperative energy transfer always outperforms the non-cooperative scheme with either perfect or estimated CSI.

4.4.3 Distributed Energy Precoder

In Sect. 4.4.2.1 with perfect CSI, we solve (4.63) under the constraint (4.64) or (4.66), which is a global constraint. Similarly, in Sect. 4.4.2.2 with estimated

CSI, (4.70) is also a globally normalized coefficient for constructing the energy precoder. In this subsection, we propose an iterative algorithm to distributively construct the energy precoders. In each iteration, two BSs need to solve (4.63) and calculate a *virtual* harvested energy with individual constraint, which is updated based on the virtual harvested energies of the last iteration.

Therefore, under both perfect CSI and estimated CSI, we first solve (4.63) with individual constraint, and then give the iterative algorithm based on the solution.

4.4.3.1 Local Energy Precoder

- Perfect CSI: At the jth BS, assuming $\alpha_{j,(l,k)}$ is the combination coefficient for energy user k in cell l, following the same derivation of (4.65), the *actual* harvested energy is given by

$$\mathscr{E}_{lk}\left(\left\{\alpha_{j,(l,k)}\right\}\right)=\eta T_{\mathrm{D}}\left[pM\left(\sum_{j=1}^{L}\alpha_{j,(l,k)}\theta_{j,(l,k)}\right)^{2}+\sigma^{2}\right],M\gg 1. \tag{4.77}$$

Then the max-min problem (4.63) with individual constraint for cell j is formulated as

$$\begin{aligned}&\max_{\left\{\alpha_{j,(l,k)}\right\}}\ \min_{\{l,k\}}\left\{\mathscr{E}_{lk}\left(\left\{\alpha_{j,(l,k)}\right\}\right)\right\}\\ &\text{s.t.}\ \ \left\|\mathbf{w}_{j}\right\|^{2}=M\sum_{l=1}^{L}\sum_{k=1}^{K_{l}}\alpha_{j,(l,k)}^{2}\theta_{j,(l,k)}=\frac{p_{j}}{p},M\gg 1.\end{aligned} \tag{4.78}$$

Suppose $\left\{\frac{p_j}{p}\right\}$ is the globally optimal power ratio among BSs, the combination coefficients should satisfy $\alpha_{b,(l,k)}=\alpha_{j,(l,k)}\ (b=1,2,\cdots,L)$. Following the same line as in the proof of Theorem 1, the BS in cell j obtains the combination coefficient, given by

$$\alpha_{j,(l,k)}=\frac{1}{\sum\limits_{j=1}^{L}\theta_{j,(l,k)}}\sqrt{\frac{p_{j}}{Mp}\left[\sum_{l=1}^{L}\sum_{k=1}^{K_{l}}\frac{\theta_{j,(l,k)}}{\left(\sum\limits_{j=1}^{L}\theta_{j,(l,k)}\right)^{2}}\right]^{-1}}, \tag{4.79}$$

and the *virtual* harvested energy of each energy user, given by

$$\mathscr{E}_j = \eta T_{\mathrm{D}} \left\{ p_j \left[\sum_{l=1}^{L} \sum_{k=1}^{K_l} \frac{\theta_{j,(l,k)}}{\left(\sum_{j=1}^{L} \theta_{j,(l,k)} \right)^2} \right]^{-1} + \sigma^2 \right\}. \tag{4.80}$$

- Estimated CSI: Replacing $\alpha_{j,(l,k)}^2$ in (4.77) with $\tilde{\alpha}_{j,(l,k)}^2 = \frac{p_j q_{lk}}{p \left\| \hat{\mathbf{g}}_j^* \right\|^2} = \frac{p_j q_{lk}}{pM} \left(\sum_{l=1}^{L} \sum_{k=1}^{K_l} q_{lk} \theta_{j,(l,k)} + \sigma_{\mathrm{BS}}^2 \right)^{-1}$ and taking into account $q_{lk} \leq q$, the max-min problem (4.63) at the BS in cell j becomes

$$\max_{\{q_{lk}\}} \min_{l,k} \left\{ \mathscr{E}_{lk} \left(\{q_{lk}\} \right) \right\} \tag{4.81}$$

$$\text{s.t. } 0 \leq q_{lk} \leq q, l = 1, 2, \cdots, L, k = 1, 2, \cdots, K_j.$$

If $\left\{ \frac{p_j}{p} \right\}$ is the globally optimal power ratio among BSs, the equivalent combination coefficients satisfy $\tilde{\alpha}_{b,(l,k)} = \tilde{\alpha}_{j,(l,k)}$ $(b = 1, 2, \cdots, L)$. Following the same deduction of Sect. 4.3.2.2 gives rise to q_{lk}, also given by (4.72), and the *virtual* harvested energy, given by

$$\mathscr{E}_j = \eta T_{\mathrm{D}} p_j \left[\sum_{l=1}^{L} \sum_{k=1}^{K_l} \frac{\theta_{j,(l,k)}}{\left(\sum_{j=1}^{L} \theta_{j,(l,k)} \right)^2} + \frac{1}{\min\limits_{\{l,k\}} \left(\sum_{j=1}^{L} \theta_{j,(l,k)} \right)^2} \frac{\sigma_{\mathrm{BS}}^2}{q} \right]^{-1} + \eta T_{\mathrm{D}} \sigma^2. \tag{4.82}$$

At the BS in cell j, for all (l,k), the virtual harvested energies are the same and calculated by $\alpha_{b,(l,k)} = \alpha_{j,(l,k)}$ $(b = 1, 2, \cdots, L)$, namely $\mathscr{E}_j = \eta T_{\mathrm{D}} \left[pM \alpha_{j,(l,k)}^2 \left(\sum_{j=1}^{L} \theta_{j,(l,k)} \right)^2 + \sigma^2 \right]$. Then, $\min\limits_{j} \left\{ \mathscr{E}_j \right\}$ is only the function of $\min\limits_{j} \left\{ \alpha_{j,(l,k)} \right\}$. On the other hand, the actual harvested energy, $\mathscr{E}_{lk} \left(\left\{ \alpha_{j,(l,k)}, j = 1, 2, \cdots, L \right\} \right)$, is calculated by (4.77). For fixed $(l_{\mathrm{m}}, k_{\mathrm{m}}) = \arg\min\limits_{l,k} \left\{ \mathscr{E}_{lk} \right\}$, due to $\min\limits_{j} \left\{ \alpha_{j,(l_{\mathrm{m}},k_{\mathrm{m}})} \right\} \leq \alpha_{j,(l_{\mathrm{m}},k_{\mathrm{m}})}$, then $\min\limits_{j} \left\{ \mathscr{E}_j \right\} \leq \min\limits_{l,k} \left\{ \mathscr{E}_{lk} \right\}$. That means $\min\limits_{j} \left\{ \mathscr{E}_j \right\}$ is a lower bound of the actual harvested energy. Therefore, if each BS adjusts the power allocation ratio to improve $\min\limits_{j} \left\{ \mathscr{E}_j \right\}$ in each iteration, the actual harvested energy is also improved, until the virtual harvested energies of all BSs become the same.

4.4.3.2 Algorithm Description

Denote $\Xi^{t-1} = \left[\mathscr{E}_1^{t-1}, \mathscr{E}_2^{t-1}, \cdots, \mathscr{E}_L^{t-1}\right]$ as the harvested energies calculated by all BSs at the $(t-1)$th iteration. At the beginning of the tth iteration, denote $l_{\mathrm{m}}^t = \min\left\{\arg\min\left\{\Xi^{t-1}\right\}\right\}$ as the smallest cell index with the minimum harvested energy and $l_{\mathrm{M}}^t = \max\left\{\arg\max\left\{\Xi^{t-1}\right\}\right\}$ as the largest cell index with the maximum harvested energy.

In the tth iteration, the BS in cell l_{m}^t increases its transmitted power by $\delta^t \frac{p}{M}$; and the BS in cell l_{M}^t reduces the same amount of transmitted power. Thus the total power of all BSs for energy users does not change. According to (4.80) for perfect CSI or (4.82) for estimated CSI, the minimum harvested energy increases and the maximum harvested energy correspondingly decreases. As the difference between the maximum and the minimum harvested energies decreases, δ^t should be reduced, otherwise it results in the oscillation between the two BSs in cells l_{m}^t and l_{M}^t. Therefore, in each iteration, we check if $\mathscr{E}_{l_{\mathrm{M}}^t}^t \le \mathscr{E}_{l_{\mathrm{m}}^t}^{t-1}$; If so, δ^t is reduced to $\frac{\delta^{t-1}}{2}$. Then, the harvested energies calculated by all BSs tend to the same over the iterations. Finally, initialized by equal power allocation, the iterative algorithm for the distributed energy precoder is summarized in Algorithm 1.

Algorithm 1 Distributed energy precoder

Initialization $(t = 0)$**:**

- Tolerable error $\varepsilon > 0$, adjustable power ratio $\delta^0 \in (0, 1)$ and $p_j^0 = \frac{p}{L}$ $(j = 1, 2, \cdots, L)$.
- All BSs exchange the large scale fading, namely $\left\{\theta_{j,(l,k)}\right\}$.
- The BS in cell $j\,(\in \{1, 2, \cdots, L\})$ calculates $\mathscr{E}_j^0$ by (4.80) for perfect CSI or by (4.82) for estimated CSI, and broadcasts $\mathscr{E}_j^0$ to other BSs. Therefore each BS obtains the vector Ξ^0.

Do {Step 1: Each BS calculates l_{m}^t and l_{M}^t according to Ξ^{t-1}.

Step 2: The BSs in cells $\left\{l_{\mathrm{m}}^t, l_{\mathrm{M}}^t\right\}$ update $p_{l_{\mathrm{m}}^t}^t = p_{l_{\mathrm{m}}^t}^{t-1} + p\delta^{t-1}$ and $p_{l_{\mathrm{M}}^t}^t = p_{l_{\mathrm{M}}^t}^{t-1} - p\delta^{t-1}$, respectively.

Step 3: The BS in cell $j\left(\in \left\{l_{\mathrm{m}}^t, l_{\mathrm{M}}^t\right\}\right)$ calculates $\mathscr{E}_j^t$ by (4.80) for perfect CSI or by (4.82) for estimated CSI, and broadcasts $\mathscr{E}_j^t$ to other BSs.

Step 4: **If** $\mathscr{E}_{l_{\mathrm{M}}^t}^t \le \mathscr{E}_{l_{\mathrm{m}}^t}^{t-1}$

{Each BS updates $\delta^t = \frac{\delta^{t-1}}{2}$, $\Xi^t = \Xi^{t-1}$, $p_{l_{\mathrm{m}}^t}^t = p_{l_{\mathrm{m}}^t}^{t-1}$ and $p_{l_{\mathrm{M}}^t}^t = p_{l_{\mathrm{M}}^t}^{t-1}$.}

Else

{Each BS updates $\delta^t = \delta^{t-1}$, and Ξ^t with $\mathscr{E}_{l_{\mathrm{m}}^t}^t$, $\mathscr{E}_{l_{\mathrm{M}}^t}^t$, $\mathscr{E}_l^t = \mathscr{E}_l^{t-1}\left(l \ne l_{\mathrm{m}}^t, l_{\mathrm{M}}^t\right)$.}

}

While $\max\{\Xi^t\} - \min\{\Xi^t\} \ge \varepsilon$

Suppose $\left\{p_j, j = 1, 2, \cdots, L\right\}$ is globally optimal, each BS

(a) *perfect CSI*: constructs $\mathbf{w}_j$ with $\left\{\alpha_{j,(l,k)}\right\}$ in (4.79) and transmits $\mathbf{x}_j = \sqrt{\frac{p}{M}}\mathbf{w}_j s$ for energy users.

(b) *estimated CSI*: constructs $\mathbf{w}_j = \frac{\hat{\mathbf{g}}_j^*}{\|\hat{\mathbf{g}}_j^*\|}$ and transmits $\mathbf{x}_j = \sqrt{\frac{p_j}{M}}\mathbf{w}_j s$ for energy users.

4.4.3.3 Convergence

The minimum harvested energy increases in each iteration of Algorithm 1. On the other hand, the harvested energy of the distributed energy precoder is upper bounded by that of the centralized precoder. Therefore, Algorithm 1 converges. Moveover, it converges to the centralized energy precoder as stated in the following result.

Theorem 3 *When the tolerable error $\varepsilon \to 0$, the energy harvesting performance of the distributed energy precoder approaches to the optimal performance, achieved by the centralized energy precoder.*

Proof Consider the sequences $\left\{\mathscr{E}_{l_{\mathrm{m}}}^{t}, t=0,1,\cdots\right\}$, $\left\{\mathscr{E}_{l_{\mathrm{M}}}^{t}, t=0,1,\cdots\right\}$ and $\left\{\mathscr{E}_{l}^{t}, t=0,1,\cdots\right\}$ $(l=1,2,\cdots,L)$ formed over the iterations of Algorithm 1, and denote $\mathscr{E}_{l}=\lim\limits_{t\to\infty}\mathscr{E}_{l}^{t}$ $(l{=}1,\cdots,L,l_{\mathrm{m}},l_{\mathrm{M}})$. We have $\mathscr{E}_{l_{\mathrm{m}}}^{t}\le\mathscr{E}_{l}^{t}\le\mathscr{E}_{l_{\mathrm{M}}}^{t}$, $\forall\ t$. On the other hand, $\lim\limits_{t\to\infty}\left(\mathscr{E}_{l_{\mathrm{M}}}^{t}-\mathscr{E}_{l_{\mathrm{m}}}^{t}\right)\le\varepsilon$. Therefore, when $\varepsilon\to 0$, we have $\mathscr{E}_{l_{\mathrm{m}}}=\mathscr{E}_{l_{\mathrm{M}}}$ and

$$\mathscr{E}_{1}\left(p_{1}\right)=\mathscr{E}_{2}\left(p_{2}\right)=\cdots=\mathscr{E}_{L}\left(p_{L}\right). \tag{4.83}$$

Under perfect CSI, substituting (4.80) into (4.83) leads to

$$\frac{1}{p_{1}}\sum_{l=1}^{L}\sum_{k=1}^{K_{l}}\frac{\theta_{1,(l,k)}}{\left(\sum\limits_{j=1}^{L}\theta_{j,(l,k)}\right)^{2}}=\cdots=\frac{1}{p_{L}}\sum_{l=1}^{L}\sum_{k=1}^{K_{l}}\frac{\theta_{L,(l,k)}}{\left(\sum\limits_{j=1}^{L}\theta_{j,(l,k)}\right)^{2}}\triangleq\vartheta. \tag{4.84}$$

Expressing p_{j} $(j=1,2,\cdots,L)$ by ϑ and taking into account $\sum_{j=1}^{L}p_{j}\left(\vartheta\right){=}p$, we can obtain the power for cell j, given by

$$\frac{p_{j}}{M}{=}\frac{\sum\limits_{l=1}^{L}\sum\limits_{k=1}^{K_{l}}\left[\theta_{j,(l,k)}\left(\sum\limits_{j=1}^{L}\theta_{j,(l,k)}\right)^{-2}\right]}{\sum\limits_{l=1}^{L}\sum\limits_{k=1}^{K_{l}}\left(\sum\limits_{j=1}^{L}\theta_{j,(l,k)}\right)^{-1}}\frac{p}{M},j=1,2,\cdots,L. \tag{4.85}$$

Taking (4.85) into (4.79), the combination coefficients satisfy

$$\alpha_{1,(l,k)}=\alpha_{2,(l,k)}=\cdots=\alpha_{L,(l,k)}=\alpha_{lk},\forall\ \ (l,k), \tag{4.86}$$

where α_{lk} is the optimal combination coefficient derived for the centralized energy precoder in Sect. 4.4.2.1. Then, the actual harvested energies of all energy users, i.e., (4.77), become (4.68).

Hence, the performance of the distributed energy precoder tends to the optimal performance achieved by the centralized energy precoder. The result holds for estimated CSI following the same line of proof.

4.4.3.4 Complexity

We have the following complexity result for Algorithm 1.

Theorem 4 *When the number of cooperative cells is L and the tolerable error is ε, the complexity of Algorithm 1 is* $\mathscr{O}\left(L\log_2\frac{1}{\varepsilon}\right)$.

Proof Under perfect CSI, $\left|\mathscr{E}_j - \mathscr{E}\right| \leq \varepsilon$ with $\mathscr{E}_j$ in (4.80) and $\mathscr{E}$ in (4.68) is a sufficient condition for Algorithm 1 to stop in consideration of the terminal condition $\max\{\Xi^t\} - \min\{\Xi^t\} \leq \varepsilon$. Based on $\left|\mathscr{E}_j - \mathscr{E}\right| \leq \varepsilon$, we have $p_j^{\mathrm{L}}(\varepsilon) \leq p_j \leq p_j^{\mathrm{H}}(\varepsilon)$ with

$$p_j^{\mathrm{L}}(\varepsilon) = \left\{ p\left[\sum_{l=1}^{L}\sum_{k=1}^{K_l}\left(\sum_{j=1}^{L}\theta_{j,(l,k)}\right)^{-1}\right]^{-1} - \frac{\varepsilon}{\eta T_{\mathrm{D}}} \right\} \sum_{l=1}^{L}\sum_{k=1}^{K_l}\left[\theta_{j,(l,k)}\left(\sum_{j=1}^{L}\theta_{j,(l,k)}\right)^{-2}\right], \tag{4.87}$$

and

$$p_j^{\mathrm{H}}(\varepsilon) = \left\{ p\left[\sum_{l=1}^{L}\sum_{k=1}^{K_l}\left(\sum_{j=1}^{L}\theta_{j,(l,k)}\right)^{-1}\right]^{-1} + \frac{\varepsilon}{\eta T_{\mathrm{D}}} \right\} \sum_{l=1}^{L}\sum_{k=1}^{K_l}\left[\theta_{j,(l,k)}\left(\sum_{j=1}^{L}\theta_{j,(l,k)}\right)^{-2}\right]. \tag{4.88}$$

Denote T_j as the iteration number of cell j, the relation between T_j and the final adjustable ratio should satisfy

$$\frac{\delta^0}{2^{T_j+1}} \leq \frac{1}{p}\left(p_j^{\mathrm{H}} - p_j^{\mathrm{L}}\right) \leq \frac{\delta^0}{2^{T_j}}, \tag{4.89}$$

namely $T_j \sim \mathscr{O}\left(\log_2\frac{1}{\varepsilon}\right)$. Therefore, the total iteration number of L cells is

$$T = \sum_{j=1}^{L} T_j \sim \mathscr{O}\left(L\log_2\frac{1}{\varepsilon}\right). \tag{4.90}$$

Following the same line for perfect CSI, the result also holds for estimated CSI.

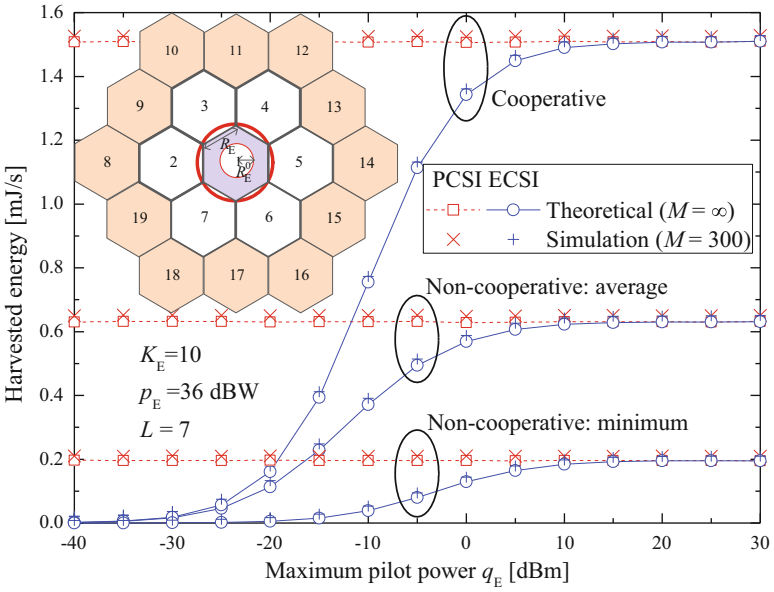

Fig. 4.7 Harvested energy versus maximum pilot power

4.4.4 Performance Evaluation

In the multi-cell scenario, the basic simulation parameters are the same to those of single cell scenario. The cell deployments are shown in the top-left corner of Fig. 4.7. We assume the numbers of energy users are the same in different cells, i.e. $K_l = K_{\mathrm{E}}$ $(l = 1, 2, \cdots, L)$. Apart from the inner circle region with radius R_{E}^0, the energy users are uniformly distributed in the hexagon regions with the side length R_{E}.

4.4.4.1 Comparison Between Non-cooperative and Cooperative Schemes

In the non-cooperative scheme, each cell only serves its own energy users, and thereby the theoretical results with PCSI and ECSI are calculated by (4.24) and (4.50), respectively. For the cooperative scheme with PCSI and ECSI, the theoretical results are given by (4.68) and (4.73), respectively. When $L = 7$, Fig. 4.7 demonstrates that the harvested energy of the cooperative scheme is higher than that of the non-cooperative scheme. By adding cells $(l = 2, 3, \cdots, 19)$ to the cooperative cluster one by one, Fig. 4.8 shows the harvested energy versus the number of cooperative cells. The average harvested energy of the non-cooperative scheme remains almost flat due to the channel orthogonality of massive MIMO. The minimum harvested energy of the non-cooperative scheme decreases with the

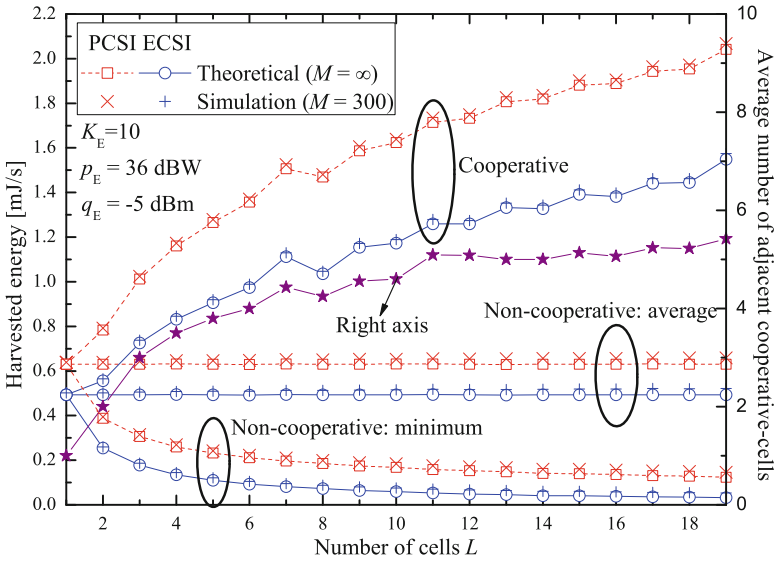

Fig. 4.8 Harvested energy versus the number of cells

increasing number of cells. By contrast, the harvested energy of the cooperative scheme increases. Moreover, the increase of the harvested energy is different when we add each cell to the cooperative cluster. Because of the path loss attenuation for the far-away cells, the increase is approximately determined by the average number of adjacent cooperative-cells. Taking $L = 4$ as an example, the number of adjacent cooperative-cells is 3 for cells 2 and 4, and 4 for both cell 1 and cell 3. Therefore, the average number of adjacent cooperative-cells is 3.5. The average numbers of adjacent cooperative-cells are also shown in Fig. 4.8. In particular, when adding cell 8 to the cooperative cluster, the average number of adjacent cooperative-cells decreases, which reduces the harvested energy. Finally, considering the overhead among cell cluster and the potential increase in the harvested energy, cooperative energy transfer among adjacent cells only is a more practical solution.

4.4.4.2 Comparison Between Centralized and Distributed Energy Precoders

In the distributed energy precoder with PCSI and ECSI, the harvested energies in each iteration of Algorithm 1 are calculated by (4.77) with $\left\{\alpha_{j,(l,k)}^{t}\right\}$ and $\left\{\tilde{\alpha}_{j,(l,k)}^{t}\right\}$, respectively. Since the power allocation among BSs is relevant to both the number of cells and the number of energy users, the adjustable power ratio is initialized by $\delta^0 = \frac{1}{LK_E}$ in our simulation. With one-time realization of user distribution, Fig. 4.9 shows the instantaneous harvested energies versus the number of iterations under

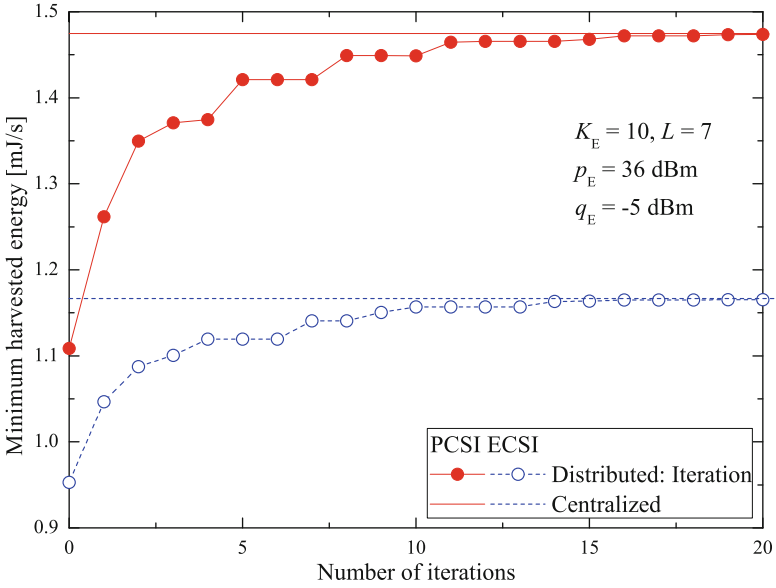

Fig. 4.9 Convergence of Algorithm 1

both PCSI and ECSI. When the number of iterations increases, the harvested energy achieved by Algorithm 1 gradually increases and eventually converges to that of the centralized energy precoder. In order to compare the energy harvesting performance of Algorithm 1 to that of the centralized energy precoder, we set $\varepsilon = 0.1\,\text{mJ/s}$. Both Figs. 4.10 and 4.11 indicate the harvested energies of the distributed energy precoder are significantly improved compared with those upon initialization, i.e., equal power allocation. The difference between the harvested energies of centralized and distributed energy precoders is limited by the tolerable error ε.

4.5 Summary

For the downlink hybrid information and energy transfer system with massive MIMO, this chapter treated the problem of precoder design for max-min harvested energy of energy users while meeting the rate requirements of information users. The precoders are in the forms of the matched-filters and the linear combination of energy users' channels for information transmission and energy transfer, respectively. With perfect CSI, the power allocation of information users and the combination coefficients of energy precoder are derived. With estimated CSI, the orthogonal pilot scheme of uplink is employed for information users; and a shared pilot scheme is proposed for energy users. Results indicate that the shared pilot scheme provides higher harvested energy than the orthogonal pilot scheme. In order

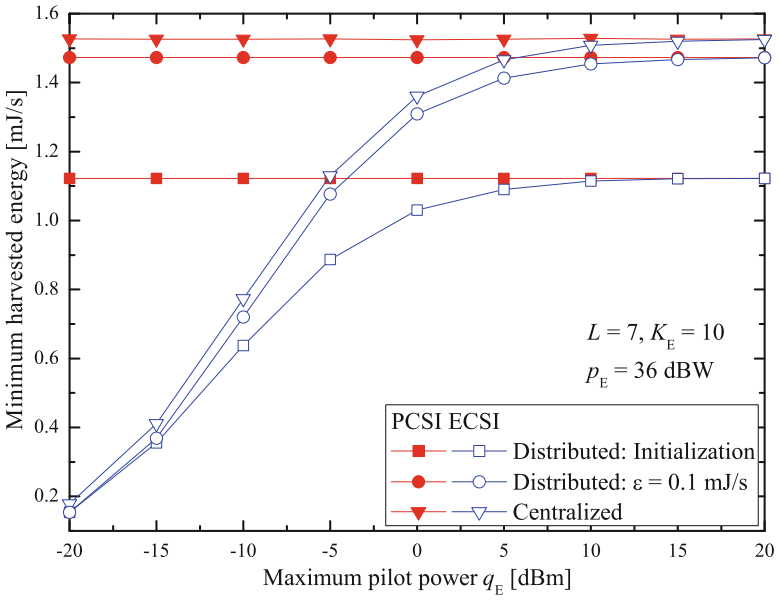

Fig. 4.10 Minimum harvested energy versus maximum pilot power

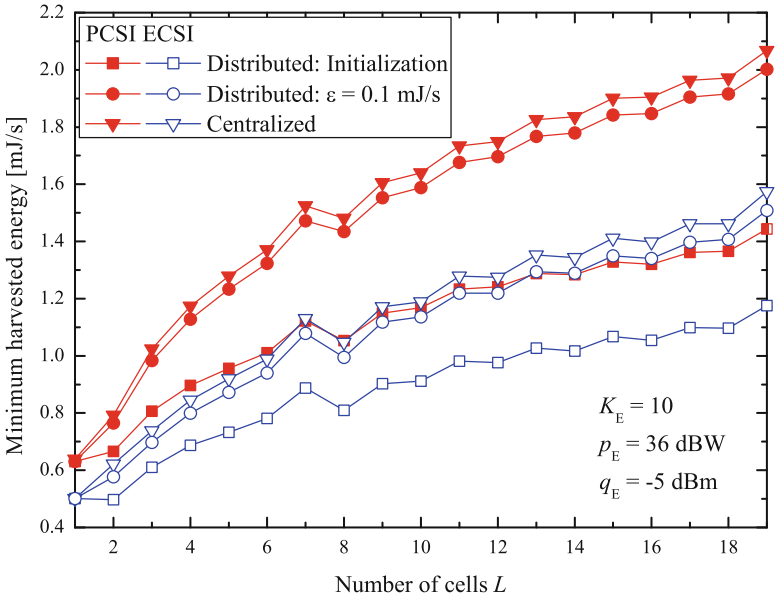

Fig. 4.11 Minimum harvested energy versus the number of cells

to exploit the inter-cell interference in the multi-cell scenario, a joint precoder is employed and its distributed implementation is given. With either perfect or estimated CSI, it is shown that the cooperative energy transfer always outperforms the non-cooperative counterpart.

References

1. I. Krikidis, S. Timotheou, S. Nikolaou, G. Zheng, D.W.K. Ng, R. Schober, Simultaneous wireless information and power transfer in modern communication systems. IEEE Commun. Mag. **52**(11), 104–110 (2014)
2. A. Massa, G. Oliveri, F. Viani, P. Rocca, Array designs for long-distance wireless power transmission: state-of-the-art and innovative solutions. Proc. IEEE **101**(6), 1464–1481 (2013)
3. K. Huang, X. Zhou, Cutting last wires for mobile communication by microwave power transfer. IEEE Commun. Mag. **53**(6), 86–93 (2015)
4. L.R. Varshney, Transporting information and energy simultaneously, in *Proceedings of IEEE International Symposium on Information Theory (ISIT)*, Toronto, July 2008, pp. 6–11
5. R. Zhang, C.K. Ho, MIMO broadcasting for simultaneous wireless information and power transfer. IEEE Trans. Wireless Commun. **12**(5), 1989–2001 (2013)
6. Q. Shi, L. Liu, W. Xu, R. Zhang, Joint transmit beamforming and receive power splitting for MISO SWIPT systems. IEEE Trans. Wireless Commun. **13**(6), 3269–3280 (2014)
7. G. Yang, C.K. Ho, R. Zhang, Y.L. Guan, Throughput optimization for massive MIMO systems powered by wireless energy transfer. IEEE J. Sel. Areas Commun. **33**(8), 1640–1650 (2015)
8. A. Osseiran, J.F. Monserrat, W. Mohr, *Mobile and Wireless Communications for IMT-Advanced and Beyond* (Wiley, West Sussex, 2011)
9. E.G. Larsson, F. Tufvesson, O. Edfors, T.L. Marzetta, Massive MIMO for next generation wireless systems. IEEE Commun. Mag. **52**(2), 186–195 (2014)
10. T.L. Marzetta, Noncooperative cellular wireless with unlimited numbers of base station antennas. IEEE Trans. Wireless Commun. **9**(11), 3590–3600 (2010)
11. H. Yang, T.L. Marzetta, Performance of conjugate and zero-forcing beamforming in large-scale antenna systems. IEEE J. Sel. Areas Commun. **31**(2), 172–179 (2013)
12. K. Zheng, L. Zhao, J. Mei, B. Shao, W. Xiang, L. Hanzo, Survey of large-scale MIMO systems. IEEE Commun. Surv. Tutorials **17**(3), 1738–1760 (2015)
13. J. Hoydis, S.T. Brink, M. Debbah, Massive MIMO in the UL/DL of cellular networks: how many antennas do we need? IEEE J. Sel. Areas Commun. **31**(2), 160–171 (2013)
14. K. Zheng, L. Zhao, J. Mei, M. Dohler, W. Xiang, Y. Peng, 10 Gb/s HetSNets with millimeter-wave communications: access and networking-challenges and protocols. IEEE Commun. Mag. **53**(1), 222–231 (2015)
15. H. Zeine, Wireless power transmission system. US 2013/0207604 A1 (Aug 2013)
16. X. Chen, X. Wang, X. Chen, Energy-efficient optimization for wireless information and power transfer in large-scale MIMO systems employing energy beamforming. IEEE Wireless Commun. Lett. **2**(6), 667–670 (2013)
17. C. Xing, N. Wang, J. Ni, Z. Fei, J. Kuang, MIMO beamforming designs with partial csi under energy harvesting constraints. IEEE Signal Process Lett. **20**(4), 363–366 (2013)
18. Z. Xing, M. Tao, Robust beamforming for wireless information and power transmission. IEEE Wireless Commun. Lett. **1**(4), 372–375 (2012)
19. G. Zheng, I. Krikidis, C. Masouros, S. Timotheou, D.A. Toumpakaris, Z. Ding, Rethinking the role of interference in wireless networks. IEEE Commun. Mag. **52**(11), 152–158 (2014)
20. X. Lu, P. Wang, D. Niyato, D.I. Kim, Z. Han, Wireless networks with RF energy harvesting: a contemporary survey. IEEE Commun. Surv. Tutorials **17**(2), 757–789 (2014)

21. Q. Sun, L. Li, J. Mao, Simultaneous information and power transfer scheme for energy efficient MIMO systems. IEEE Commun. Lett. **18**(4), 600–603 (2014)
22. C. Shen, W. Li, T. Chang, Wireless information and energy transfer in multi-antenna interference channel. IEEE Commun. Lett. **62**(23), 6249–6264 (2014)
23. T. Yoo, N. Jindal, A. Goldsmith, Multi-antenna downlink channels with limited feedback and user selection. IEEE J. Sel. Areas Commun. **25**(7), 1478–1491 (2017)
24. Y. Liang, Y. Wang, T. Chang, Y. P. Hong, C. Chi, On the impact of quantized channel feedback in guaranteeing secrecy with artificial noise, in *Proceedings of IEEE International Symposium on Information Theory (ISIT)*, Seoul, June 2009, pp. 2351–2355
25. L. Zhao, K. Li, K. Zheng, M.O. Ahmad, An analysis of the tradeoff between the energy and spectrum efficiencies in an uplink massive MIMO-OFDM system. IEEE Trans. Circuits Syst. II Express Briefs **62**(3), 291–295 (2015)
26. H.Q. Ngo, E.G. Larsson, T.L. Marzetta, Energy and spectral efficiency of very large multiuser MIMO systems. IEEE Trans. Commun. **61**(4), 1436–1449 (2013)
27. B. Hochwald, T. Marzetta, V. Tarokh, Multi-antenna channel hardening and its implications for rate feedback and scheduling. IEEE Trans. Inform. Theory **50**(9), 1893–1909 (2004)
28. H.Q. Ngo, E.G. Larsson, T.L. Marzetta, Aspects of favorable propagation in massive mimo, in *Proceedings of the 22nd European Signal Processing Conference (EUSIPCO)*, Lisbon, Sept 2014, pp. 76–80
29. Z. Xiang, M. Tao, X. Wang, Massive MIMO multicasting in noncooperative cellular networks. IEEE J. Sel. Areas Commun. **32**(6), 1180–1193 (2014)
30. A. Ashikhmin, T.L. Marzetta, Pilot contamination precoding in multi-cell large scale antenna systems, in *Proceedings of IEEE International Symposium on Information Theory (ISIT)*, Cambridge, MA, July 2012, pp. 1137–1141

Chapter 5
Conclusion and Outlook

5.1 Conclusion

This monograph aims to elaborate that massive MIMO technology can be utilized to provide high QoS for 5G communications and future services. The physical-layer and MAC-layer techniques of massive MIMO are first summarized and compared in detail. Based on the basic theory of massive MIMO, two typical application scenarios of massive MIMO, i.e., mm-wave communications and wireless energy transfer, are discussed, demonstrating the feasibility and efficiency of massive MIMO in these two scenarios. It is concluded that massive MIMO can be used to efficiently support information transmission and energy transfer.

5.2 Future Research Directions

The investigation of massive MIMO has stimulated strong research interest in both academia and industry alike. However, much more efforts are needed for practical applications of massive MIMO in the near future. Based on our discussions in the preceding chapters, the following challenges and open issues lie ahead.

Design of AAs Finding practical antenna configurations is an important issue for massive MIMO systems, because it affects not only the channel properties, but also their array gains, diversity gains and multiplexing gains. Moreover, AAs may be constrained to a limited physical size. Therefore, the employment of antennas has to be carefully designed to enhance the attainable performance given the physical area constraint.

Green Massive MIMO Networks With increasing carbon emissions imposed by the excessive power consumption of wireless communications networks, EE has

L. Zhao et al., *Massive MIMO in 5G Networks: Selected Applications*,
SpringerBriefs in Electrical and Computer Engineering,
https://doi.org/10.1007/978-3-319-68409-3_5

become a significant performance metric of evaluating future wireless networks. However, the evaluation of EE in massive MIMO systems in the literature focuses primarily on the EE in the single-cell environment. Furthermore, only the radiated power of the PAs is considered, while ignoring the power dissipation of signal processing circuit and the efficiency of the PAs [1, 2]. Therefore, the realistic EE performance of massive MIMO systems needs to be analyzed by considering both the radiated power and circuit power in multi-cell scenarios.

Performance Analysis of Large-scale DASs Centralized and distributed antenna deployments constitute two important scenarios of massive MIMO systems. The majority of current work focuses on the family of centralized massive MIMO systems. As argued, large-scale DASs are capable of significantly improving both the coverage quality and the capacity of wireless communications networks. The coverage quality of both indoor and outdoor environments should be evaluated in the near-future in terms of the Probability Density Function (PDF) of their SINRs. Stochastic geometry has been widely used for the analysis of wireless networks, with an emphasis on the 2D plane. However, stochastic geometry needs to be extended to the 3D space to analyze large-scale DASs.

Complexity Versus Performance A massive MIMO system often entails considerably complex signal processing. Hence, substantial efforts have been devoted to streamline and optimize both signal processing algorithms and their implementations. However, low-complexity algorithms generally decrease the performance of massive MIMO. For example, having more accurate CSI leads to improved performance at the expense of increased processing complexity. When low-complexity linear channel estimation is adopted, the attainable performance is constrained by the pilot contamination phenomenon, especially in multi-cell scenarios. However, pilot contamination can be overcome by using complex channel estimation algorithms [3, 4]. There exists a tradeoff between the complexity of channel prediction as well as the TPC design and the experienced channel, when the UEs move around in a cell. Therefore, simple but efficient algorithms have to be conceived for channel estimation, channel prediction, TPC and detection.

Effects of Non-ideal Hardware Massive MIMO relies mainly on the law of large numbers to average out noise, channel fading characteristics, etc. However, in practice, low-cost imperfect components are employed to implement the massive MIMO system. Therefore, the imperfections of non-ideal hardware, such as the nonlinearities of the amplifier, I/Q imbalance, A/D and D/A nonlinearities, should be taken into account [5, 6] in practical massive MIMO systems. Some existing studies have been reported on evaluating the effects of non-ideal hardware. However, more efforts are required for designing efficient algorithms to mitigate these non-ideal factors.

Duplex Mode There are two basic duplex modes in wireless communications networks, namely TDD and FDD. Owing to a limited number of orthogonal pilot sequences, TDD is assumed at present in most existing work related to massive MIMO. A full-duplex system, where the UL and DL transmissions occur

simultaneously, is also a good choice. However, preliminary studies on full-duplex systems use only three antennas. Extending the full-duplex research to massive MIMO systems may be a topic of interest in the near future.

New Application Scenarios Since massive MIMO is introduced to wireless networks, it has been undergoing rapid changes. As a benefit of its large DoF, the R-TDD scheme has been proposed for alleviating the interference in HetNets. When eNBs are equipped with massive AAs, a wireless backhaul can be established among the eNBs. However, both R-TDD and wireless backhaul techniques are not mature in practice to date, hence studies need to be carried out. Moreover, when a relay node employs a large number of antennas, the channel properties are different from those of a regular relay equipped with a small number of antennas [7]. Although much attention has been dedicated to the design of massive MIMO systems in the mm-wave band, there are still many uncertain issues surrounding the practical mm-wave communication systems, such as their hardware design, interference control and resource management. Also, the applications of massive MIMO on wireless energy transfer and wireless control need further studies.

References

1. H.Q. Ngo, E. Larsson, T. Marzetta, Energy and spectral efficiency of very large multiuser MIMO systems. IEEE Trans. Commun. **61**(4), 1436–1449 (2013)
2. H. Yang, T. Marzetta, Performance of conjugate and zero-forcing beamforming in large-scale antenna systems. IEEE J. Sel. Areas Commun. **31**(2), 172–179 (2013)
3. H.Q. Ngo, E. Larsson, EVD-based channel estimation in multicell multiuser MIMO systems with very large antenna arrays, in *Proceedings of the IEEE International Conference Acoustics, Speech and Signal Processing (ICASSP)*, Kyoto, May 2012, pp. 3249–3252
4. R.R. Müller, M. Vehkaperä, L. Cottatellucci, Blind pilot decontamination, in *Proceedings of the17th ITG Workshop on Smart Antennas*, Stuttgart, Mar 2013, pp. 1–6
5. A. Pitarokoilis, S.K. Mohammed, E.G. Larsson, Uplink performance of time-reversal MRC in massive MIMO systems subject to phase noise. IEEE Trans. Wirel. Commun. **15**(99), 1 (2014)
6. E. Björnson, J. Hoydis, M. Kountouris, M. Debbah, Massive MIMO systems with non-ideal hardware: energy efficiency, estimation, and capacity limits. IEEE Trans. Inf. Theory **60**(11), 7112–7139 (2014)
7. H.Q. Ngo, H. Suraweera, M. Matthaiou, E. Larsson, Multipair full-duplex relaying with massive arrays and linear processing. IEEE J. Sel. Top. Sign. Process. **32**(9), 1721–1737 (2014)